NUREG/CR-2784

Behavior of Water Spray Injected into Air/Steam Environment

Prepared by S. Y. Lee, R. S. Tankin

Department of Mechanical and Nuclear Engineering
Northwestern University

Prepared for
U.S. Nuclear Regulatory Commission

8208260433 820831
PDR NUREG
CR-2784 R PDR

NOTICE

This report was prepared as an account of work sponsored by an agency of the United States Government. Neither the United States Government nor any agency thereof, or any of their employees, makes any warranty, expressed or implied, or assumes any legal liability of responsibility for any third party's use, or the results of such use, of any information, apparatus, product or process disclosed in this report, or represents that its use by such third party would not infringe privately owned rights.

Availability of Reference Materials Cited in NRC Publications

Most documents cited in NRC publications will be available from one of the following sources:

1. The NRC Public Document Room, 1717 H Street, N.W.
   Washington, DC 20555

2. The NRC/GPO Sales Program, U.S. Nuclear Regulatory Commission,
   Washington, DC 20555

3. The National Technical Information Service, Springfield, VA 22161

Although the listing that follows represents the majority of documents cited in NRC publications, it is not intended to be exhaustive.

Referenced documents available for inspection and copying for a fee from the NRC Public Document Room include NRC correspondence and internal NRC memoranda; NRC Office of Inspection and Enforcement bulletins, circulars, information notices, inspection and investigation notices; Licensee Event Reports; vendor reports and correspondence; Commission papers; and applicant and licensee documents and correspondence.

The following documents in the NUREG series are available for purchase from the NRC/GPO Sales Program: formal NRC staff and contractor reports, NRC-sponsored conference proceedings, and NRC booklets and brochures. Also available are Regulatory Guides, NRC regulations in the *Code of Federal Regulations*, and *Nuclear Regulatory Commission Issuances*.

Documents available from the National Technical Information Service include NUREG series reports and technical reports prepared by other federal agencies and reports prepared by the Atomic Energy Commission, forerunner agency to the Nuclear Regulatory Commission.

Documents available from public and special technical libraries include all open literature items, such as books, journal and periodical articles, and transactions. *Federal Register* notices, federal and state legislation, and congressional reports can usually be obtained from these libraries.

Documents such as theses, dissertations, foreign reports and translations, and non-NRC conference proceedings are available for purchase from the organization sponsoring the publication cited.

Single copies of NRC draft reports are available free upon written request to the Division of Technical Information and Document Control, U.S. Nuclear Regulatory Commission, Washington, DC 20555.

Copies of industry codes and standards used in a substantive manner in the NRC regulatory process are maintained at the NRC Library, 7920 Norfolk Avenue, Bethesda, Maryland, and are available there for reference use by the public. Codes and standards are usually copyrighted and may be purchased from the originating organization or, if they are American National Standards, from the American National Standards Institute, 1430 Broadway, New York, NY 10018.

GPO Printed copy price: $6.50

NUREG/CR-2784
R2

Behavior of Water Spray Injected into Air/Steam Environment

Manuscript Completed: May 1982
Date Published: August 1982

Prepared by
S. Y. Lee, R. S. Tankin

Department of Mechanical and Nuclear Engineering
Northwestern University
Evanston, IL 60201

Prepared for
Division of Accident Evaluation
Office of Nuclear Regulatory Research
U.S. Nuclear Regulatory Commission
Washington, D.C. 20555
Under NRC Grant No. G-1000

ABSTRACT

BEHAVIOR OF WATER SPRAY INJECTED INTO AIR/STEAM ENVIRONMENT

The behavior of a water spray injected into both an air and a steam environment was studied. The water spray was divided into two parts - sheet portion and droplet portion. An analytical model is proposed for explaining the spray behavior. Experiments were performed to substantiate the analytical results. Holographic pictures were used to obtain the droplet size distribution. These size distributions were used for computing the motion of spray droplets in the analytical model. For the sprays used in this study, the sheet portion plays a very important role in the heat transfer phenomenon. The spray angle is primarily governed by the sheet portion. In addition, the axial extent (length) of sheet is very important parameter in determining the spray angle. A correlation is obtained experimentally for breakup length in terms of the Weber number and the Jakob number.

TABLE OF CONTENTS

LIST OF TABLES

LIST OF FIGURES

NOMENCLATURE

a	constants
$\bar{a}$	distribution parameter
A	constants
A_o	flow area of the nozzle (m^2)
b	constants
C	constants
C_D	drag coefficient
C_p	specific heat of water (KJ/Kg^oC)
d	thickness of water sheet (m)
D	diameter of droplets (μm)
D_i	initial droplet diameter (μm)
D_m	maximum droplet diameter (μm)
D_n	nozzle diameter (m)
Dc	Dc number $(\frac{\lambda_f \rho_f C_{p,f}}{\lambda_L \rho_L C_{p,L}} \frac{1}{Ja})$
E	length of the initial part of drop portion (see Fig. II-3)
F_o	Fourier number $(4\alpha t/D_i^2)$
g	gravity
h	enthalpy (KJ/Kg)
Ja	Jakob number $(C_p(T_s - T)/\lambda)$
Je	Jet number $(We \cdot (\rho_a/\rho_L)^{0.55})$
k	thermal conductivity (KW/m^oC)
L	length of water spray sheet in axial direction (m)
$\dot{m}_c$	condensation rate between z- z+dz (Kg/sec)
$\dot{m}_e$	vapor entrained between z - z+dz (Kg/sec)

$\dot{m}_L, \dot{m}$	mass flow rate of liquid (Kg/sec)
$\dot{m}_{Lo}$	mass flow rate of spray water at nozzle exit (Kg/sec)
$\dot{m}_v$	mass flow rate of vapor (Kg/sec)
n	integer number
N	number of droplets
ΔP	pressure difference (N/m^2)
Pe	Peclet number
P_{oz}	pressure of vapor (or air) at z, outside the water sheet (N/m^2)
P_z	pressure of vapor (or air) at z, inside the water sheet (N/m^2)
Q	volume flow rate of liquid (ml/sec)
r	radial distance from the axis of the spray (m)
R	radius of spray cross-section at z (m)
Re	Reynolds number
R_r'	position of droplets in radial direction from breakup point (m)
R_t'	position of droplets in tangential direction from breakup point (m)
S	direction of flow of liquid sheet
T	temperature (^oC)
T_{Lo}	temperature of spray water at the nozzle exit (^oC)
T_i	temperature of water droplet at breakup point (^oC)
T_s	temperature of steam (^oC)
t	time (sec)
v	volume of droplets
V_a	velocity of air ($\sqrt{V_{vz}^2 + V_{vr}^2}$)
V_{Lz}	liquid velocity (axial direction) (m/sec)
V_{Lr}	liquid velocity (radial direction) (m/sec)
V_{Lo}	liquid velocity of the sheet portion (m/sec)

V_o velocity difference between liquid and steam (or air) (m/sec)

V_{vz} steam (or air) velocity (axial direction) (m/sec)

V_{vr} steam (or air) velocity (radial direction) (m/sec)

V_t tangential velocity of water (m/sec)

We Weber number $(\rho_L V_{Lo}^2 D_n/\sigma)$

We_T $2\sigma/\rho_L V_{Lo}^2 d$

y $\ell n[\bar{a}\ D_i/(D_m - D_i)]$

z axial distance from the nozzle tip (m)

α thermal diffusivity (m^2/sec)

δ distribution parameter

λ heat of vaporization (KJ/Kg)

Γ $[1 + C_p(T_s - T_{Lo})/\lambda]^{1/3} - 1$

ρ density (Kg/m^3)

η $\tan^{-1}(dr/dz)$

σ surface tension (N/m)

ζ radius of curvature

ψ stream function

ϕ normal direction to the flow

ξ vorticity

ν kinematic viscosity (m^2/sec)

SUBSCRIPTS

a	air
f	condensate film
L	liquid
v	vapor

I. INTRODUCTION

The purpose of a spray is to increase the surface area of the injected liquid in order to promote the heat and mass transfer. In most cases, the behavior of spray can be described by spray angle, dispersion (drop size distribution) and penetration. These parameters are determined by the spray nozzle, breakup mechanism and aerodynamic effects after breakup, which in turn depends on the ambient pressure (density), injection pressure, liquid and gas properties for a particular nozzle.

Since 1930, a great deal of research has been performed on the breakup mechanism and the effects of ambient pressure, injection pressure, liquid properties [1-19] including extensive review works [20, 21]. The aerodynamic behavior of spray was studied by Rothe and Block [22].

Castleman [1] explained the mechanism of atomization of the jets by the drag of the ambient air; a portion of the large mass (jet) caught up by air stream and anchored at the other end is drawn out to fine drops by Rayleigh instability. Schweitzer [2] explained the breakup mechanism by the turbulent motion which occurred inside the nozzle. The radial dis-turbance (velocity) tends to break the interface as soon as the restraint imposed by the orifice wall ceases. A laminar boundary layer may retard this disintegration up to certain distances. Tanasawa et al. [3] studied the breakup mechanism using the photographic method, the light source being an electric spark of 0.1 micro-second duration. As a criterion for defining the various patterns of the breakup regime, they introduced a nondimensional number, Je (Jet number, $We \cdot (\rho_a/\rho_L)^{0.55}$), defined as the function of Weber number $(\rho_L V_{Lo}^2 D_n/\sigma)$ and density ratio of liquid and gas. The breakup regime is divided into four patterns; dripping ($Je < 0.1$), longitudinal oscillation ($0.1 < Je < 10$), lateral oscillation ($10 < Je < 500$) and atomizing ($Je > 500$). Basically, Castleman explains that the initiation of breakup is due to the drag of the surrounding air; whereas the model of Schweitzer emphasizes the turbulent motion which originates from nozzle hole. Yet there is no definite explanation on the breakup mechanism; the effect of turbulent motion, drag of surrounding fluids, properties of liquid and surroundings (such as, viscosity and surface tension), shape of the nozzle are all considered as governing parameters of breakup. However, as far as breakup patterns are concerned, the type of classification used by Tanasawa is generally accepted.

For the purpose of application to practical systems (such as engine design), the study of sprays was conducted in a different manner. That is, the phenomena of spray were studied experimentally by changing the governing parameters; such as ambient pressure, injection pressure (flow rate) and fluid properites. DeJuhasz [4], Lee [5,6] reported that the drop size distribution becomes even and initial spray cone angle increases by increasing of ambient pressure, injection pressure and decreasing of liquid viscosity. Ranz [7] introduced the concept of stress on the atomizing mechanism. In his report, the condition of atomization depends on the ratio of inertial stress (velocity of droplet) and surface normal stress (surface tension effect), which leads to a form of the Weber number. Also the theoretical dispersion angle is predicted as a function of viscosity parameter. He suggested the possibility of modelling the spray using the Weber number as the criterion. Recently, Reitz et al. [8] used an ultra-high-speed-filming camera (about 10^6 frames/sec) to study spray phenomena; such as, intact length, spray angle, etc. He found the spray cone angle increases as ambient pressure increases and decreases slightly with increasing liquid viscosity, and strongly depends on nozzle design.

Most of the above studies were conducted on a solid-injection nozzle. However, in many applications, other types of nozzles - such as, swirl (centrifugal) nozzle, poppet type nozzle and fan spray nozzle - are used for better atomization (Fig. I-1). Fraser et al. [9] concentrated on determining the drop sizes for swirl and fan sprays as a function of injection pressure and flow number (which depends on the atomizer design). Their results show the drop size is inversely proportional to the injection pressure. Also, the effect of ambient pressure (at sub atmospheric pressure) on drop sizes was studied. More data of this type were obtained later by Dombrowski et al.[10]. Dombrowski et al. [11-17] also studied the disintegration of a liquid sheet which is produced by fan spray nozzles. Two principal modes of disintegration were discussed; due to the growth of aerodynamic waves; and due to the perforation in the sheet. The aerodynamic instability is caused by unbalance of the aerodynamic forces and interfacial tension. This unstable wave propagates at the same velocity as the sheet with exponentially increasing amplitude (Kelvin - Helmholtz type instability) until breakup occurs. On the other hand, perforation occurs by the presence of nonwettable particles in the liquid or by certain turbulence characteristics in the nozzle. Coalescence of expanding perforation produces the network of unstable ligaments which eventually break into

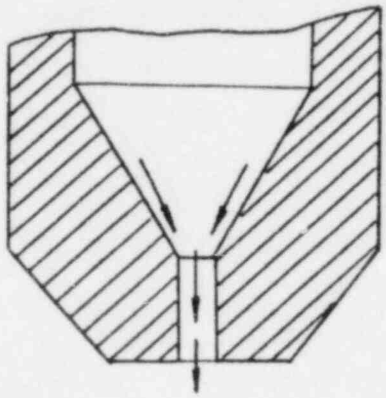

(a) Solid injection nozzle

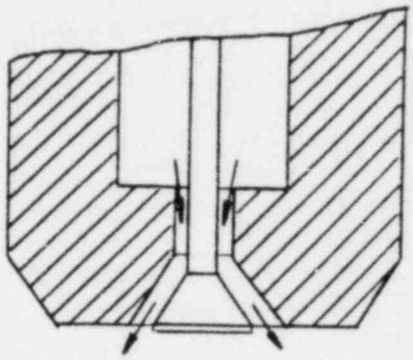

(b) Poppet type nozzle

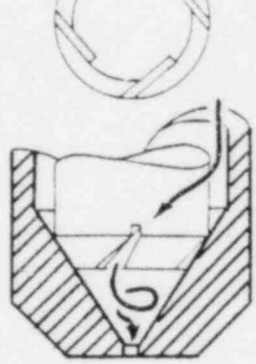

(c) Swirl (Centrifugal) nozzle (9)

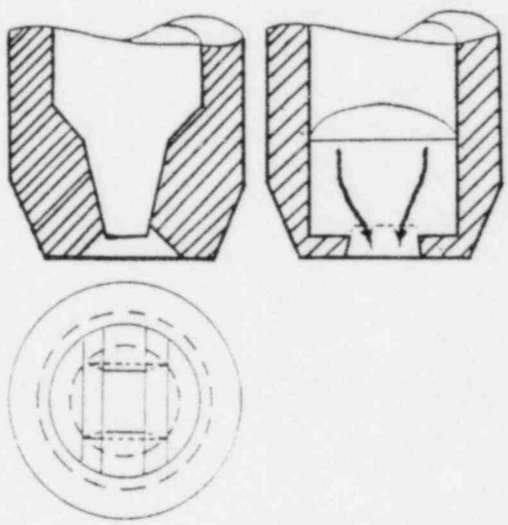

(d) Fan spray nozzle (9)

Fig.I-1 Typical types of nozzles

droplets. DeCorso [18,19] studied the effect of ambient and injection pressure on spray angle and drop sizes. Experiments were conducted with the centrifugal nozzle and diesel fuel. He concluded that the spray angle decreases markedly with increasing fuel and ambient pressure. This conclusion seems to contradict to the results reported by other researchers [3-5,8]. This is because the swirl (or centrifugal) nozzle has different flow characteristics compared to the solid injection nozzle. It is generally explained [20] as follows; for the plain atomizer (solid injection) the axial velocity of liquid is always larger than radial velocity (5 to 15 times). With an increase of air density (due to increase of ambient pressure), the decrease of axial velocity will be greater than the radial velocity and the spray angle will increase. However, in case of swirl nozzle, higher ambient pressure causes larger air core diameter to exist inside the nozzle. With the vortex type flow of liquid, the tangential velocity at the air core periphery must decrease, which results in decrease of spray angle. For a centrifugal nozzle, it is also reported [20] that the effect of injection pressure on the spray angle turned out to be small. Rather, the large decrease of spray angle observed by DeCorso seems to originate from a different definition of spray angle DeCorso used. He defined the equivalent spray angle which is primarily determined by the spray radius downstream. If the spray is injected into air, it will drag the air in the axial direction, induce the entrainment of the ambient air inwards in lateral direction, and then drag the droplets inwards. If the ambient pressure (or ambient gas density) increases, the inward drag force increases; thus the equivalent spray angle (or spray radius downstream) becomes smaller. He also reported that the drop sizes (Sauter Mean Diameter) becomes smaller up to a certain ambient pressure, and then increases above that pressure. It is conjectured that increasing the ambient pressure above a certain value causes the coalescence of droplets. However, this secondary effect has not been clearly documented experimentally.

Recently, Rothe et al. [22] proposed a one-dimensional model to obtain the spray shape assuming the breakup is completed at injection. The continuity and momentum equation were set up for the whole spray region with the drag force on each droplet taken into account. Their solution gave the spray outline shape. In this model, the drop size is assumed to be uniform. This model greatly simplifies the actual system and from a practical point of view, it is questionable to define the boundary of spray based on a uniform drop size.

The effect of condensation on a spray is not taken into account in the above research. The phenomenon of direct contact condensation of steam is important to various fields. For example. a cold water spray is injected into steam when LOCA situation occurs in a nuclear reactor; a cold water spray is injected into steam in direct contact type condensers (heat exchangers); etc. Although direct contact condensation has been a subject of importance for a long time, only very limited research has been done on the behavior of cold water sprays in direct contact with steam.

Brown [23,24] studied the effects of mean droplet diameter and water feed rate on heat transmission for water spray droplets in a steam environment. This theory suggests that the value of the heat transfer coefficient varied from 2300 to 11600 Btu/ft^2-hr-F (3.98 - 20.1 Kw/m^2-C) for the droplets whose sizes range from 100 to 500 microns. Similar range of heat transfer coefficient was reported by Lim et al. [25] in case of the stratified steam-water flow. Lim's work consisted of experimental measurements over a wide range of steam and subcooled water flow rates.

Kutateladze [26] studied condensation on a free falling jet, obtaining an expression for the temperature change of the water as a function of the length of jet with an outflow velocity of 3-5 m/sec. However, it was pointed out by others [27] that the turbulent exchange coefficient (eddy diffusivity) included in his formulation is based on an eddy diffusivity coefficient evaluated from pipe flow correlations - which differs from the case of jet flow with free surface.

Weinberg [28] studied the heat transfer for sprays of water in a steam atmosphere at low pressure. The spray was divided into two regions - film region and the droplet region - corresponding to the flow of water as a film and as drops. In Weinberg's analysis, it was concluded for the centrifugal nozzle that the film region is much more important than the droplet region with regard to heat transfer.

Hasson et al. [27,29] studied the heat transfer by direct contact condensation for laminar liquid jets, and experiments were conducted by measuring the variation of water sheet thickness to substantiate their analytical model. According to their results, the heat transfer coefficient for a laminar water sheet is very high; ranging from 100,000 to 200,000 Kcal/hr-m^2-C (120-240 Kw/m^2-C), surface resistance being neglected.

More recently, a water spray in steam atmosphere was studied by Sandoz et al. [30,31] and the General Electric Company [32] for LOCA situations. They studied modeling of environmental effect on the water sprays from nozzles used in reactors. However, these studies do not contain a detail behavior of the spray, i.e., drop size distribution, breakup lengths, etc. They concentrated on a prototype experiment for design purposes. The G.E. Report [32] mentions the effects of ambient steam pressure and spray water subcooling temprature as follows:

1. With spray water at saturation temperature, the spray cone outline appears substantially the same in steam as in air at 1 atm.
2. The spray cone outline narrows as the ambient pressure increases.
3. The spray cone outline narrows as the spray water temperature decreases (from saturation temperature).

Takahashi et al. [33] have studied the water spray phenomena for a mixture type steam condenser to be used in geothermal power plants. They conclude that the rising temperature of water spray from centrifugal nozzles can be correlated to H/D where H represents the height of fall of cooling water and D is nozzle orifice diameter. Most of the water temperature rise occurs before breakup where H/D is less than 20.

Lekic et al. [34-38] have studied the water spray behavior in greater detail. First, they studied the behavior of drops experimentally and devised an analytical model of the spray. Droplet size distributions were studied experimentally by photographic method, and their theoretical considerations include the motion of droplets (vertical direction only) and heat transfer rate. In their analysis, the thermal utilization* for a given length of spray is obtained. The drop size is found to be the most important parameter influencing thermal utilization. In Lekic's paper, the initial drop sizes were takên from the photograph of the spray injected into steam at the location about 30 mm from the nozzle tip. As mentioned earlier [28,33], most of the heat transfer (or droplet growth) occurs within very short distance from the nozzle tip. The measured size might be different from the original droplet size, D_i. Also in Lekic's experiments, a slit is placed inside of the spray to facilitate photographing the droplets. This slit disturbs the shape of the spray; thus, it no longer has the advantage of an optical non-disturbing experimental method. There have been studies in which the drop sizes have been measured [37,39] and several mathematical expressions were proposed for fitting the droplet distribution curves [40]; such as, Nukiyama-Tanasawa, Rosin-Rammler, Log-probability, Upper-limit, etc., (Table I-1). The Upper-limit function fits the droplet distribution best and is simple to use. Lekic [36] mentions this in his paper.

More recently, Kashiwagi et al. [41] studied direct contact condensation for coolant fluid jets. Here, theoretical investigations were carried out for direct contact condensation for plane, cylindrical and spherical jets with the effect of the condensate film resistance taken into account. These results were obtained numerically. They introduced a dimensionless number, Dc, $(\lambda_f \rho_f C_{p,f} / \lambda_L \rho_L C_{p,L} \cdot 1/Ja)$, defined as the

------

* Thermal utilization is defined as the ratio between the actual heat transfer rate at distance z from the nozzle and the theoretical heat transfer rate.

Name	Function Form	Comments
Nukiyama-Tanasawa	$\frac{dn}{dD} = B\,D^2 e^{-bD^{\delta}}$ where, $b = \frac{2}{\delta\,D'^{\delta}}$ $B = \delta\,b^{3/\delta}/\Gamma(3/\delta)$ n : Number fraction of droplets D': Diamater of maximum probability	∘ δ is chosen for best fitting ∘ Function for number distribution
Rosin-Rammler	$1 - v = e^{-(D/\bar{D})^{\delta}}$ where, v : Accumulated volume fraction of droplets	∘ $\bar{D}$, δ are chosen for best fitting
Log-probability	$\frac{dv}{dy} = \frac{\delta}{\sqrt{\pi}} e^{-\delta^2 y^2}$ where, $y = \ln(D/\bar{D})$	∘ $\bar{D}$, δ are chosen for best fitting
Upper-limit	$\frac{dv}{dy} = \frac{\delta}{\sqrt{\pi}} e^{-\delta^2 y^2}$ where, $y = \ln[\bar{a}\,D/(D_m - D)]$ D_m : Maximum droplet diameter	∘ $\bar{a}$, δ, D_m are chosen for best fitting ∘ Modified form of Log-probability

Table I-1 Functional forms for drop size distribution inverse of the Jakob number ($C_p(T_s - T)/\lambda$) multiplied by the ratio of thermal conductivity, density and specific heat between the coolant and condensate film. In our case where the coolant and vapor are water and steam, Dc number is just inverse of Jakob number. The computational results show that the accurate local Nusselt number cannot be obtained by neglecting the condensate film resistance if Dc < 10. Also, they obtained the non-dimensional thickness of condensate film with parameters of the Dc number.

Tanaka [42] studied the heat transfer of a spray droplet in a nuclear reactor containment for the LOCA situation. He developed a computer program (CONDENSE) for the rigid-droplet model and complete-mixing droplet model. This program was developed to calculate the spray heat transfer efficiency as a function of falling distance with the input data of droplet size, initial velocity, spray angle, and gas temperature. This work was done for a single droplet, and it does not explain the effect of drop size distribution on the whole spray pattern.

Ohba et al. [43] studied the direct contact condensation of steam on a high speed spray-jet of subcooled water. In their theoretical model, the internal circulating motion within the droplet is assumed. The drop size distribution was obtained by using the oil bath method. This drop size distribution is used as the weighting function to obtain the mean temperature of spray as a function of distance. The Peclet number (Pe = Pr•Re) was used to represent the strength of internal circulation. Temperature of the water spray was measured and compared with the temperature obtained from a theoretical model. Neglecting breakup length may be the cause for most of the deviation between the theoretical model and the experiments. Their liquid nozzle consists of many small holes such as seen in a shower nozzle, and breakup length for such a nozzle may not be negligible. The heat transfer for a liquid column (before break-up) is very much different from that of liquid droplets (after breakup).

Most of the previous studies on sprays dealt with particular aspects of sprays - such as, breakup mechanism, spray angle, condensation and/or evaporation of single droplets, etc. Very little research has been performed on the overall behavior of a spray starting with initial condition at the nozzle exit. Even less has been done taking into account condensation effects. In this research, a model is proposed and experiments have been conducted to predict the overall behavior of water spray injected into steam environment. To study the behavior of droplets, the holographic method is used to obtain 3-dimensional, instantaneous pictures of the water spray. Nd:YAG pulsed laser is used for this purpose. To examine the outline shape of the sheet portion, 2-dimensional pictures were taken with the same laser (back lighting). In addition to the outline shape of the sheet portion, the breakup length was measured from these pictures. Injection pressure (or flow rate), ambient pressure and subcooling temperature were taken as experimental parameters, and the difference between the steam and air environment was studied.

II. ANALYTICAL MODEL

Generally, the spray consists of a sheet (or film) region and droplet region, which occurs before and after the breakup, respectively. Usually, the sprays used in direct contact condensation have a wide spray angle; which means, basically, these sprays are classified as hollow cone sprays*. In this chapter, the general flow pattern of the spray is considered and then the analysis will be presented for the two regions of the spray; i.e., the region of spray that is a liquid sheet and the region that is droplets.

1. General Flow Pattern of the Spray

Generally, a spray consists of two regions, i.e., sheet and droplet regions; the sheet region usually extends a small distance from the nozzle. In case of no condensation (water-air, or saturated water-steam), the water spray behavior will be as seen in Fig. II-1. When the water sheet leaves the nozzle, the water sheet will drag the adjacent air with it. Also, the droplets formed (from the breakup of the liquid sheet) will drag the air in the spray core downwards entraining air from sides. This air flow pattern within the sheet is confirmed by an experiment which is discussed in Chapter IV. It appears to form closed streamlines as indicated in Fig. II-1. With this assumption, it is possible to determine the pressure distribution inside the sheet by using the method of Parlange [44], who calculated the pressure distribution

------

* The spray angle of the full cone nozzle is at most 10 to 11 degrees [8]. The usual definition of a full cone spray is as follows: the water droplets have even distribution at certain distance downstream. In this study, the full cone spray means no hollow portion exists before breakup occurs.

inside of water bells. The details of this derivation are given in Appendix 1. The calculated results show the pressure changes (for our range of flow rates) due to the air circulation inside the water sheet is negligibly small. Thus, the sheet shape can be calculated with surface tension and inertia forces taken into consideration.

In case of significant condensation, the flow pattern is assumed to be similar to that seen in Fig. II-2. A major difference between models proposed in Fig. II-1 and Fig. II-2 is that the entrainment of vapor from surroundings is more vigorous when condensation is present. The proposed flow patterns are deduced from the experimental observations. Small secondary flow may be formed at the edge of the sheet which may enhance the breakup of the sheet. Experimentally it is found that for the same water flow rates, the length of the water sheet is shorter in condensing flows than in non-condensing flows. With these general concepts, an analytical model of the spray with condensation is proposed. The analytical model for spray flow pattern is assumed to be similar to that shown in Fig. II-3, where the two regions (sheet and droplets) will be treated separately.

2. Water Sheet Portion

We will discuss the condensation case and obtain computed values; the non-condensible case will be treated as a special solution. Along the sheet region, vapor condensation occurs on the inside surface of the sheet as well as the outside surface. The sheet itself acts as a vapor sink. The vapor interior to the sheet enters from a region downstream of the breakup zone. If a small segment of the sheet is isolated as in

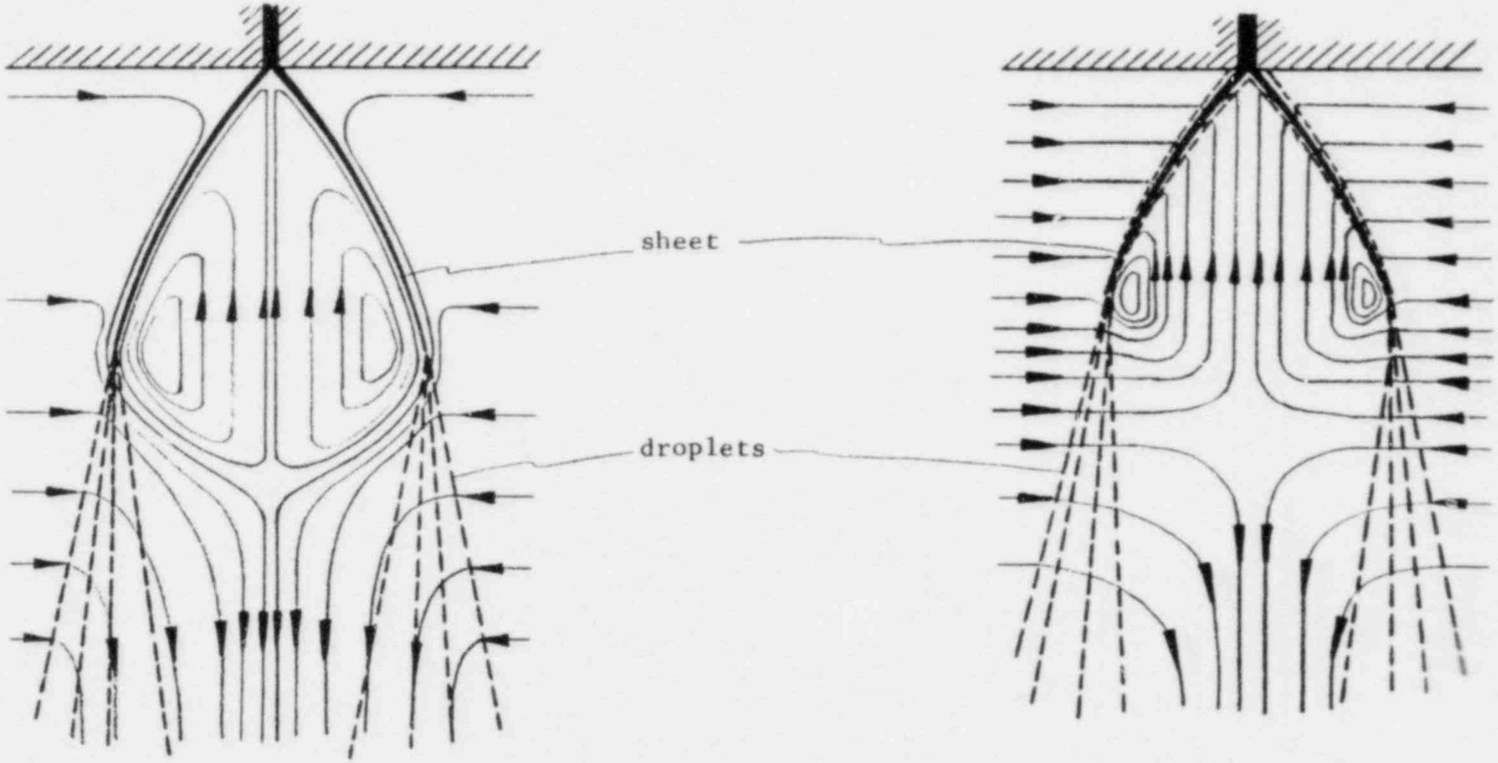

Fig. II-1 General flow pattern of spray in case of non-condensation

Fig. II-2 General flow pattern of spray in case of condensation

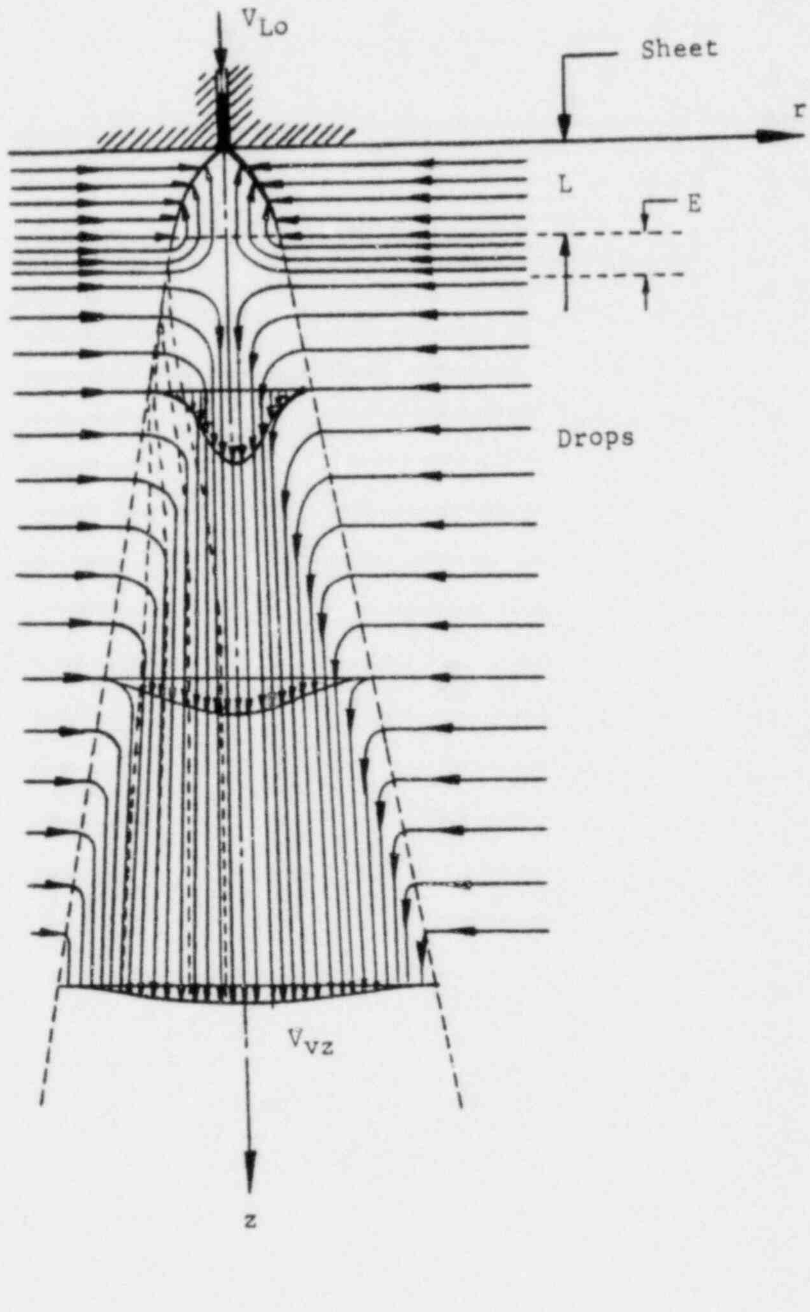

Fig. II-3 Model spray pattern

Fig. II-4, the governing equations can be established. The following assumptions are made:

(1) Condensation has a negligible effect on liquid sheet thickness (the mass flow rate of the condensate is very small compared to mass flow rate of water).

(2) Effect of the friction drag on the liquid sheet is neglected.

(3) Pressure and velocity of vapor inside the sheet (hollow portion) are uniform along the cross section (away from the sheet boundary).

(4) Gravity force neglected.

Then, (see Fig. II-4) the equation of motion in normal direction to the surface of the sheet will be [45]

$$\frac{2\sigma}{\zeta} + \frac{2\sigma}{r/\cos\eta} + \Delta p - \frac{V_{zo}^2 \rho_L d}{\zeta} - \frac{V_c^2 \rho_L d}{r/\cos\eta} = 0 \qquad (1)$$

where, ζ is the radius of curvature defined as:

$$\frac{1}{\zeta} = - \frac{d^2r/dz^2}{\left[1 + (dr/dz)^2\right]^{3/2}} \qquad (2)$$

The first two terms of Eq. (1) are the effects of the surface tension, and the third term is the pressure difference caused by condensation or internal circular motion of the air flow. These forces are balanced by the centrifugal forces (or inertia terms) which show up on the fourth and fifth terms of Eq. (1).

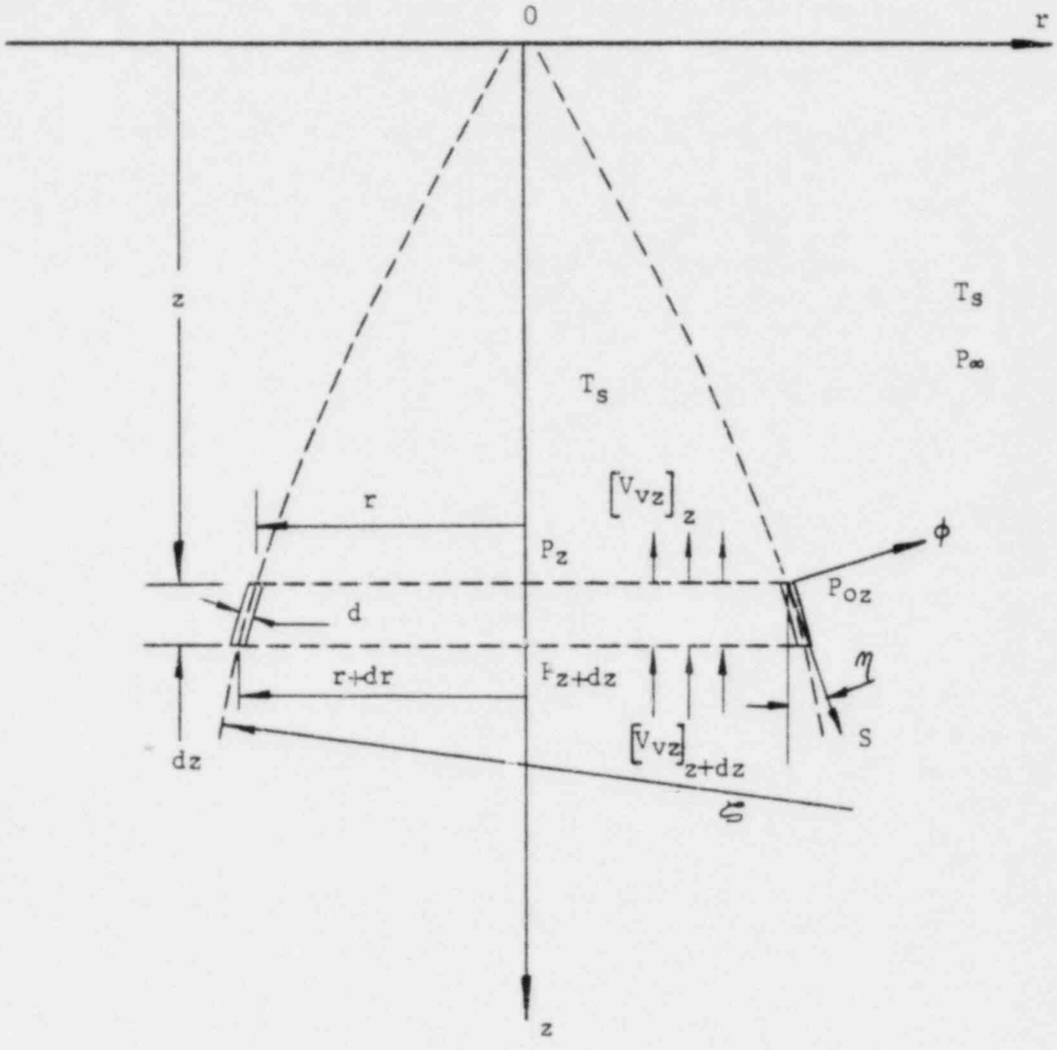

Fig.II-4 Calculation model of the water sheet portion

In case of no condensation, as explained previously, ΔP is negligibly small. However, in case of significant condensation, ΔP is not negligible.

With no frictional drag by the vapor,

$$V_{Lo} = \text{const} \tag{3}$$

and also

$$V_t \cdot r = \text{const} \tag{4}$$

and the thickness of spray sheet is

$$d = \frac{\dot{m}_{Lo}}{2\pi r \rho_L V_{Lo}} \tag{5}$$

In case of condensation, the heat transfer coefficient between the liquid and vapor is very high (about 100 Kw/m^2- C) [27,29]. Similar range of Nusselt numbers is obtained by Lim et al.[25] where the thickness of the water layer is large. Thus, it is assumed there is no heat transfer resistance on the vapor side of the interface. The removal of heat from the interface is assumed to be by means of conduction in the liquid sheet. Therefore, the heat balance equation is

$$V_{Lo} \frac{\partial T}{\partial S} = \alpha \frac{\partial^2 T}{\partial \phi^2} \tag{6}$$

with boundary conditions

$$\begin{aligned} T(S,0) &= T_s \\ T(S,d) &= T_s \\ T(0,\phi) &= T_{Lo} \end{aligned} \tag{7}$$

where, S denotes the direction of flow of liquid sheet and ϕ is taken normal to the flow direction (Fig. II-5). The derivation and solution of Eq. (6) are explained in Appendix 3.

If temperature distribution T is known at each segment, the enthalpy of each segment will be,

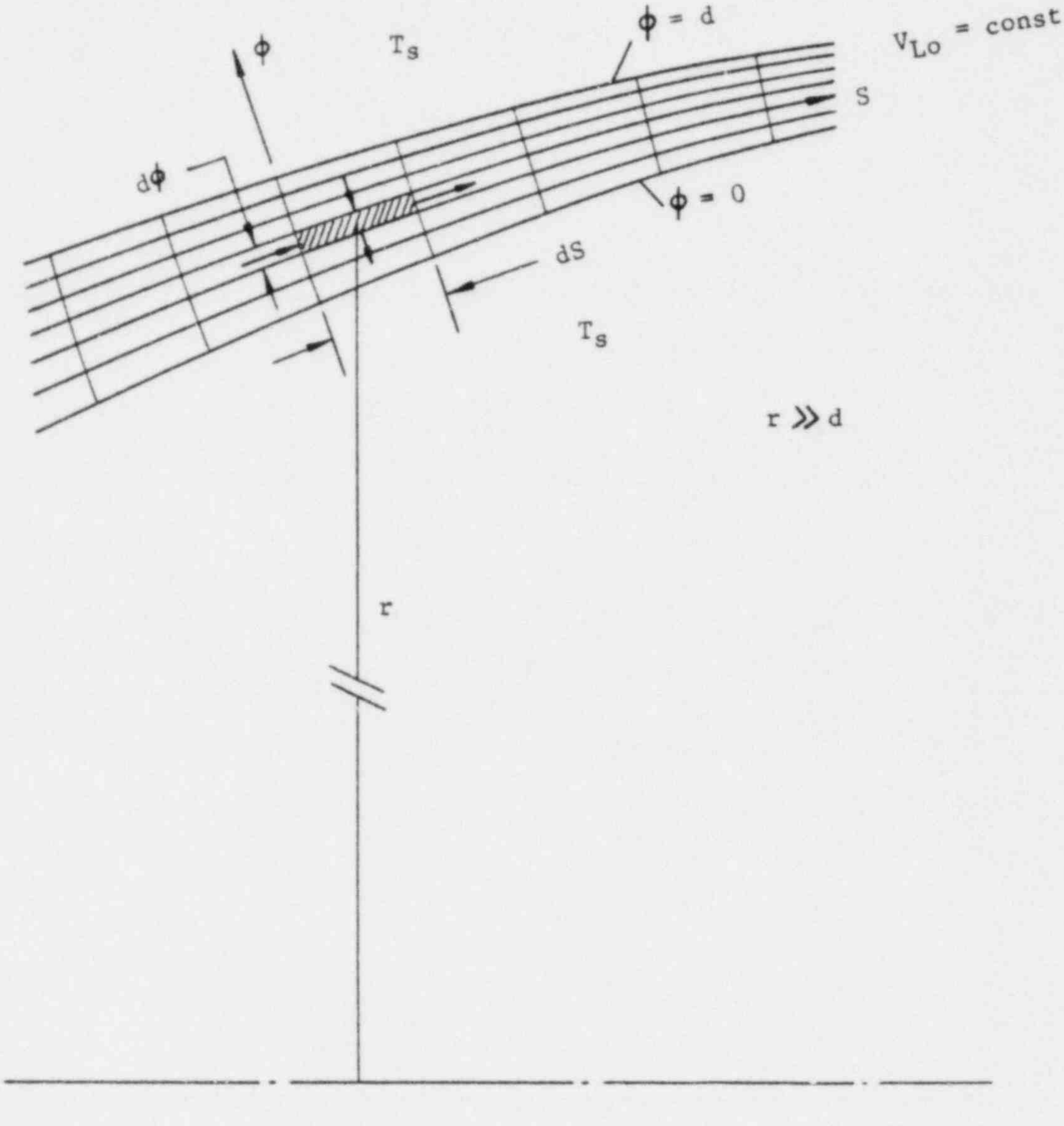

Fig.II-5 Heat balance of the liquid sheet

$$h_z = \int_o^d \left[C_p \, T\rho_L 2\pi r \sqrt{1 + (dr/dz)^2} dz \right] d\phi \tag{8}$$

and, the condensation rate for the segment dz can be obtained from the enthalpy change as follows:

$$\lambda \dot{m}_c = \frac{d}{dt} h_z \tag{9}$$

Half of the condensation occurs on inside and outside of the sheet respectively; thus,

$$\int_o^z \frac{1}{2} \frac{\dot{m}_c}{dz} \, dz = \rho_v V_{vz} \pi r^2 \text{ (inside)} \tag{10}$$

$$\frac{1}{2} \dot{m}_c = \rho_v 2\pi r \, V_{vr} dz \qquad \text{(outside)} \tag{11}$$

The vapor pressure at inside and outside surface of the sheet is,

$$P_z = P_\infty - \frac{1}{2} \rho_v V_{vz}^2 \text{(inside)} \tag{12}$$

$$P_{oz} = P_\infty \qquad \text{(outside)} \tag{13}$$

The vapor pressure outside the surface of spray sheet is same as the ambient pressure. Therefore, the static pressure difference between inside and outside of the sheet will be,

$$\Delta P = P_{oz} - P_z = \frac{1}{2} \rho_v V_{vz}^2 \tag{14}$$

The pressure drop due to flow of vapor past the droplets at the edge of the breakup zone is considered negligible. The relation between time and axial distance is

$$dz = V_{Lz} dt \tag{15}$$

From the equations presented, the radius of water sheet can be obtained numerically by proceeding step by step.

3. Droplet Portion

In the droplet portion of the spray, the liquid droplets are entrained by the surrounding vapor. Due to continuity, the vapor moves into the spray which drags the drops inwards; thus, decreasing the spray cone radius. In case of steam and a subcooled-water spray, the steam condenses on the cold liquid drops. This increases the momentum transfer. The behavior of droplets can be computed with the following assumptions:

(1) All the droplets are spherical shape.

(2) The droplets have a size distribution given by the Upper-limit function.

(3) The velocity and temperature of droplets at breaking point are assumed to be same as the sheet velocity and temperature obtained from the sheet portion.

(4) The pressure in this region is assumed to be uniform and equal to the ambient pressure.

(5) No influence between the droplets, i.e., no secondary breakup or coalesce.

(6) Gravity force is neglected.

The equation for the drop size distribution is [40]

$$y = \ln[\bar{a}\ D_i/(D_m - D_i)] \tag{16}$$

$$\frac{dv}{dD_i} = \frac{\delta}{\sqrt{\pi}} \frac{D_m}{D_i(D_m - D_i)} \exp(-\delta^2 y^2) \tag{17}$$

where, $\bar{a}$ and δ are distribution parameters which represent skewness and uniformity respectively, and D_m is the maximum droplet diameter. The number of drops produced per unit time with diameter between $D_i + 1/2dD_i$ and $D_i - 1/2dD_i$ is

$$dN_i = \frac{\dot{m}_{Lo}}{\rho_L} \frac{\delta}{\sqrt{\pi}} \frac{D_m}{D_i(D_m - D_i)} \frac{6}{\pi D_i^3} \exp(-\delta^2 y^2) dD_i \tag{18}$$

The effect of condensation on the droplet size is [35]

$$D = D_i \{1 + \Gamma[1 - \exp(-\pi^2 F_o)]^{1/2}\} \tag{19}$$

where,

$$\Gamma = [1 + C_p(T_s - T_i)/\lambda]^{1/3} - 1 \tag{20}$$

$$F_o = \frac{4\alpha t}{D_i^2} \tag{21}$$

Equations (19) - (21) are obtained by assuming zero surface resistance and neglecting internal motion within the droplet. Kashiwagi et al. [41], who studied the heat resistance at the surface shows insignificant surface resistance for steam-water. Ohba et al. [43] studied the heat transfer augmentation by internal circular motion of a droplet. However, the experimental results do not clearly substantiate their analytical model. Hence, the assumption of heat transfer by conduction appears to be reasonable.

3a. Motion of Each Single Droplet

The equation of motion for a single droplet is

$$\left(\frac{\pi}{6} D^3\rho_L\right) \frac{d\vec{V}_L}{dt} = - \left(\vec{V}_L - \vec{V}_v\right) \frac{d}{dt} \left(\frac{\pi}{6} D^3\rho_L\right) - \frac{1}{2} \rho_v C_D \left(\frac{\pi}{4} D^2\right) V_o \left(\vec{V}_L - \vec{V}_v\right) \tag{22}$$

where, $V_o = |\vec{V}_L - \vec{V}_v|$. The acceleration of a droplet on the left hand side of Eq. (22) is balanced by the effect of mass change of droplets (the first term on the right) and drag force term (the last term). Equation (22) can be written in its component directions as:

z-direction

$$\frac{dV_{Lz}}{dt} = - \frac{3}{D} \frac{dD}{dt} \left(V_{Lz} - V_{vz}\right) - \frac{3}{4} \frac{C_D}{D} \frac{\rho_v}{\rho_L} V_o \left(V_{Lz} - V_{vz}\right) \tag{23}$$

r-direction

$$\frac{dV_{Lr}}{dt} = - \frac{3}{D} \frac{dD}{dt} \left(V_{Lr} - V_{vr}\right) - \frac{3}{4} \frac{C_D}{D} \frac{\rho_v}{\rho_L} V_o \left(V_{Lr} - V_{vr}\right) \tag{24}$$

tangential direction

$$\frac{dV_t}{dt} = - \frac{3}{D} \frac{dD}{dt} V_t - \frac{3}{4} \frac{C_D}{D} \frac{\rho_v}{\rho_L} V_o V_t \tag{25}$$

where, the velocity V_o is defined as,

$$V_o = \left[(V_{Lz} - V_{vz})^2 + (V_{Lr} - V_{vr})^2 + V_t^2\right]^{1/2} \tag{26}$$

and C_D (drag coefficient) is chosen from Ref. [46] and the list of C_D as functions of Reynolds number is in Table II-1. Also Yuen et al. [47] studied the drag coefficient with the mass transfer taken into account.

3b. Momentum Balance of the Spray

The z-directional momentum of the spray should be balanced as follows:

$$\underbrace{\int_{D_i} \frac{\pi}{6} D^3 \rho_L \, dN_i V_{Lz}}_{\text{momentum of drops}} + \underbrace{\int_R \rho_v 2\pi r \, dr \, V_{vz}^2}_{\text{momentum of vapor}} = \text{const} \qquad (27)$$

3c. Velocity Profile of Vapor

If it is assumed that the sheet portion is relatively small, one would expect vapor profile to be similar to that of a free circular jet. Thus, the velocity profile of vapor is assumed to have a shape similar to that seen in Fig. II-6. A simple, approximate mathematical expression of such a profile is assumed

$$V_{vz} = C_1(z) \left(1 + \frac{r}{R}\right)^2 \left(1 - \frac{r}{R}\right)^2 \quad , \qquad (28)$$

and the radial velocity profile is assumed to be linear,

$$V_{vr} = - C_2(z) \frac{r}{R} \qquad (29)$$

Recommended Drag Correlations: Standard Drag Curve, $w = \log_{10} \mathrm{Re}$

Range		Correlation
(A)	$\mathrm{Re} < 0.01$	$C_D = 3/16 + 24/\mathrm{Re}$
(B)	$0.01 < \mathrm{Re} \leq 20$	$\log_{10}\left[\frac{C_D \mathrm{Re}}{24} - 1\right] = -0.881 + 0.82w - 0.05w^2$
		i.e., $C_D = \frac{24}{\mathrm{Re}}\left[1 + 0.1315\,\mathrm{Re}^{(0.82 - 0.05w)}\right]$
(C)	$20 \leq \mathrm{Re} \leq 260$	$\log_{10}\left[\frac{C_D \mathrm{Re}}{24} - 1\right] = -0.7133 + 0.6305w$
		i.e., $C_D = \frac{24}{\mathrm{Re}}\left[1 + 0.1935\,\mathrm{Re}^{0.6305}\right]$
(D)	$260 \leq \mathrm{Re} \leq 1500$	$\log_{10} C_D = 1.6435 - 1.1242w + 0.1558w^2$
(E)	$1.5 \times 10^3 \leq \mathrm{Re} \leq 1.2 \times 10^4$	$\log_{10} C_D = -2.4571 + 2.5558w - 0.9295w^2 + 0.1049w^3$
(F)	$1.2 \times 10^4 < \mathrm{Re} < 4.4 \times 10^4$	$\log_{10} C_D = -1.9181 + 0.6370w - 0.0636w^2$
(G)	$4.4 \times 10^4 < \mathrm{Re} \leq 3.38 \times 10^5$	$\log_{10} C_D = -4.3390 + 1.5809w - 0.1546w^2$
(H)	$3.38 \times 10^5 < \mathrm{Re} \leq 4 \times 10^5$	$C_D = 29.78 - 5.3w$
(I)	$4 \times 10^5 < \mathrm{Re} \leq 10^6$	$C_D = 0.1w - 0.49$
(J)	$10^6 < \mathrm{Re}$	$C_D = 0.19 - 8 \times 10^4/\mathrm{Re}$

[a] Sources of data: Achenbach (A3); Arnold (A7); Bailey and Hiatt (B1); Beard and Pruppacher (B5); Davies (D2); Dennis and Walker (D3); Goin and Lawrence (G9); Goldburg and Florsheim (G10); Gunn and Kinzer (G14); Hoerner (H14); Ihme *et al.* (I1); LeClair (L5); Liebster (L12); Masliyah (M2); Maxworthy (M7, M8); Millikan and Klein (M10); Möller (M11); Pettyjohn and Christiansen (P4); Pruppacher and Steinberger (P8); Rafique (R1); Rimon and Cheng (R8); Roos and Willmarth (R10); Schmiedel (S2); Shakespear (S9); Vlajinac and Covert (V3); Wieselsberger (W4); Woo (W9).

[b] Number of data points: C—149; D—74; E—61; F—52; G—142.

Table II-1 Drag coefficient on liquid droplets as function of Reynolds number [46]

where,

$C_1(z)$ = center-line velocity of vapor

$C_2(z)$ = radial velocity of vapor at spray boundary

R = radius of spray outline.

Other power relations were tried for the vapor velocity profile (Eq. (28) and (29)) and they had little effect on the results. These will be discussed later.

Large radial velocity of vapor is expected at the beginning of the drop portion, designated by E in Fig. II-3, because most of the vapor for condensation at inner side of water sheet will flow through this region. For computation, the length of E was assumed to be the same as water sheet length L. Various lengths of E were tried and they had little effect on the results (this implies the droplet portion is not important for determination of spray outline shape).

The mass flux of the liquid and vapor should be balanced as follows (Fig. II-6):

$$[\dot{m}_v + \dot{m}_L]_z + [\dot{m}_e]_z = [\dot{m}_v + \dot{m}_L]_{z+dz}$$

$$\begin{aligned}[\dot{m}_e]_z &= [\dot{m}_v]_{z+dz} - [\dot{m}_v]_z + [\dot{m}_L]_{z+dz} - [\dot{m}_L]_z \\ &= [\dot{m}_v]_{z+dz} - [\dot{m}_v]_z + [\text{Condensate rate}]_z^{z+dz}\end{aligned}$$

That is,

$$2\pi R\, dz\, V_{vr}\rho_v = \int_0^{R+dR} 2\pi r\, dr\, \rho_v [V_{vz}]_{z+dz} - \int_0^R 2\pi r\, dr\, \rho_v [V_{vz}]_z + \frac{\pi}{6}\rho_L \int_{D_i} (D^3_{z+dz} - D^3_z)\, dN_i \qquad (30)$$

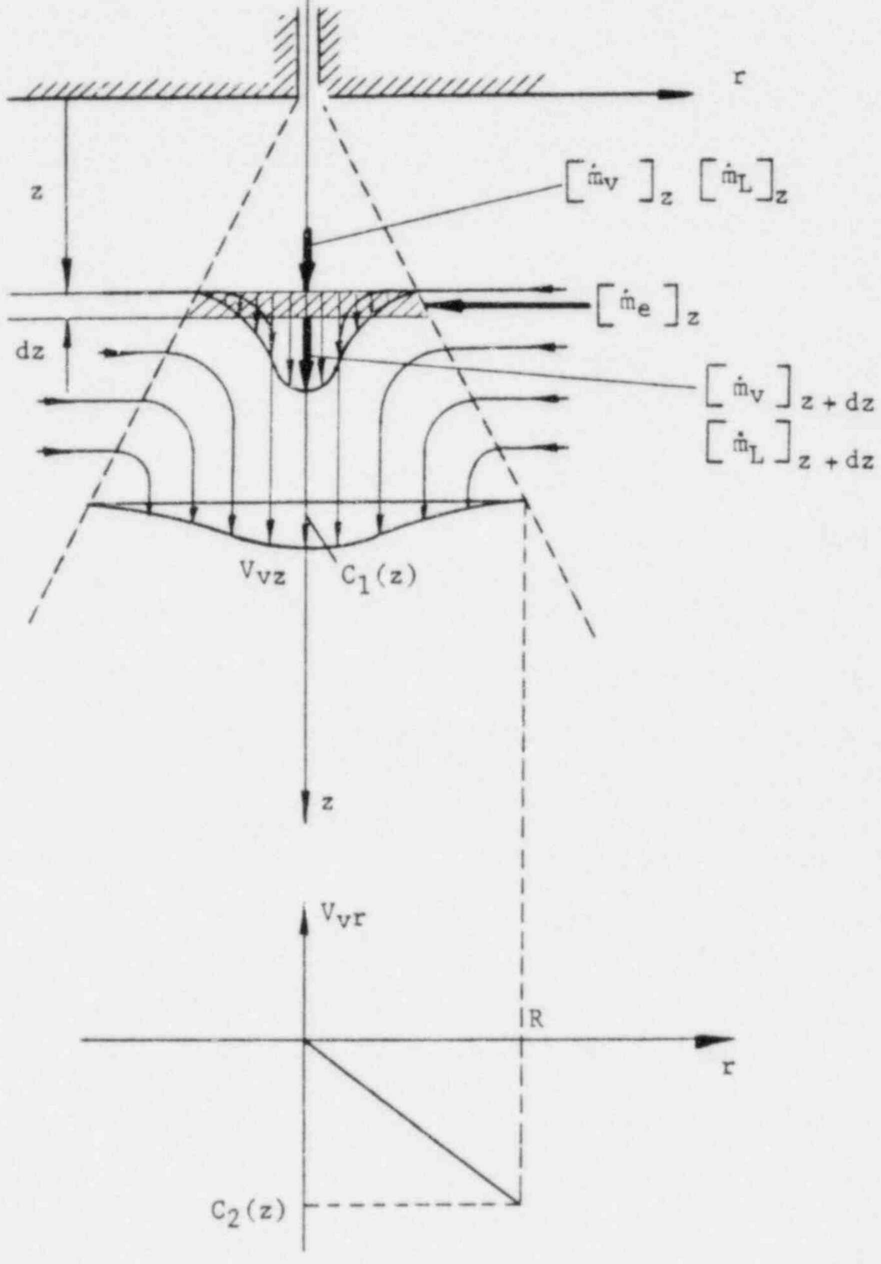

Fig.II-6 Vapor velocity profile model at droplet portion

The velocities of droplets can be obtained as;

$$[V_{Lz}]_{z+dz} = [V_{Lz}]_z + [\frac{dV_{Lz}}{dt}]_z \, [dt]_z \qquad (31)$$

$$[V_{Lr}]_{z+dz} = [V_{Lr}]_z + [\frac{dV_{Lr}}{dt}]_z \, [dt]_z \qquad (32)$$

$$[V_t]_{z+dz} = [V_t]_z + [\frac{dV_t}{dt}]_z \, [dt]_z \qquad (33)$$

and the radial positions of the droplets will be (Fig. II-7)

$$[R_r']_{z+dz} = [R_r']_z + [V_{Lr}]_z \, [dt]_z \qquad (34)$$

$$[R_t]_{z+dz} = [R_t]_z + [V_t]_z \, [dt]_z \qquad (35)$$

$$[R]_{z+dz} = \left([R_r']^2_{z+dz} + [R_t]^2_{z+dz}\right)^{1/2} \qquad (36)$$

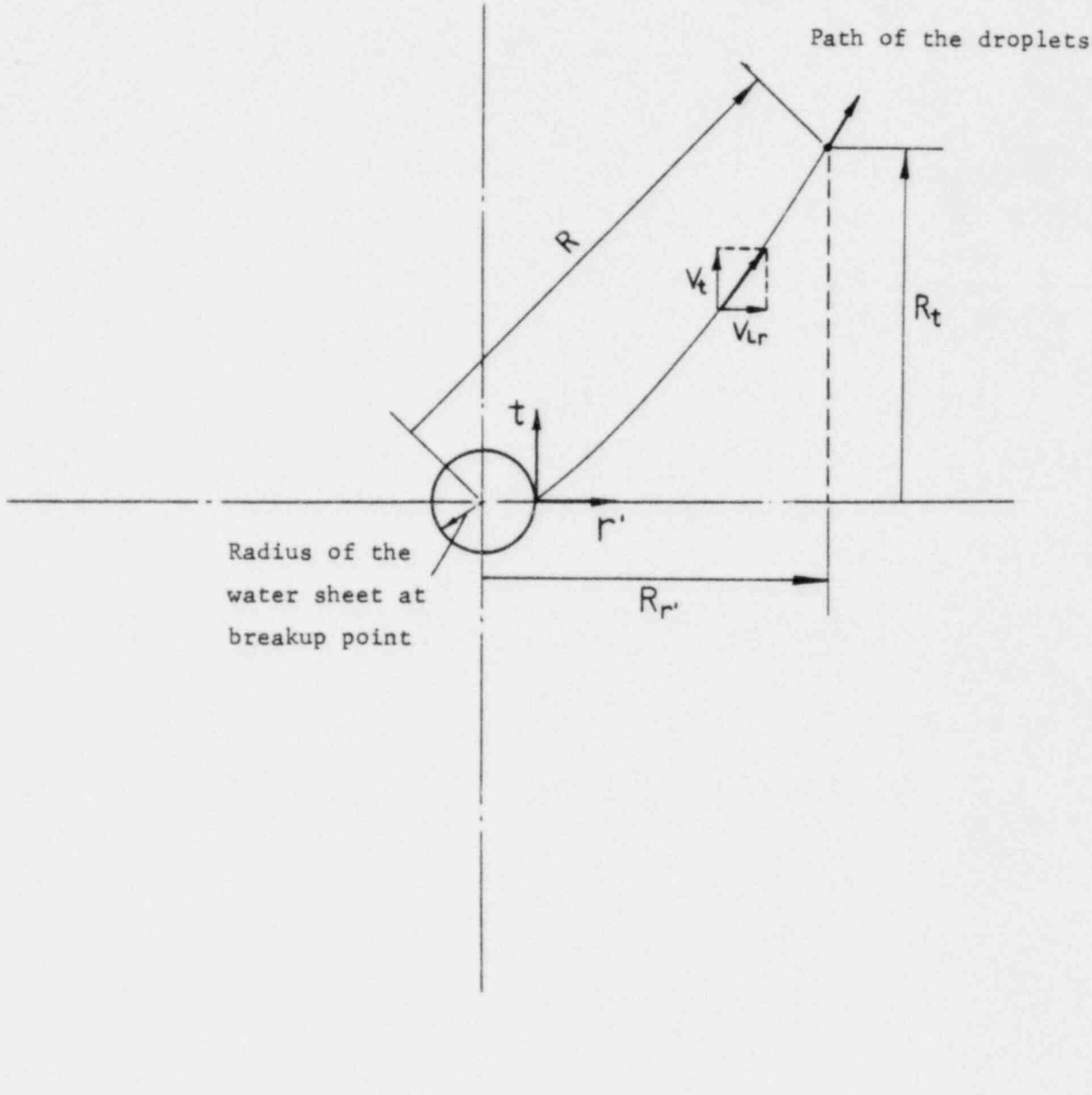

Fig.II-7 Radial position of droplets

III. EXPERIMENTS

1. Test Section and Experimental Apparatus

Fig. III-1 and Fig. III-2 show the schematic diagram of experimental apparatus. Water is boiled with an electric heater located in the bottom of the test chamber. Thus the saturated steam is generated inside the test chamber which is maintained at a desired pressure by relief valve. Subcooled water spray is injected through the nozzle at pre-selected flow rate and temperature. The experiments were conducted with various spray water flow rates, temperatures and pressures (mostly saturated steam or air at 1 atm.). Some of the higher pressure (3 atm.) experiments were conducted to determine the drop size distribution at higher pressure.

The test section, which is made of brass, is 25 cm in diameter, 30 cm high, and contains windows (50 mm diameter) made of 25 mm thick pyrex glass for taking holograms and photographs. Spray water flow rate is measured with calibrated rotameter (Fisher and Porter) and the pressure inside the test section and the nozzle are measured by calibrated burdon type pressure gage. Fig. III-3 shows the calibration curve for the rotameter obtained by measuring the amount of water flow over a fixed time duration. Fig. III-4 shows the calibration curve for the pressure gauge. Calibration was made with a dead-weight-gage calibrater. The pressure gage to be calibrated is connected to a chamber filled with fluid whose pressure can be adjusted by means of some type of pump and bleed valve. The chamber is also connected to a vertical piston-cylinder to which various standard weights may be applied. The pressure is slowly increased until the piston and weights are seen to "float," at

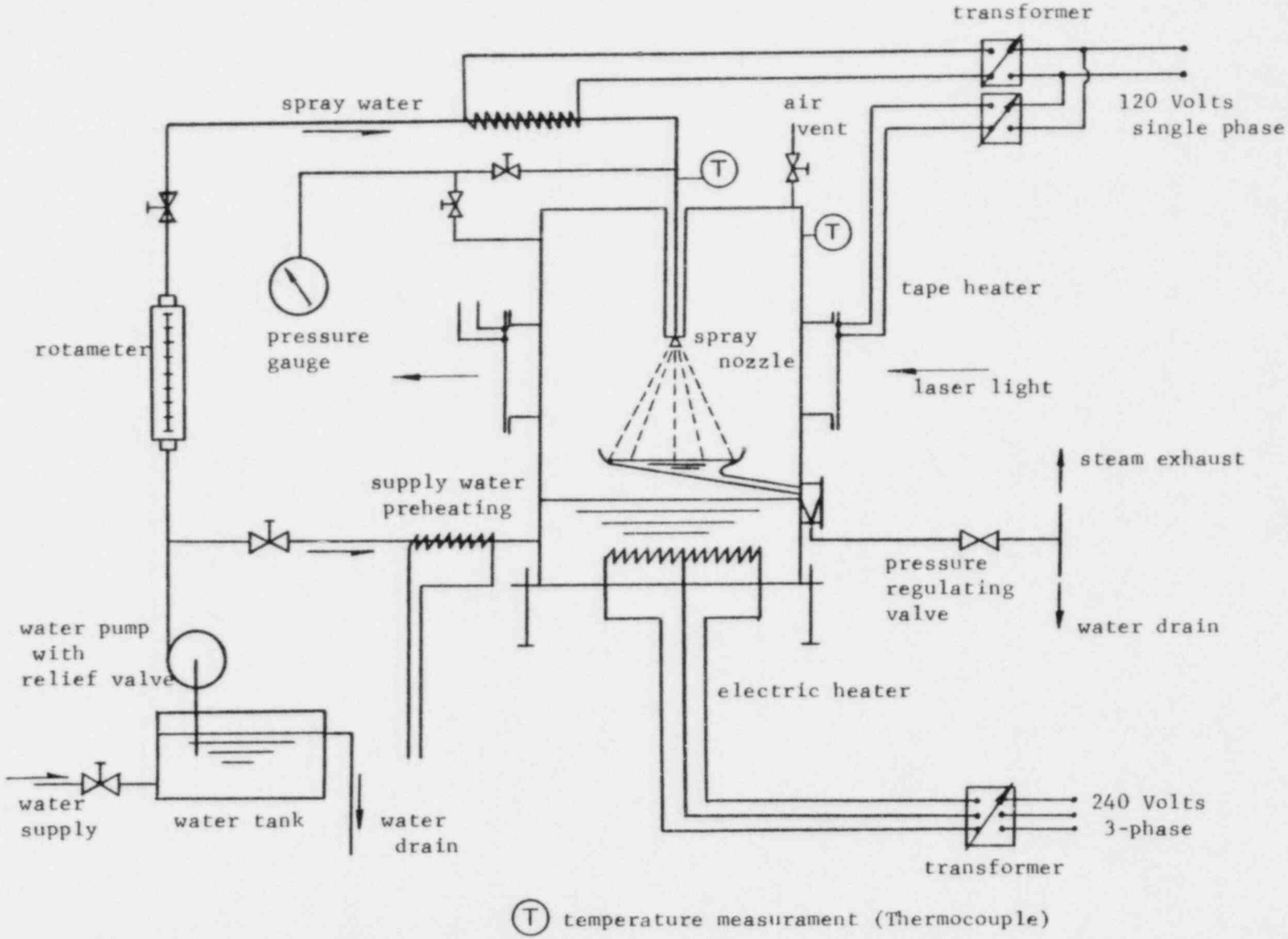

Fig.III-1 Schematic diagram of the experimental system

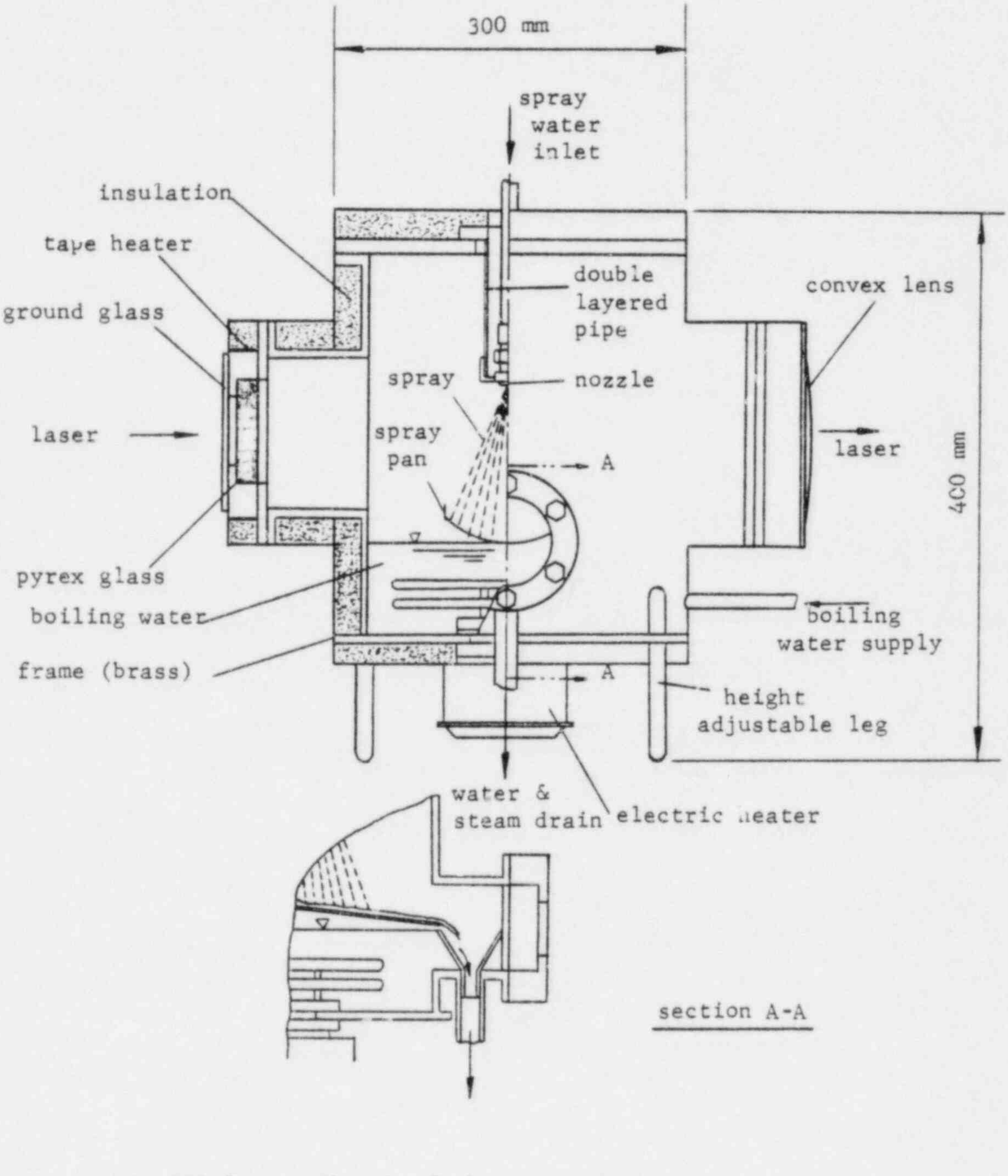

Fig.III-2 Sketch of the test section

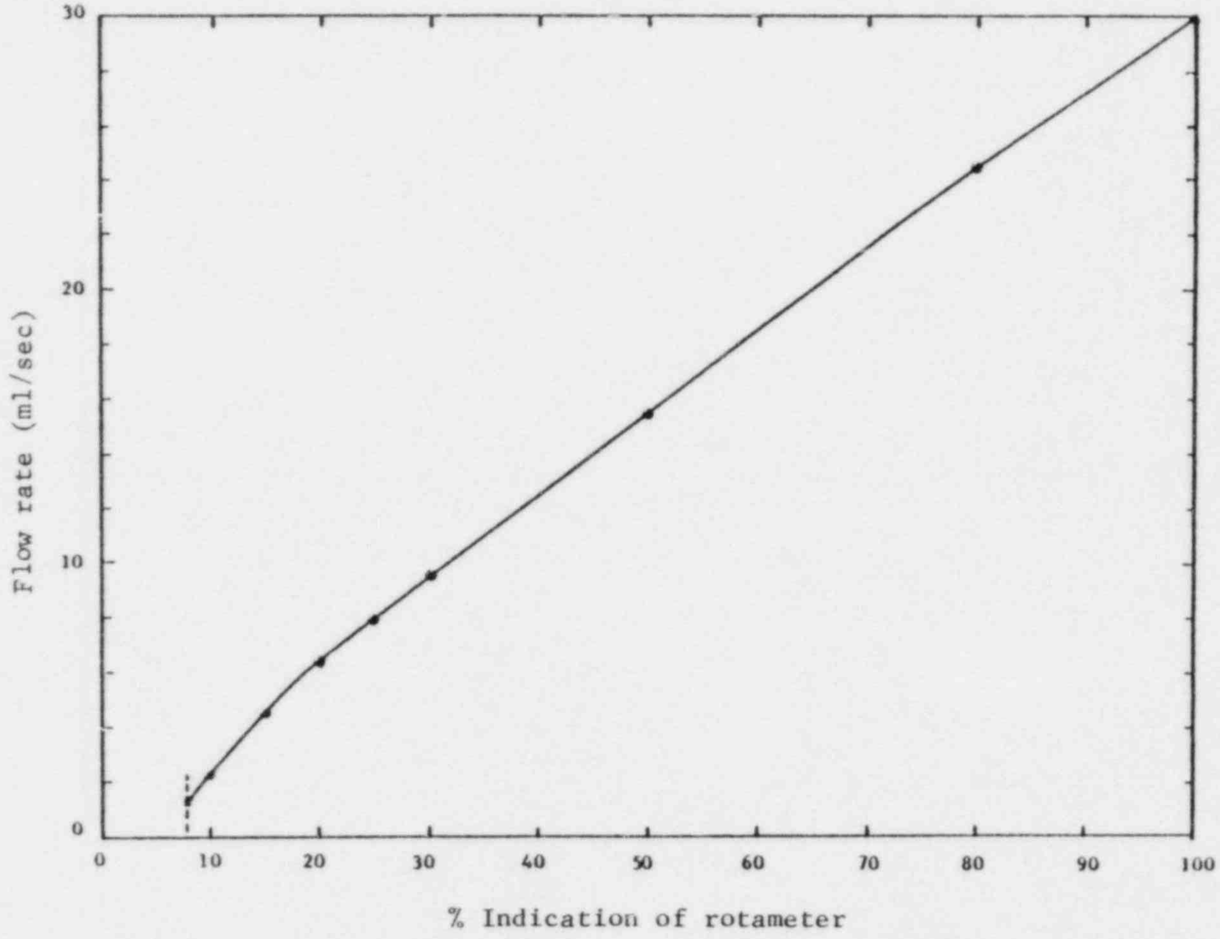

Fig.III-3 Calibration curve for rotameter which point the fluid "gage" pressure must equal the dead weight supported by the piston, divided by the piston area. For temperature measurements, calibrated chromel-alumel thermocouples are used. Three of the nozzles used were manufactured by Spraying Systems Company (#1/4TTG0.3, #1/4TTG0.4 and #1/4TTG0.7) and their specifications are listed in Table III-1. These nozzles have two (or four) slots inside the nozzle chamber and produce the swirl motion. The other two nozzles used were poppet type which were designed and constructed in our machine shop (see Fig. III-5,6).

A gear type water pump is used to supply water for the spray. Tap water is used for the experiments. To reduce heat transfer from the steam to the inlet water, a double pipe is used to connect the water supply line to the nozzle inside the test chamber. In order to eliminate the condensate on the window, electrical tape heaters are used for heating the pyrex windows. A spray pan is installed inside the test chamber in order to deflect the spray water directly from the test chamber without mixing with the boiling water. Before holograms (or photographs) are taken, the water inside the test chamber is boiled for at least an hour exhausting steam to the atmosphere - thus eliminating air from the test chamber. The water spray is turned on when steady state conditions have been achieved, the laser and ELN-1 are turned on to take holograms (or photographs).

Holographic plates are developed in KODAK D-19 developer (5-6 min.) and put into stop bath (30 sec.) and then put into the rapid fixer (2-4 min.). Once the holograms were obtained, photographs of the 3-dimensional image in the holograms were taken with a 35 mm camera. A He-Ne Laser is

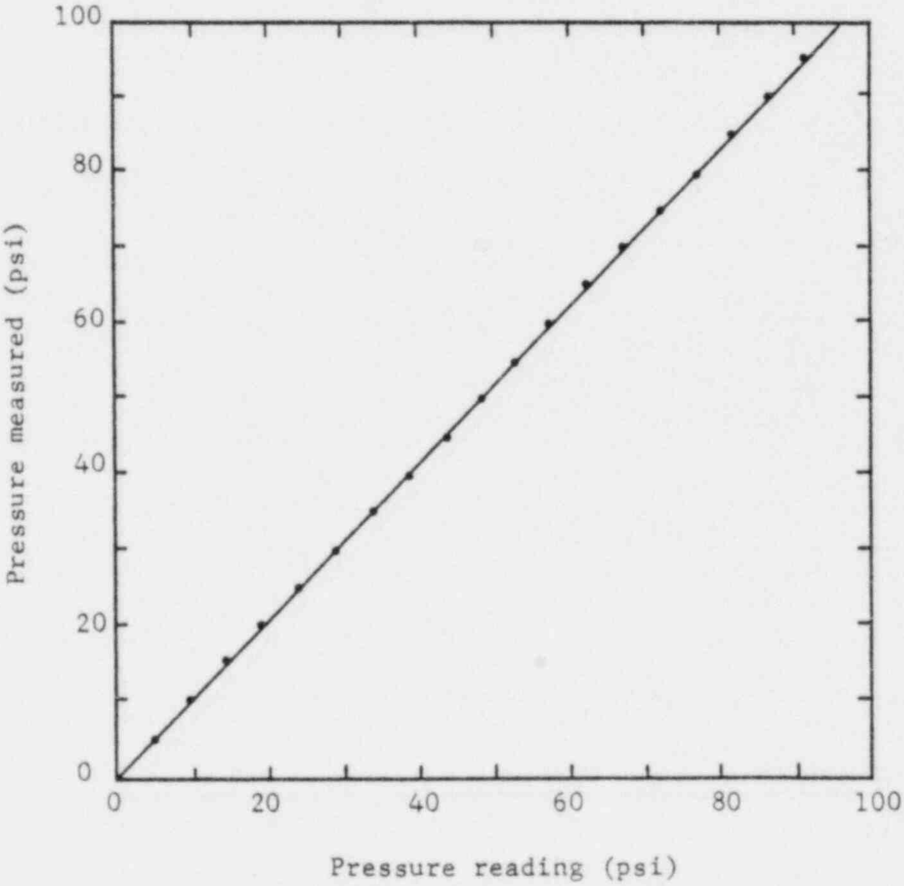

Fig.III-4 Calibration curve for pressure gauge

Nozzle #	Type	Specifications
1	Spraying Systems, Type TG Full Cone Spray Nozzle, ¼TTG0.3	D_n(Orifice diameter) = 0.02" (= 0.508 mm) with two slots for swirling inside the nozzle
2	Spraying Systems, Type TG Full Cone Spray Nozzle, ¼TTG0.4	D_n(Orifice diameter) = 0.023"* (= 0.584 mm) with two slots for swirling inside the nozzle
3	Poppet type nozzle	Equivalent hydraulic diameter of orifice = 0.406 mm Flow area = 0.858 mm^2 (See Fig.III-5)
4	Poppet type nozzle	Equivalent hydraulic diameter of orifice = 0.445 mm Flow area = 0.439 mm^2 (See Fig.III-6)
5	Spraying Systems, Type TG Full Cone Spray Nozzle, ¼TTG0.7	D_n(Orifice diameter) = 0.03" (= 0.762 mm) with four slots for swirling inside the nozzle

* Original specification in catalogue shows 0.022". However, the measured size is 0.023" (measured with Electric Comparator)

Table III-1 Specifications of the nozzles used in experiments

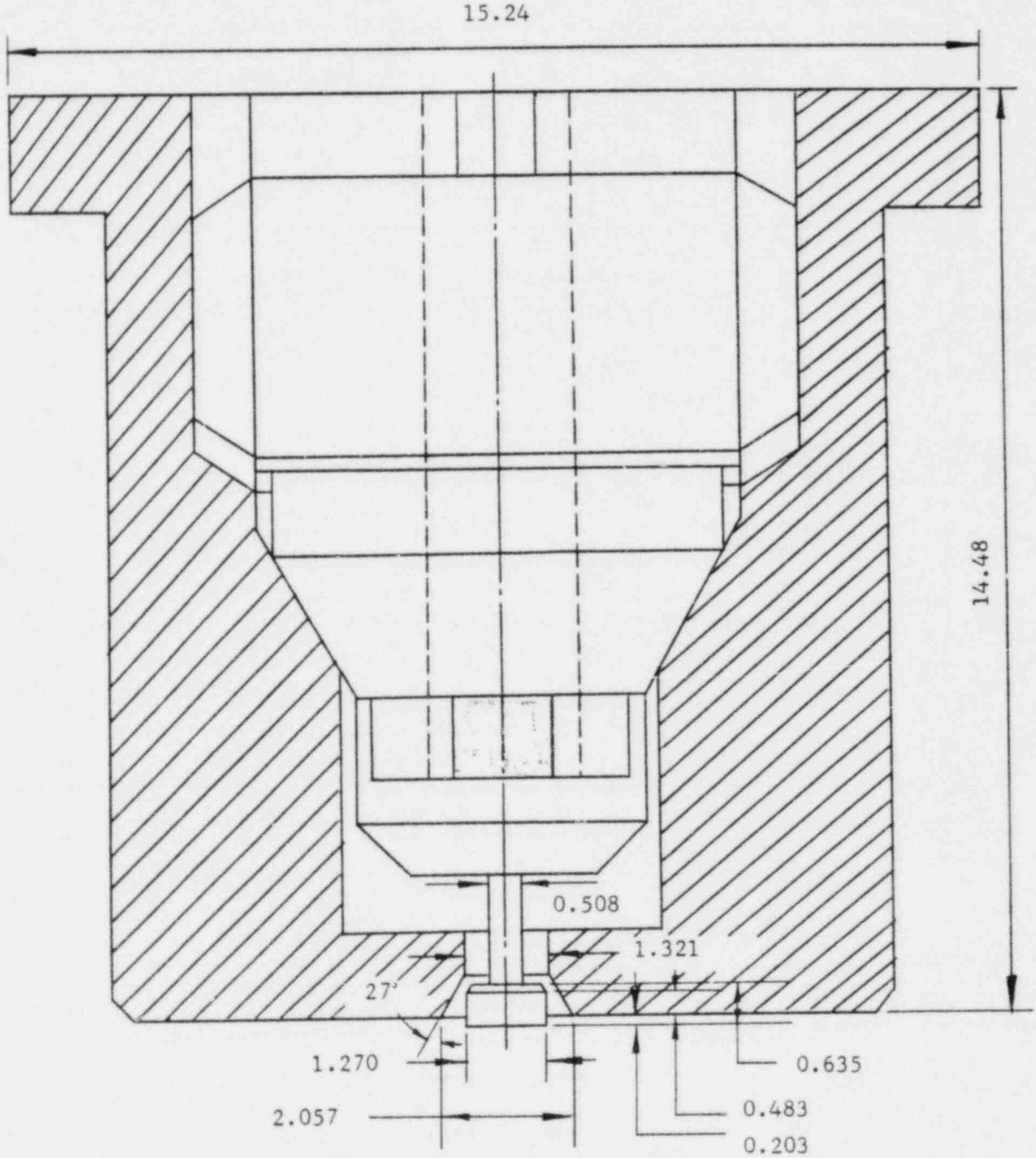

unit: mm

Fig.III-5 Poppet type nozzle for experiments (nozzle #3)

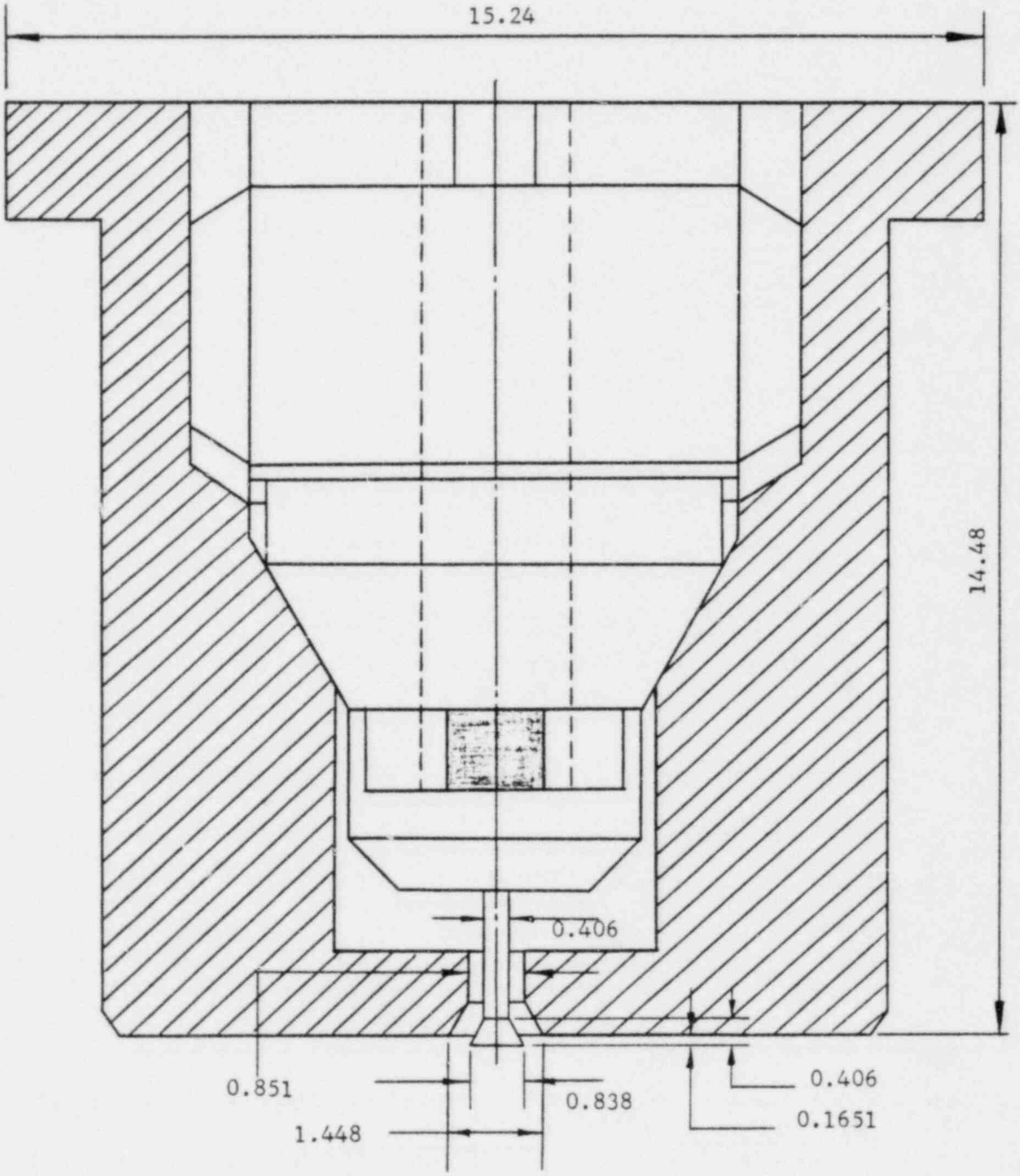

unit: mm

Fig.III-6 Poppet type nozzle for experiments (nozzle #4) used in the reconstruction. KODAK Tri-X Pan ASA 400 film, used for taking two dimensional pictures, is developed with Microdol developer (10 min.) and then fixed with Rapid Fixer (2-4 min.). For data taking, enlarged positive prints were made using standard photographic paper. Also, 2-dimensional pictures of the spray were taken by back lighting with the Nd:YAG pulsed Laser. Thus, the laser was used as a light source and shutter. These photographs are then analyzed to determine droplet size distributions, cone angle, breakup point, spray radius, etc. The details of the holographic method is explained in the next section.

2. Holographic Method

As explained above, holograms of the water spray were taken to determine the drop size distribution. If a coherent reference wave of light is combined with light scattered from an object of interest, it will result in an interference pattern that would be a function of the phase and amplitude of the light scattered from the object. If this interference pattern is recorded on film, which is called hologram, then a 3-dimensional image of the object can be reconstructed using the hologram and coherent light source. This imaging technique is known as holography. The basic theory and application of the holography can be found in many recent text books dealing with lasers and optics. The main advantage of the holographic method is that it contains information concerning the shape, size and position of the droplets 3-dimensionally without disturbing the spray. In this case of counting droplets, the holographic method requires a great deal of tedious data handeling.

That is, to obtain the size and position of the droplets in the spray requires making measurements and counts from the many photographs, which is laborious work. There are techniques for electronically counting and measuring the droplets, but these devices are generally quite expensive. Lekic [37,38] used a device called Quantimat for counting droplets. However, there is some uncertainty in applying this counting equipment to holography because normal photographs which are taken from 3-dimensional hologram show the unfocused droplets as well as focused droplets. It is difficult to judge one from another by the Quantimat system. We have a T.V. camera and CRT screen which is used to examine the enlarged images of the spray. In the present experiments, the size and position of the droplets were measured manually from photographs. Though it is time consuming to analyze holograms in this manner, it is accurate. Later, if electronic measurments are made, those can be checked against our manual measurements. In Fig. III-7 the holographic configuration is shown. This holographic configuration was originally set up by Stachniak [48], but was modified; thus improving the holograms. A Q-switched Nd:YAG pulsed laser is used as a coherent light source and off-axis holographic configuration is chosen because it allows us to operate at higher density flows. The Nd:YAG laser is capable of supplying pulsed light (0.532 micron and 1.064 micron) with a pulse repetition rate between 2 to 22 Hz. The average pulse time duration is approximately 6 nano-seconds with a peak power per pulse of 9 MW (0.532 micron) and 22 MW (1.064 micron). Coherence length of the light is less than 10 cm but using an Electronic Line-width Narrower (ELN-1) accessory, the coherence length can be extended to about 3 meters. The

Nd:YAG laser beam strikes a prism that separates the 0.532 micron (green) and 1.064 micron (infra-red) light and directs both beams across the room. The 1.064 micron infra-red light is collected in a light trap while the 0.532 micron green light is reflected across the room to the iris stop, where the laser beam is about 30 mm in diameter. The original diameter of the beam emitted by the laser is approximately 6.5 mm. This iris stop is used to select the uniform portion of the laser light. The portion of the laser beam that is allowed to pass is then expanded by plano-concave lens and an off-axis paraboloid mirror. The lens and mirror are separated by a distance equal to the difference of their focal lengths. The light reflected by the off-axis mirror is a parallel light which is directed to 1:1 beam splitter, where the laser beam is divided into a reference beam and an object beam. The reference beam is directed to the holographic plate by two folding mirrors, and the object beam is reflected by a folding mirror through the test section. Before the object beam strikes the test section, it passes through a ground glass diffuser, which provides uniform illumination of the object field. An image of the illuminated object field is formed near the holographic film by a pair of plano-convex lenses. The distance between the image (or object when no lenses are present) and the recording plane affects the quality of the hologram. By placing the two imaging lenses so that they are separated by a distance equal to the sum of their focal lengths, the magnification factor is constant over the field of view. The focal lengths of the lenses in our case are 212 mm and 483 mm. The size of the image becomes larger proportional to the ratio of focal lengths and depth of field becomes larger proportional to

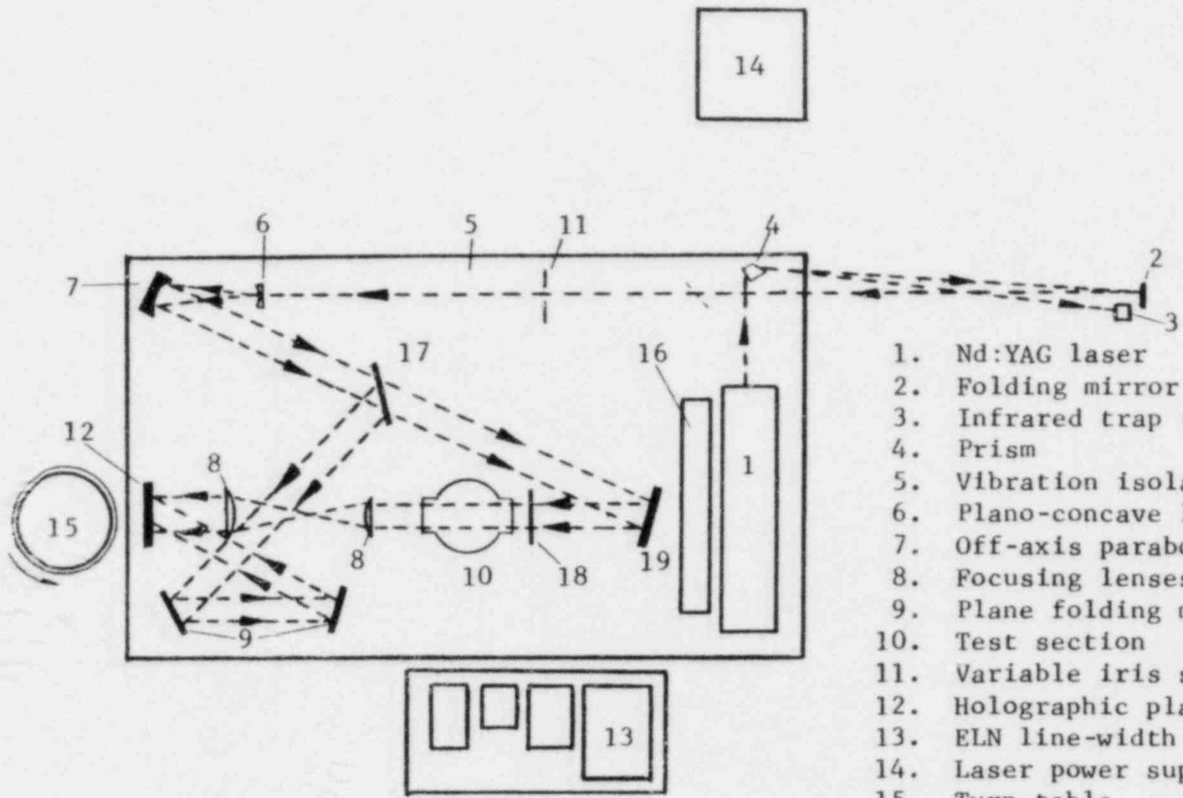

1. Nd:YAG laser
2. Folding mirror
3. Infrared trap (1.06μ)
4. Prism
5. Vibration isolated table
6. Plano-concave lense
7. Off-axis paraboloid mirror
8. Focusing lenses
9. Plane folding mirrors
10. Test section
11. Variable iris stop
12. Holographic plate
13. ELN line-width narrower
14. Laser power supply
15. Turn table
16. He-Ne laser (for reconstruction)
17. Beam splitter
18. Ground glass diffuser
19. Plane mirror (for objective beam)

Fig.III-7 Schematic diagram of off-axis holographic set-up the square of the ratio of focal lengths as shown in Fig. III-8. The angle between the object and the reference beam is approximately 25 degrees. The film used to record the hologram is AGFA-Gevaert 10E56-AH (4" x 5") glass plates with a film resolution of 2800 lines/mm (Table III-2) [49]. However, because of the laser speckle, the resolution ability of this holographic method is about 50 microns. Droplets smaller than the 50 microns are not practically measurable. For reconstruction, the He-Ne 15 mW laser (Spectra Physics) is used with the configuration shown in Fig. III-9. The He-Ne laser beam is routed across the table by plane folding mirror. The plano-concave lens used in taking the hologram is removed and the beam is expanded by a double-convex lens - pin hole assembly and off axis paraboloid mirror. The double-convex lens and the paraboloid mirror are separated by a distance equal to the sum of the two focal lengths to obtain a parallel beam of light. The reference beam reflects off of beam splitter and two plane folding mirrors to the holographic plate. These were the same mirrors that were used during construction. Thus the beam of light during reconstruction traces the same path as during construction. The object beam is shielded because it is not used for reconstruction. The difference in dimensions which occur because of the different wavelength between the construction wave and the reconstruction wave was checked by taking the hologram of two objects of known sizes and distances between them. The 35 mm camera and the traveling carriage was placed behind the reconstructed hologram and the camera was traversed until a few water droplets closest to the camera appeared to be in focus. With that position as the starting point, photographs were taken by traversing the

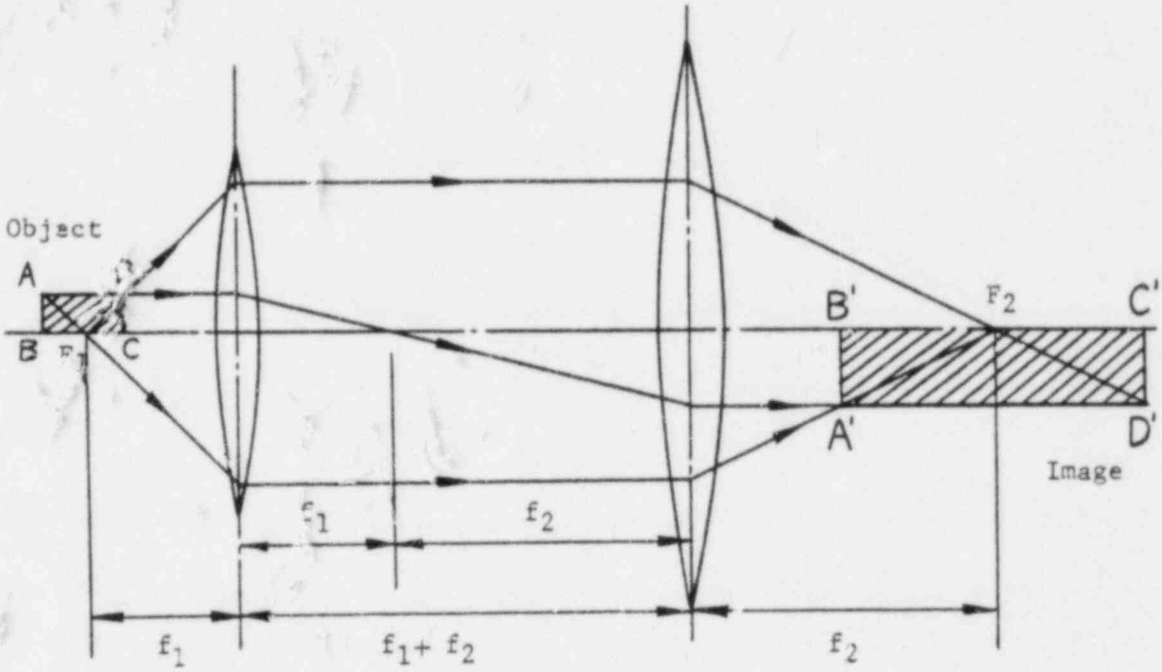

$$A'B' = \left(\frac{f_2}{f_1}\right) AB$$

$$A'D' = \left(\frac{f_2}{f_1}\right)^2 AD$$

Fig.III-8 Imaging lens systems

Material	Resolution lines/mm	Exposure for density of one erg/cm^2	Comments P=Panchromatic O=Orthochromatic
KODAK			
649F	2000	1000	P
649G,6490	2000	1000	O
S0243	500	5	P
High Contra-st Copy	200	0.5	P
HRP	2000	1000	O
Tri-X Pan	150	0.1	P
AGFA-Gevaert			
8E70	3000	200	Peaked for He-Ne
10E70	1500	50	and Ruby lasers
AGE PEFF	280	2.5	O
AGEPAN	220	1	P
10E56	2800	50	Peaked for Argon lasers
39C56	165	3	O

Table III-2 Properties of the most common photographic emulsions[49]

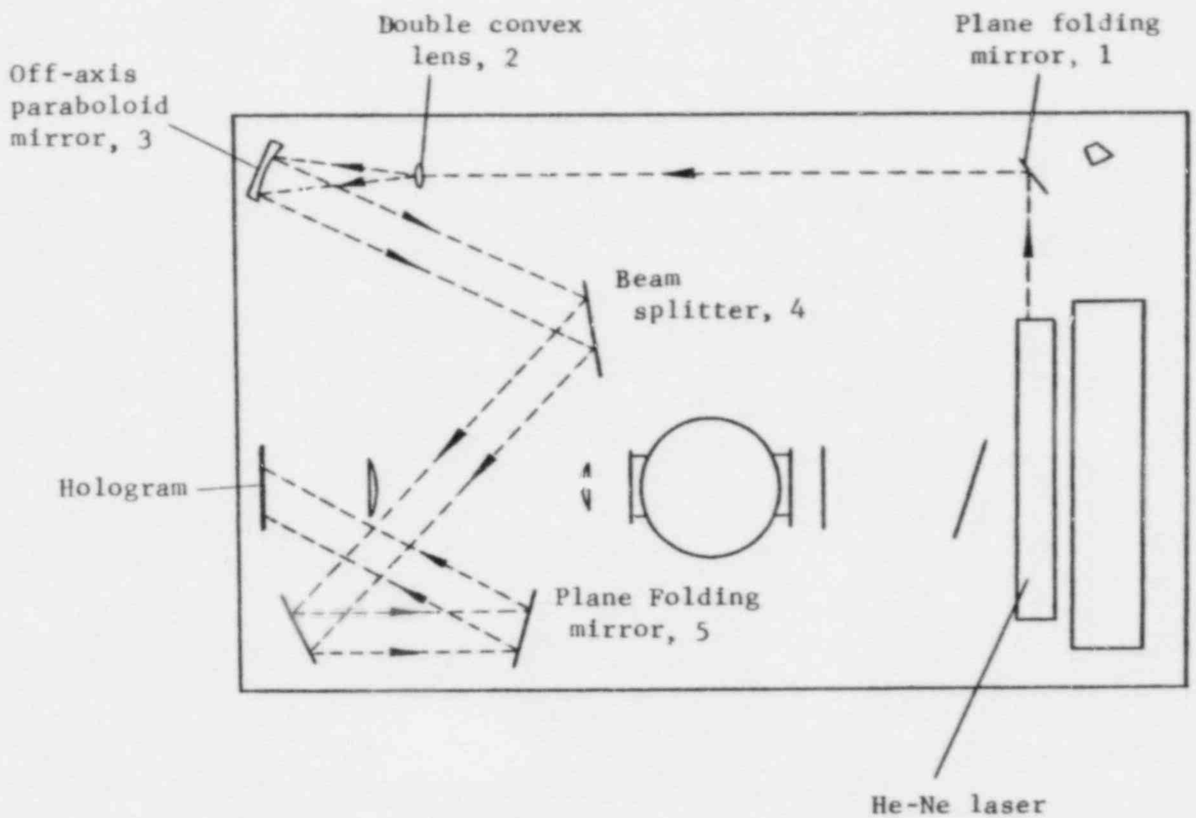

Fig.III-9 Schematic diagram of hologram reconstruction camera in 10 mm increments and taking pictures. The incremental distance in the real image is 2.7 mm. The focus and all other camera settings were never changed while photographs were being taken. Thus the processed photographs have information on the location (x,y,z) and sizes of droplets. Extracting this information for analysis is a rather tedious process.

IV. RESULTS AND DISCUSSION

1. Droplet Portion

Experiments were conducted for the test conditions listed in Table IV-1 using nozzle #1. In the region z = 10-25 mm (axial distance from the nozzle), the diameters and positions of the droplets are measured and recorded. Figure IV-1 shows a typical photograph of the droplets taken from a hologram. The diameters are grouped in 50 micron increments and counted. In determining the volume of droplets, non-spherical droplets are handled as ellipsoids or cylinders. For the test conditions #1-#7, the droplet sizes range from 50 to 750 microns. The droplet data can be expressed with one of the usual distribution equations. It is known that the spray droplets have a random distribution, and the Upper-limit equation is the best-fit curve [36,40]. The Upper-limit equation is the modified form of the Log-probability equation. The mathematical expressions are:

$$\frac{dv}{dD} = \frac{\delta}{\sqrt{\pi}} \frac{D_m}{D(D_m - D)} \exp(-\delta^2 y^2) \quad (37)$$

$$y = \ln[\bar{a}\, D/(D_m - D)] \quad (38)$$

where, a and δ are the distribution parameters which represents skewness and uniformity respectively, and D_m is the maximum droplet diameter. To determine these parameters, the least square method was used to fit the experimental data. This provides the best fit to the data points, and the parameters obtained for each test conditions are listed in Table IV-2. Figure IV-2 - Fig. IV-8 show the droplet size distributions for test

Condition	#1	#2	#3	#4	#5	#6	#7
Environment	Air 1 atm		Saturated Steam 1 atm			Air 3 atm	Saturated Steam 3 atm
Spray water flow rate (ml/sec)	3.52	2.23	2.23	3.52	3.52	3.52	3.52
Spray water temperature (°C)	13.0	13.1	24.5	24.5	61.1	15.0	24.5
Saturation temperature (°C)	-	-	100	100	100	-	134.0

Table IV-1 Test conditions for measuring the drop size distribution (Nozzle #1)

Condition	#1	#2	#3	#4	#5	#6	#7
$\bar{a}$	2.79	1.97	2.44	1.79	1.77	2.03	2.32
δ	1.40	1.17	1.19	1.07	1.33	1.22	1.16
D_m (microns)	972.3	936.0	1320.0	908.8	676.0	688.5	966.5

Table IV-2 Parameters of drop size distribution functions of each test conditions (Nozzle #1)

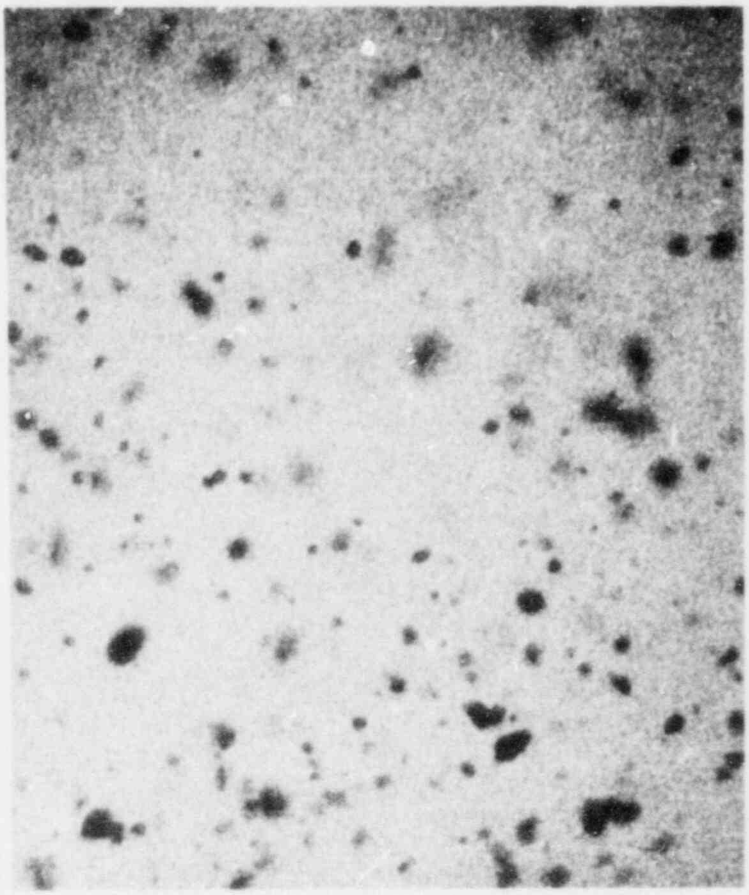

⟶| |⟵ 1 mm

Fig.IV-1 Typical photograph of the spray droplets conditions #1-#7. In Fig. IV-2, the number distribution is shown (Fig. IV-2(a)) as well as the volume distribution (Fig. IV-2(b)). The volume distribution is skewed to the right compared to the number distribution because it is weighted in proportion to D^3. Figure IV-9 shows the effect of flow rate, ambient pressure, subcooling temperature and comparison between air and steam environment. Droplet sizes become more uniform and smaller when ambient pressure and/or injection pressure increases. Also, the average drop sizes are larger in a steam environment than in an air environment (Fig. IV-9(a,b,g)). This seems to be due to the earlier breakup of water sheet in a steam environment. The effects of ambient and injection pressure on droplet sizes agree with results of other researchers [3,4,5]. (At injection pressure higher than 5000 psi, it is reported that the effect of injection pressure on drop size is negligible [20].) When the subcooling temperature decreases, then drop sizes become smaller (Fig. IV-9(h)) and the distribution shape become close to that for the air environment (Fig. IV-9(a)).

These droplet size distributions were used for calculating the droplet trajectories after breakup. As a trial, calculations were performed with the sheet portion neglected because the sheet portion is usually very short (less than 20 orifice diameters). As seen in Fig. IV-10, it is assumed that the nozzle hole is the source of droplets. The droplets emitted from nozzle were assumed to have the measured size distributions with uniform velocities and temperature. Computations were done using Eqs. (16)-(36) of Chapter II. The PDP-11/44 computer and the TEKTRONIX 4052 graphic terminal was used for numerical computations and plottings. Figures IV-11,12 show the computed results of

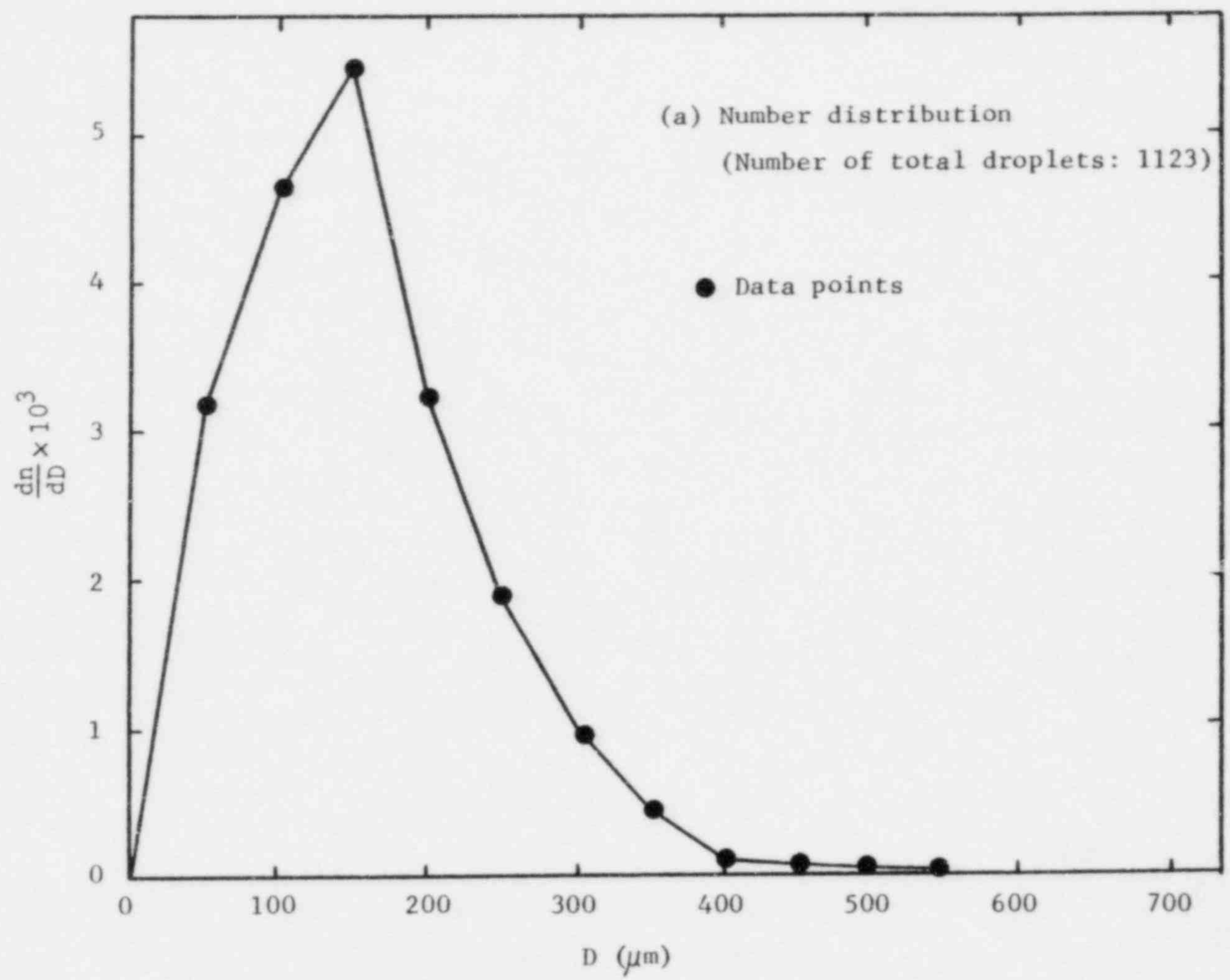

Fig.IV-2 Drop size distribution (Air 1 atm, Q = 3.52 ml/sec)

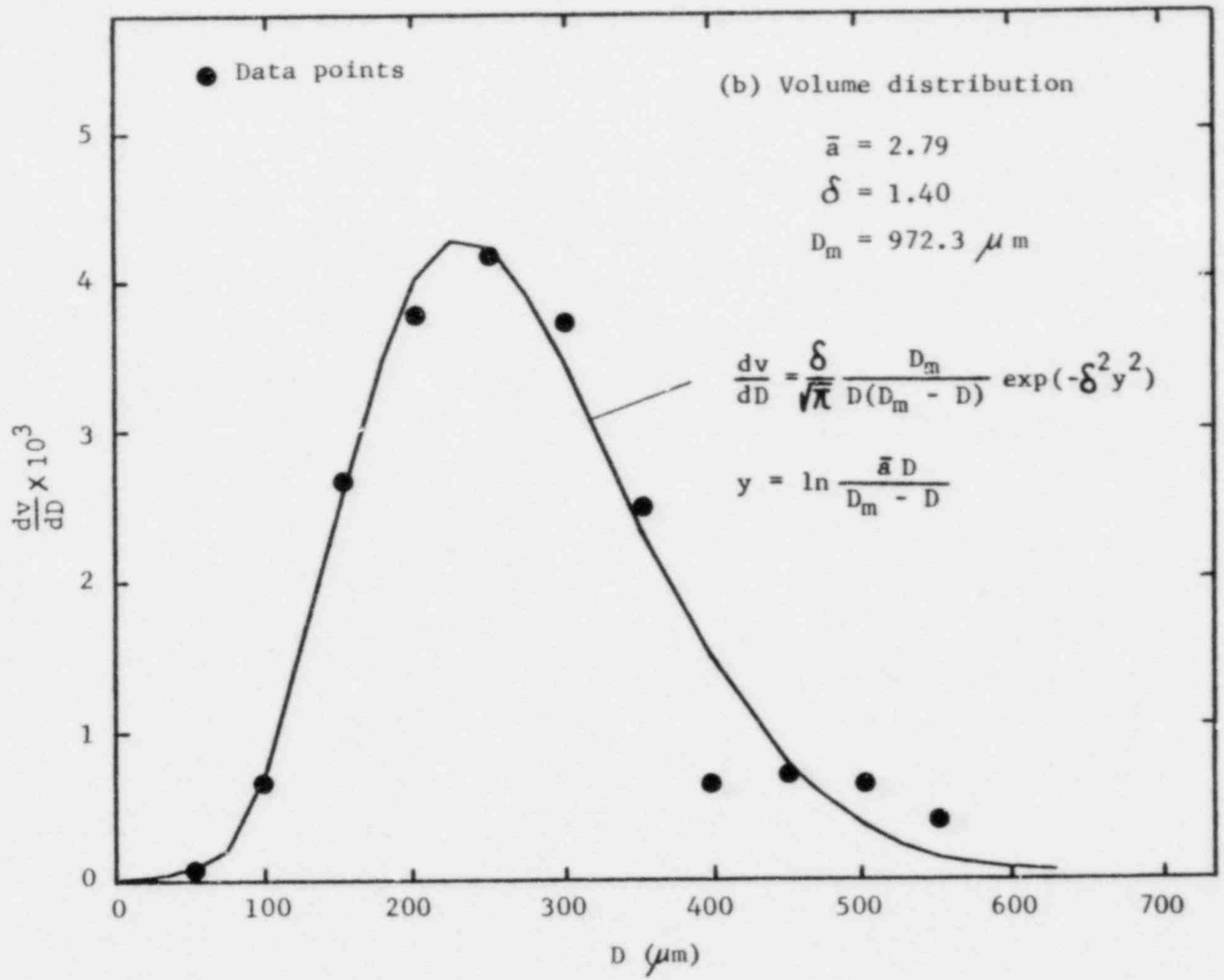

Fig.IV-2 (Cont'd)

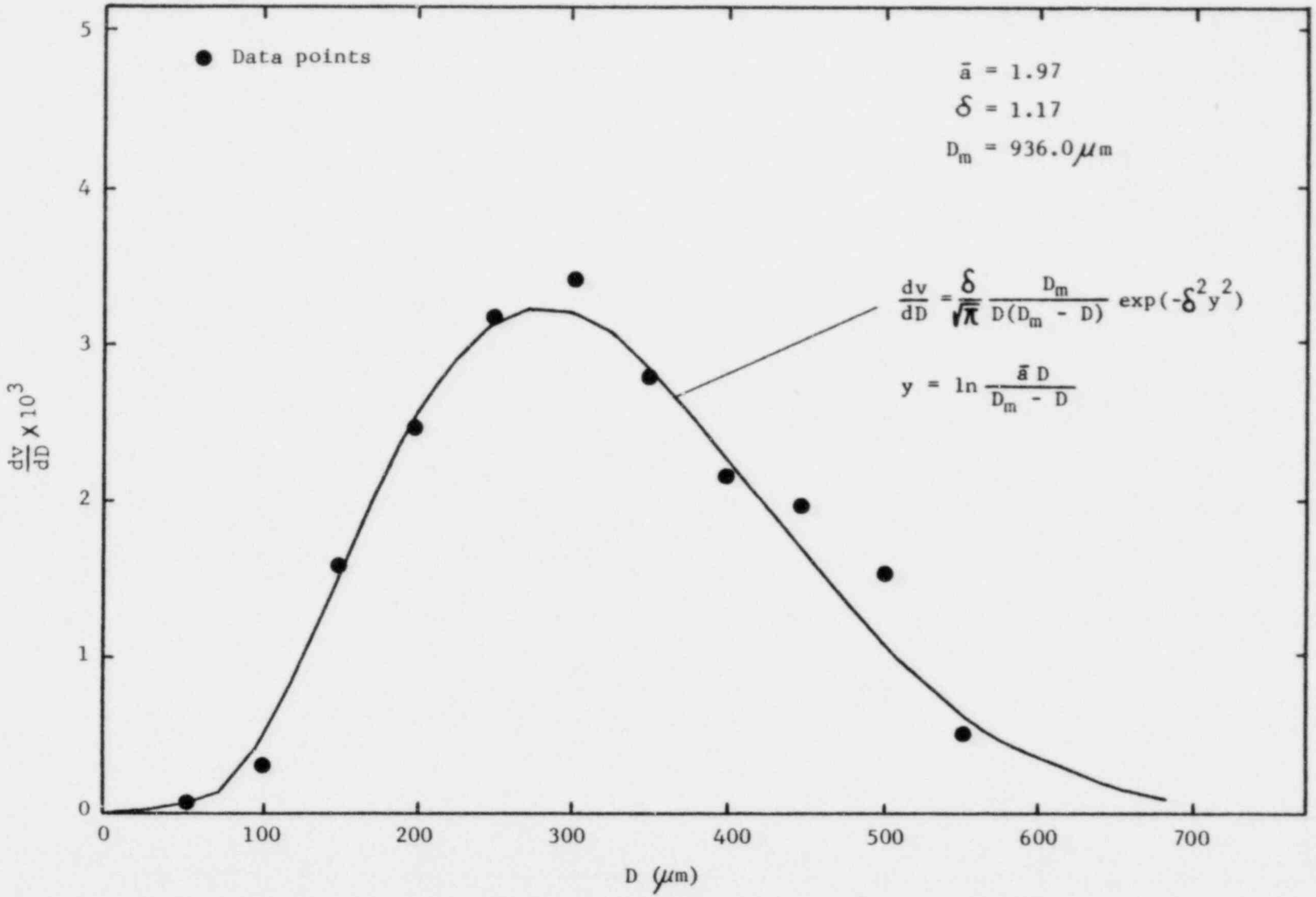

Fig.IV-3 Drop size distribution (Air 1 atm, Q = 2.23 ml/sec)

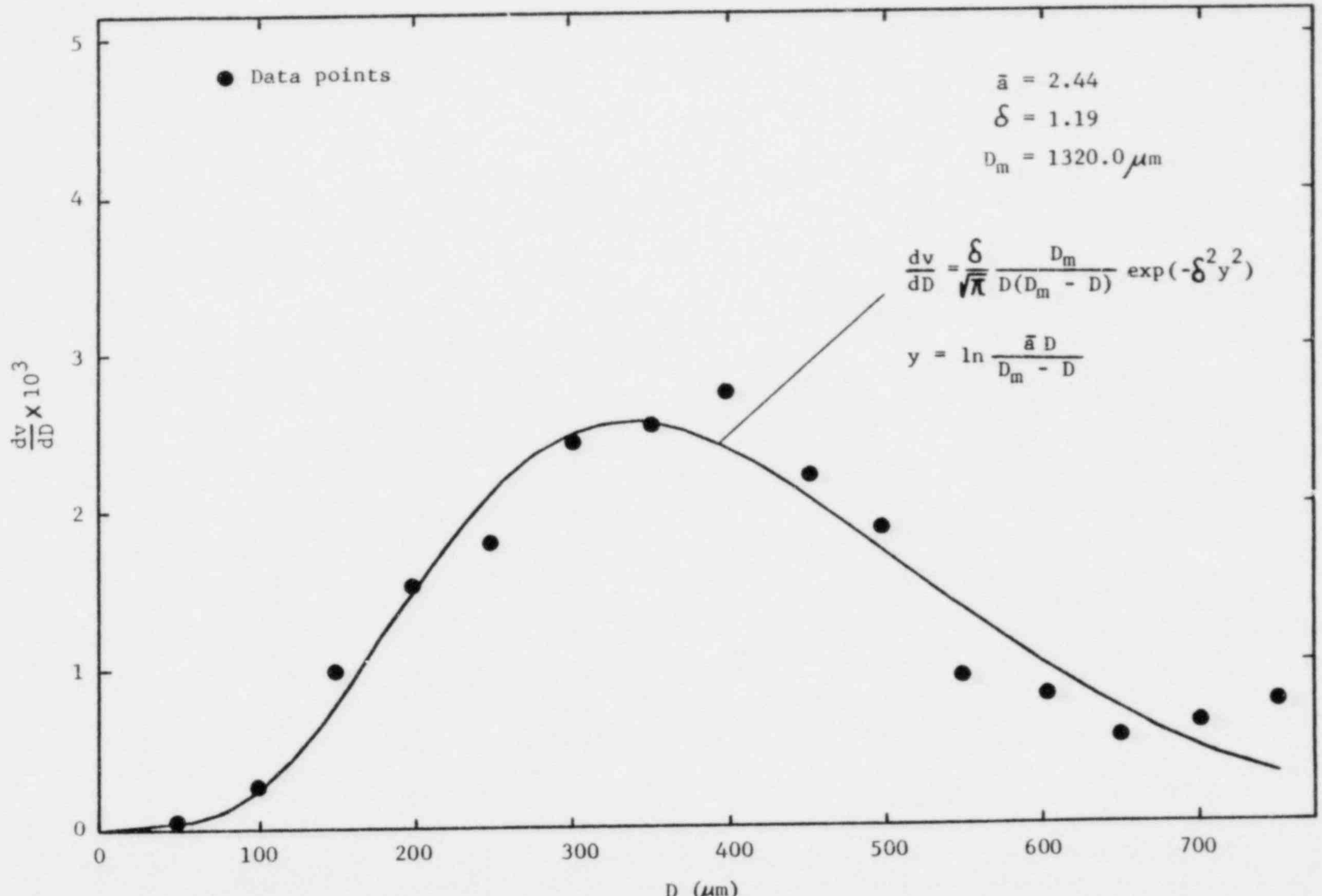

Fig. IV-4 Drop size distribution (Steam 1 atm, Q = 2.23 ml/sec, T_s = 100°C, T_{Lo} = 24.5°C)

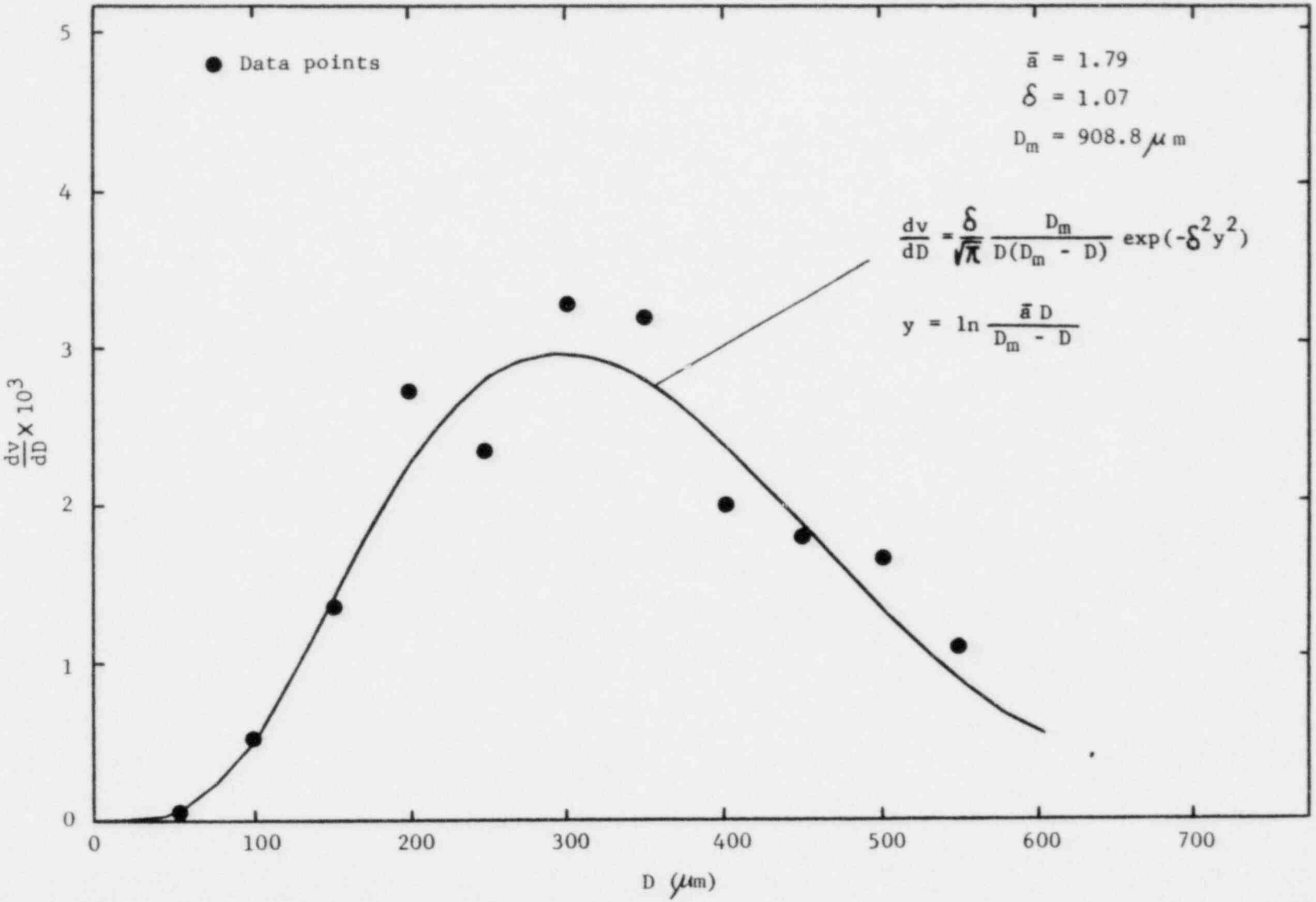

Fig.IV-5 Drop size distribution (Steam 1 atm, Q = 3.52 ml/sec, T_s = 100°C, T_{Lo} = 24.5°C)

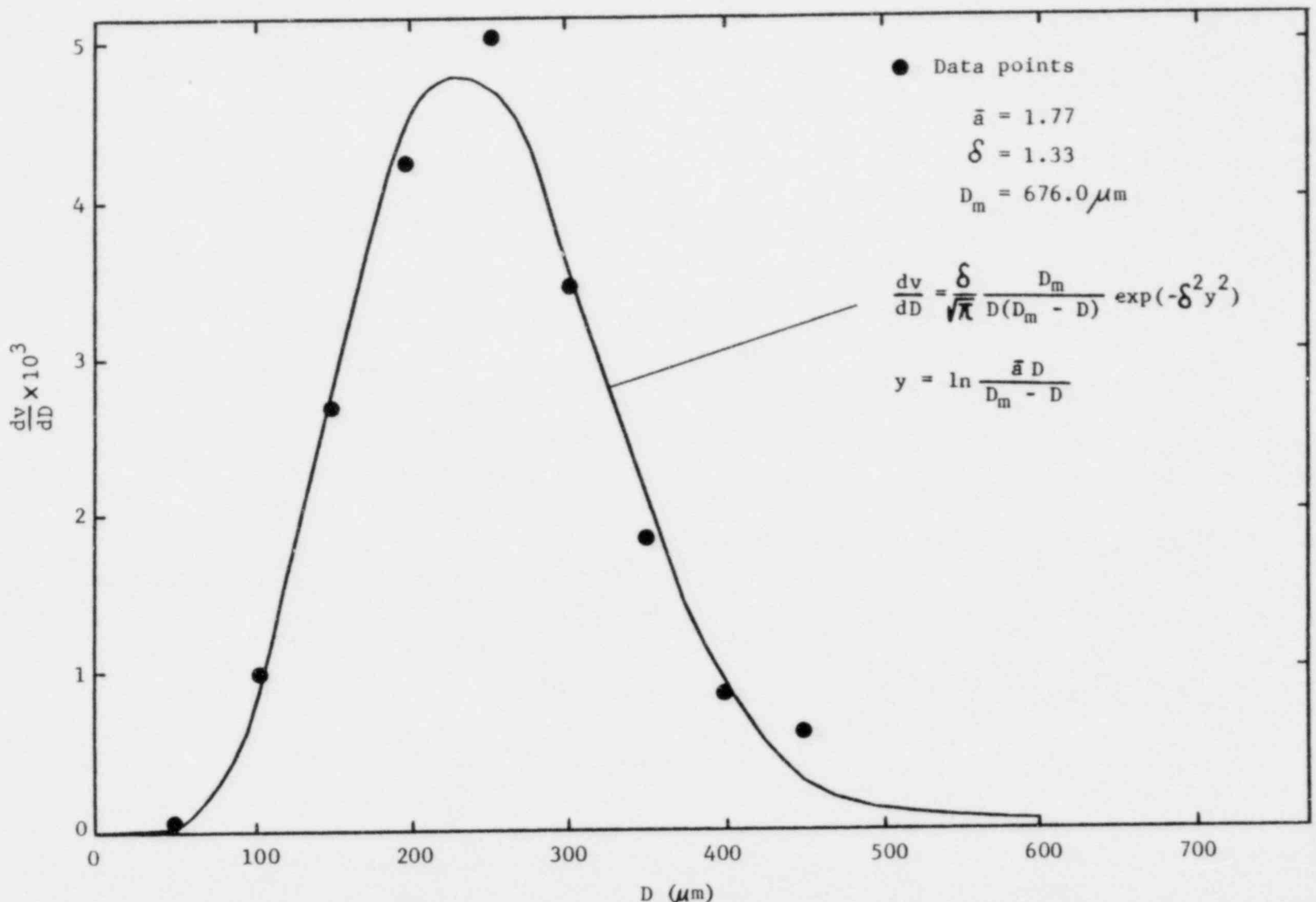

Fig.IV-6 Drop size distribution (Steam 1 atm, Q = 3.52 ml/sec, T_s = 100°C, T_{Lo} = 61.1°C)

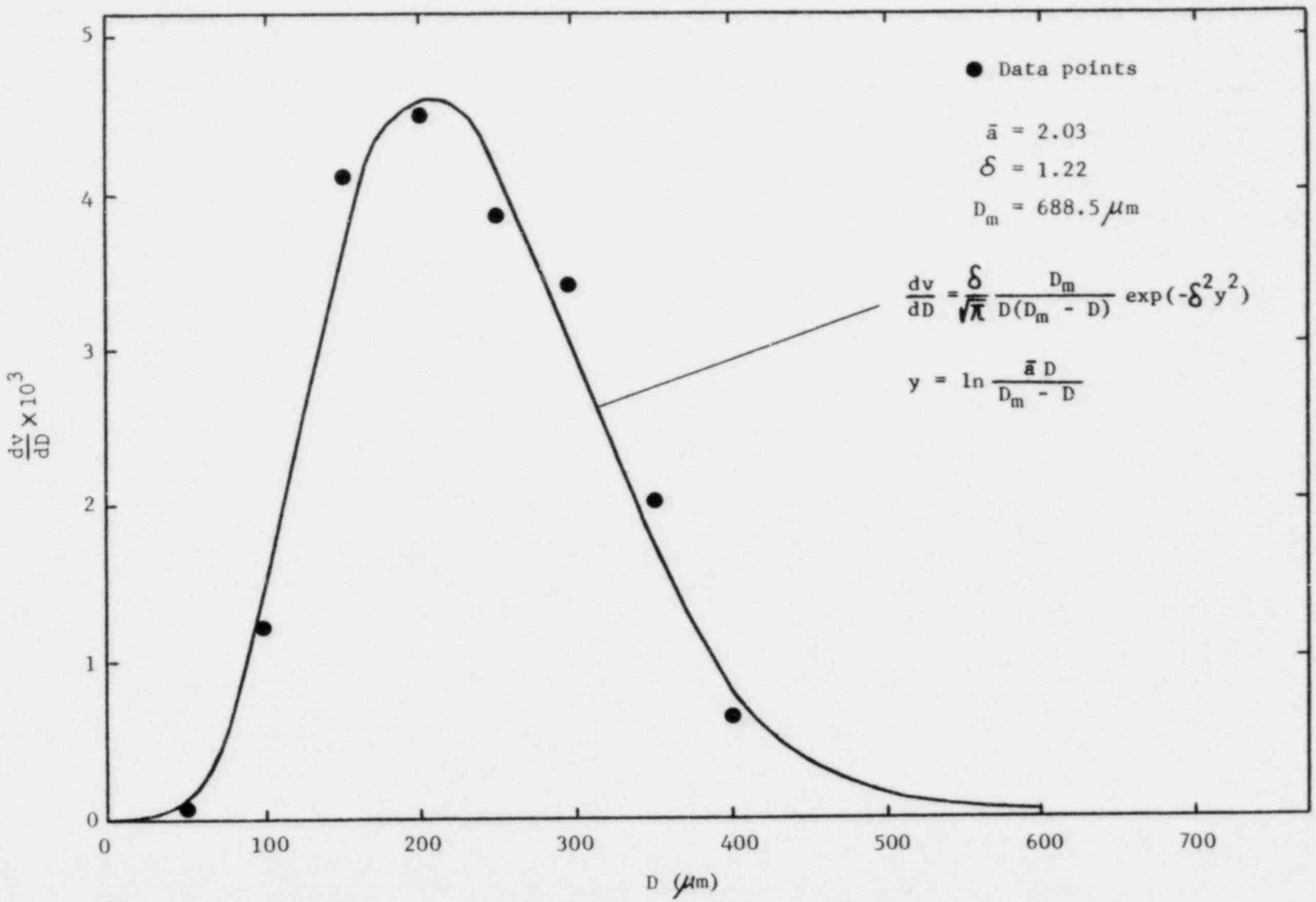

Fig.IV-7 Drop size distribution (Air 3 atm, Q = 3.52 ml/sec)

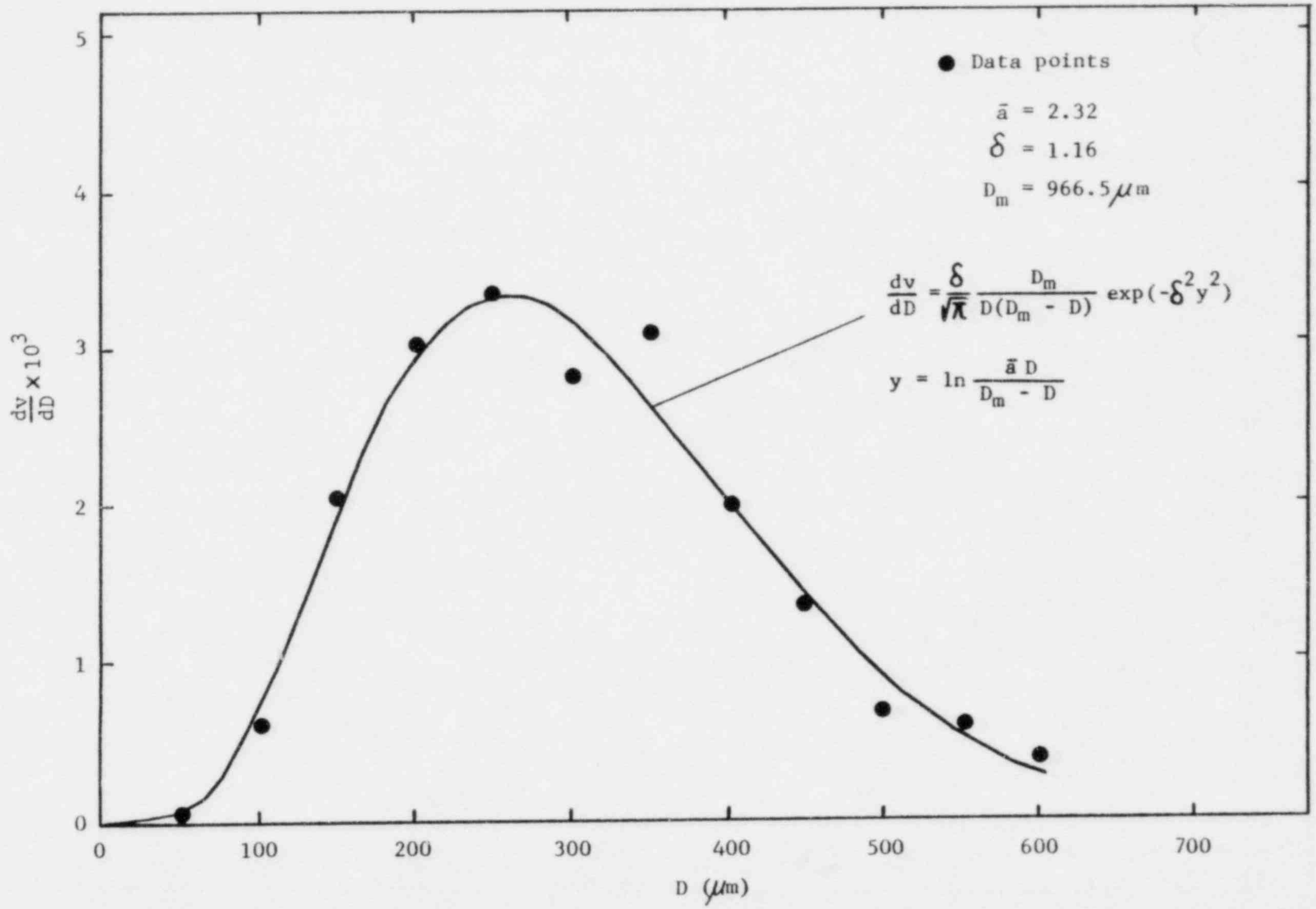

Fig. IV-8 Drop size distribution (Steam 3 atm, $Q = 3.52$ ml/sec, $T_s = 134.0°C$, $T_{Lo} = 24.5°C$)

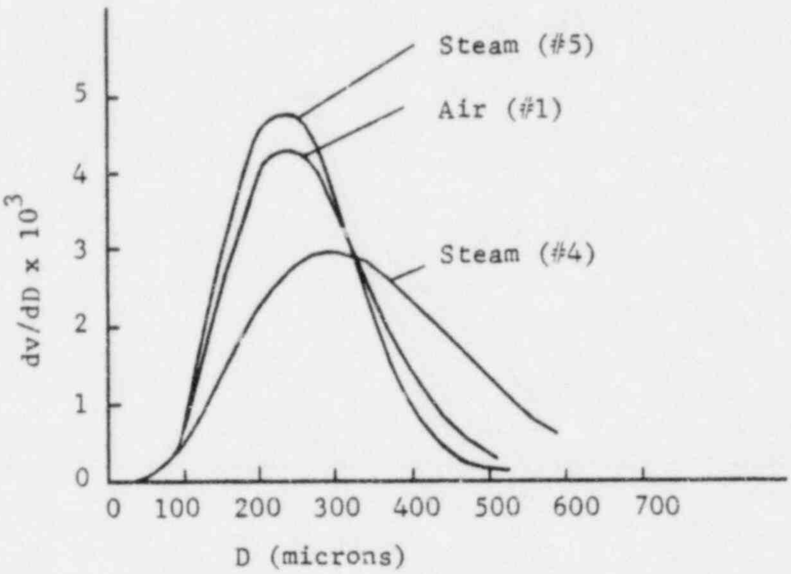

(a) Comparison between steam and air environment (Q = 3.52 ml/sec), 1 atm

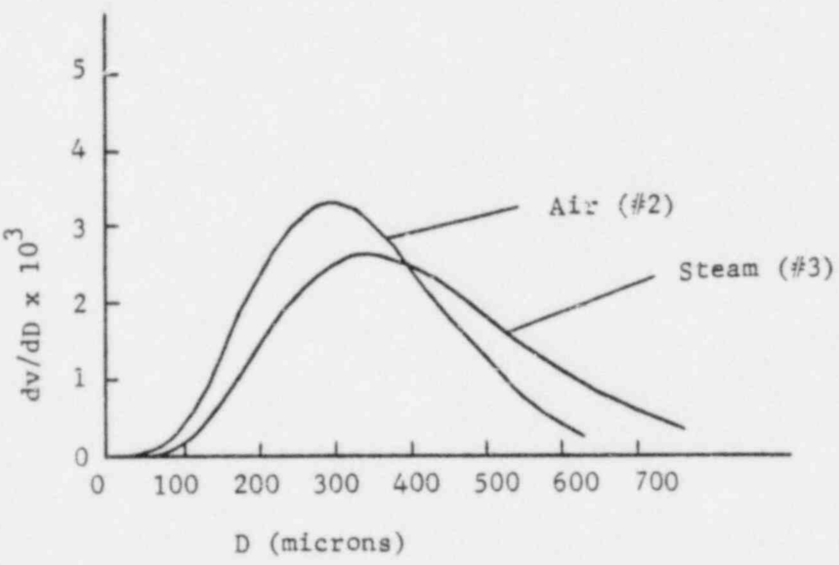

(b) Comparison between steam and air environment (Q = 2.23 ml/sec), 1 atm

Fig.IV-9 Comparison of drop size distribution between each test conditions.

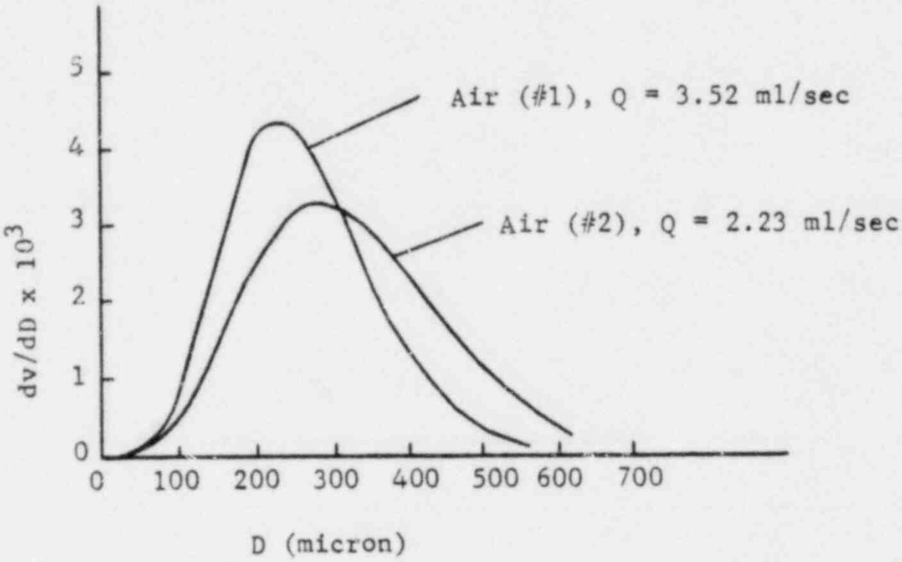

(c) Effect of flow rate (Air environment)

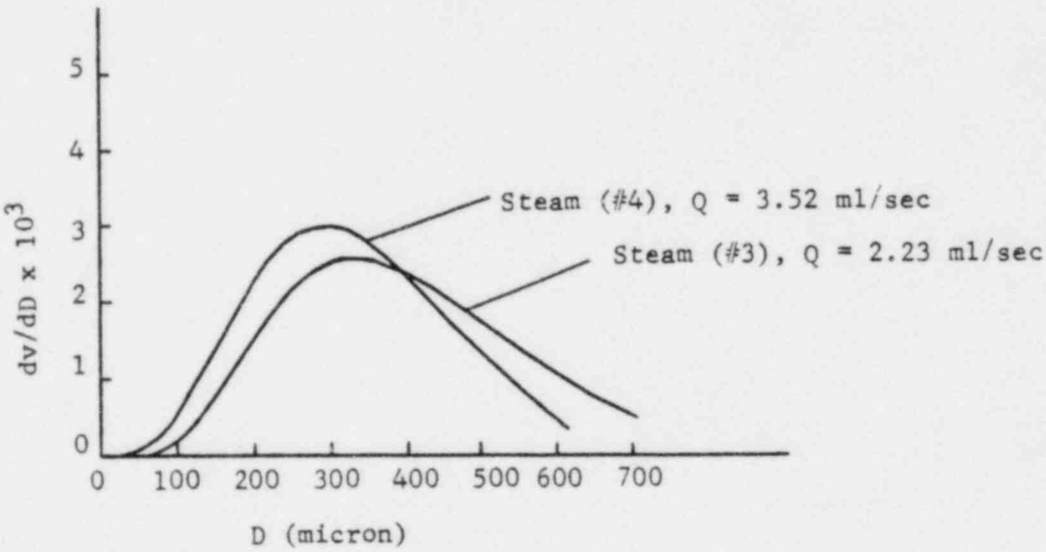

(d) Effect of flow rate (Steam environment)

Fig.IV-9 (cont'd)

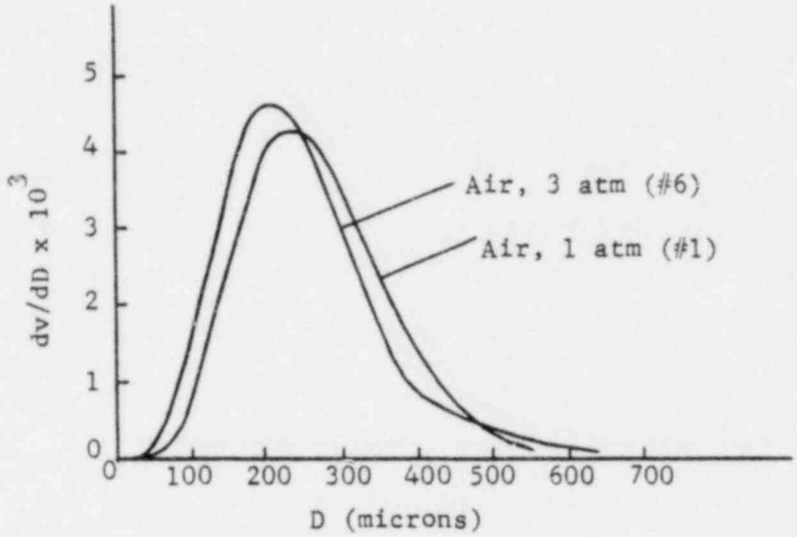

(e) Effect of ambient pressure (Air environment, Q = 3.52 ml/sec)

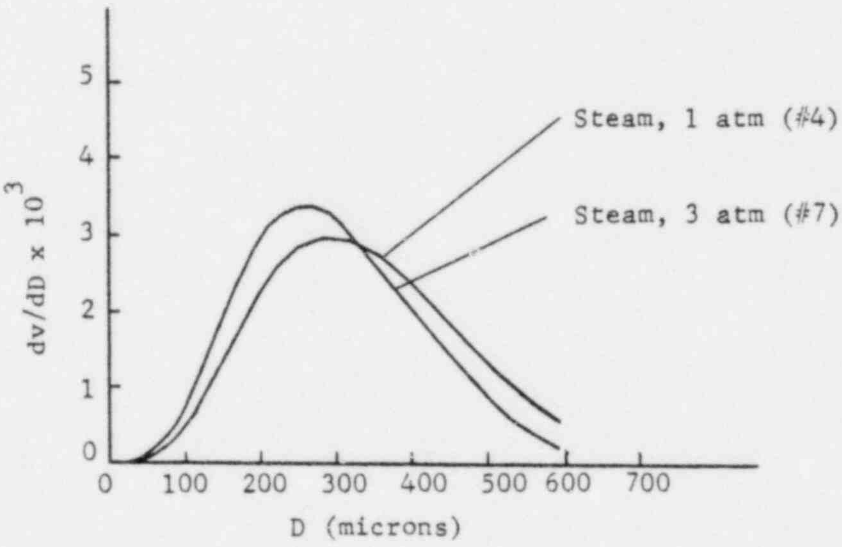

(f) Effect of ambient pressure (Steam environment, Q = 3.52 ml/sec)

Fig.IV-9 (Cont'd)

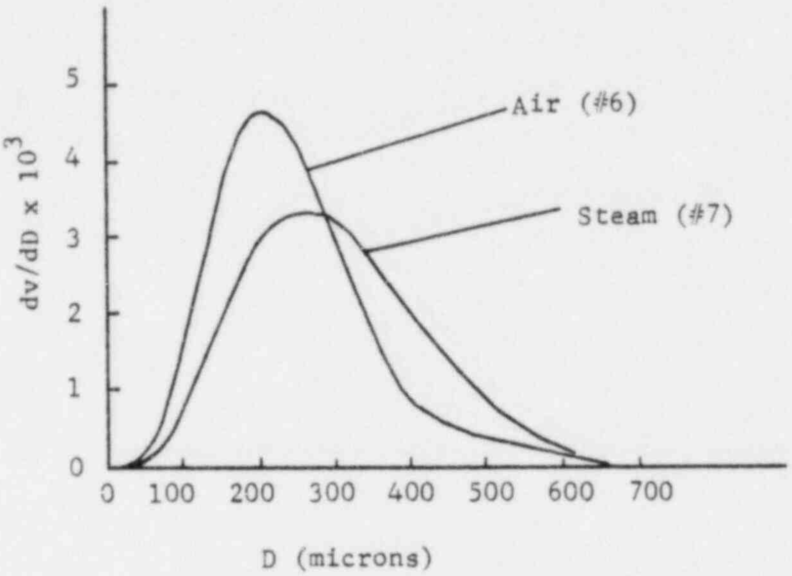

(g) Comparison between steam and air environment (Q = 3.52 ml/sec), 3 atm

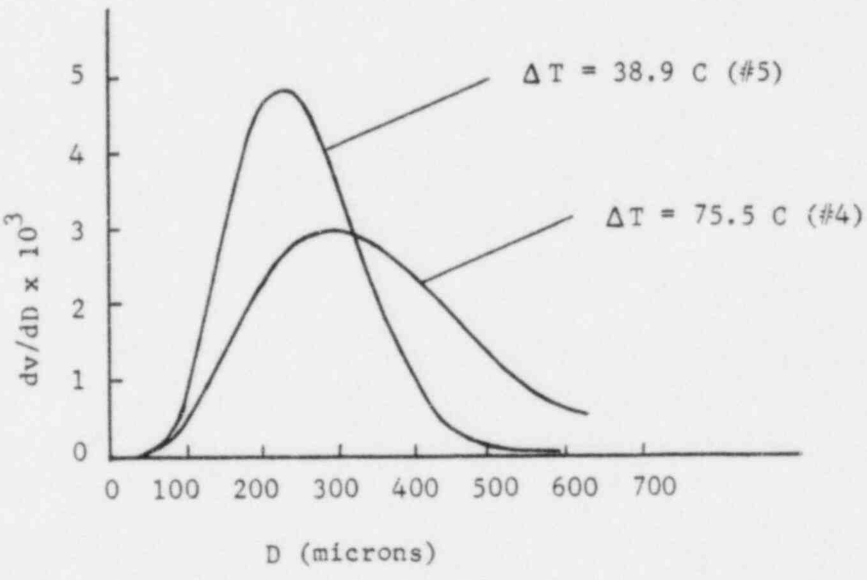

(h) Effect of subcooling temperature (Steam environment, 1 atm, Q = 3.52 ml/sec)

Fig.IV-9 (Cont'd)

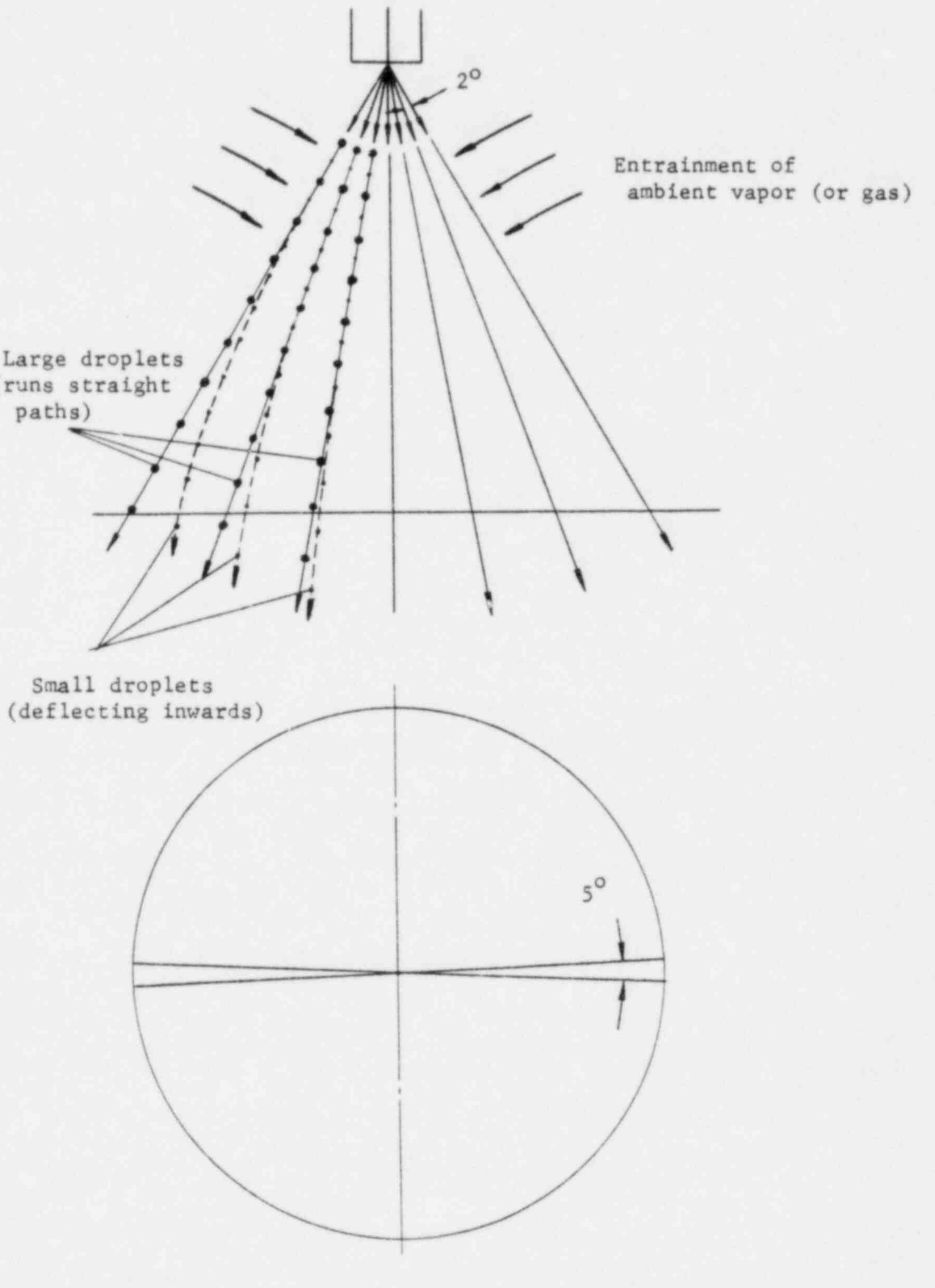

Fig.IV-10 Computational model without sheet portion (Drop model) space distributions of droplets. The plotting was done for the range of 5 degree in azimuthal direction of spray with 50 micron increments of drop sizes and 2 degree increments of spray angle (Fig. IV-10). In Figs. IV-11,12, one side of the plots (Number distributions) show the position of droplets in space - each point indicates a single droplet regardless of its size - and the other side of the plots (Volume distribution) shows the relative volume distribution of droplets in space. Since the plots were made with a range of 5 degrees in azimuthal direction, both plots of Number and Volume distribution of droplets in space are seen to be more dense at the edge than at the center of the spray (the edge volume is larger than the center volume). The large droplets follow their initial trajectory; whereas, the small droplets are deflected inwards. In Fig. IV-11, we can see a group of droplets that are deflected inwards which were initially injected at the edge portion. We can verify the deflecting droplets to be small ones by following methods: if plots were made (by computer) without 50 and 100 micron droplets, this group of deflecting droplets in Fig. IV-11 vanishes. The deflection of small droplets are seen to be greater in air environment than in steam en-vironment even though condensation is present in latter case. Air has a higher density than steam; thus the drag force due to entrainment is larger in case of air. Also from Figs. IV-11,12, the outline shape of the spray does not change appreciably between the case of condensation and non-condensation. That is, the large droplets follow their initial trajectory - inward deflection is negligible. Therefore, it is believed that the contraction of spray angle in steam is primarily due to the contraction of the sheet portion - even though this region of

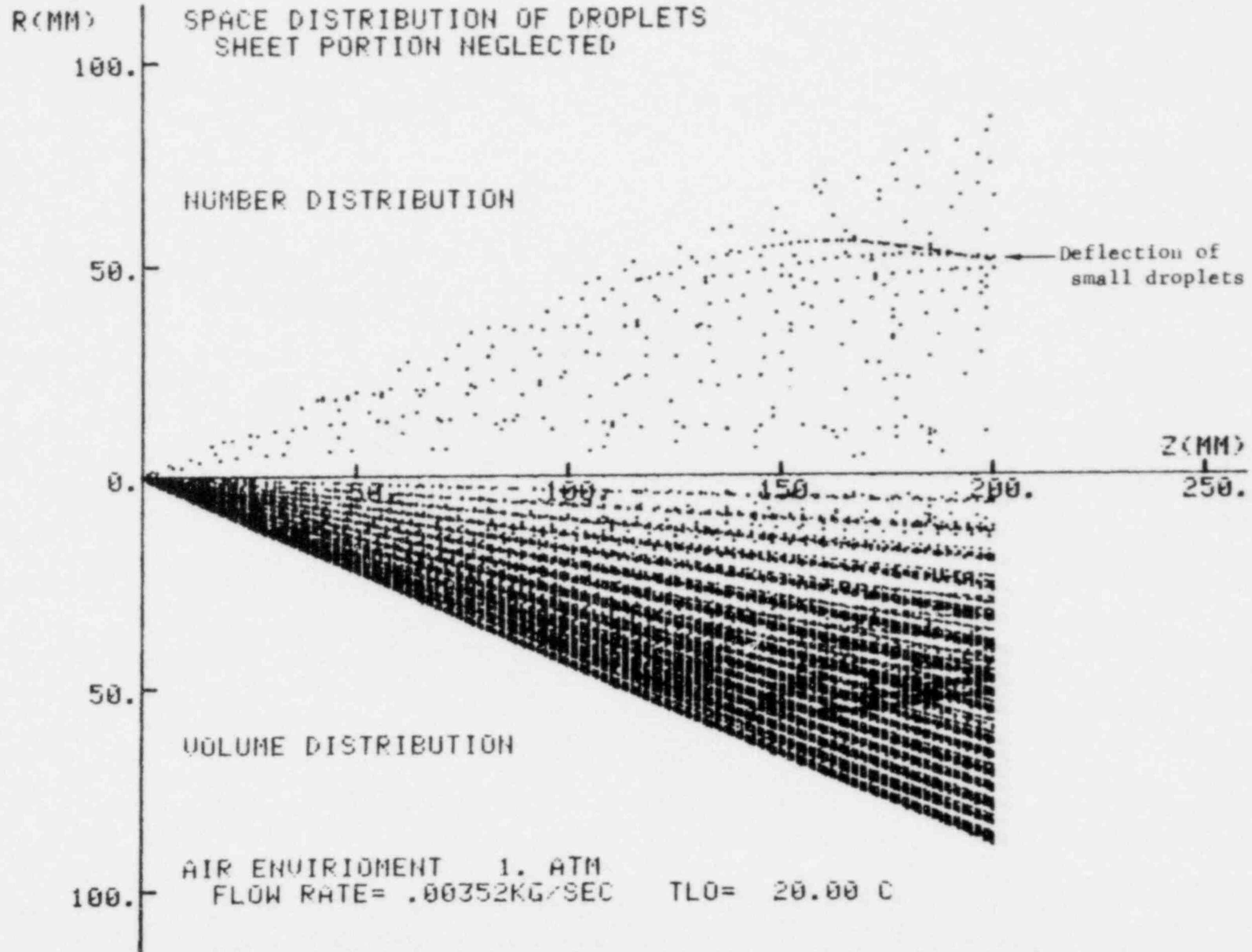

Fig.IV-11 Calculation of spray shape with drop model (no water sheet)

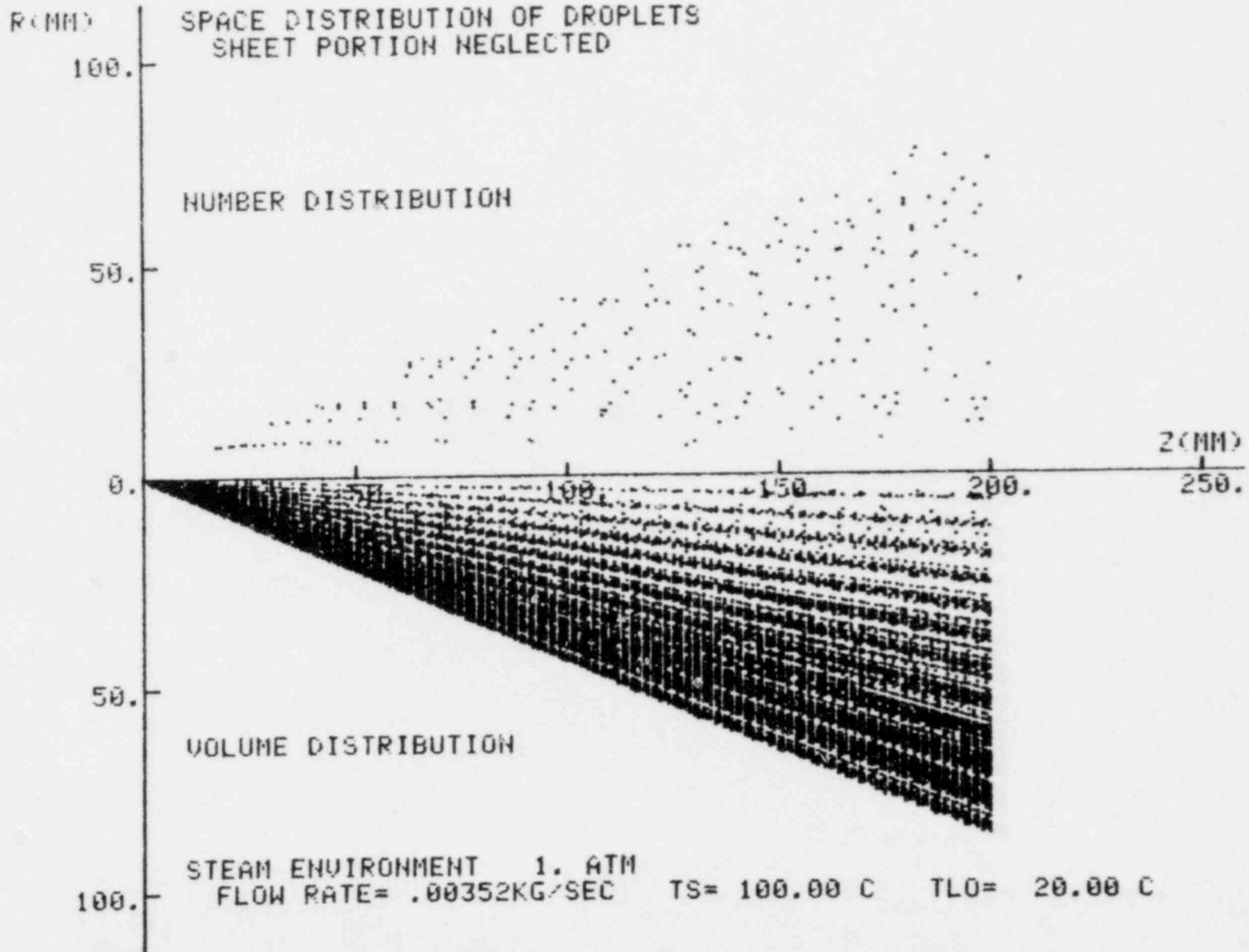

Fig.IV-12 Calculation of spray shape with drop model (no water sheet) the spray is very short. Similar conclusions are reported by Chan et al. [50]. The method of Rothe and Block [22] used a uniform drop size and obtained contraction. If the average size droplet were used in our computation, we would have also observed contraction in the spray angle.

2. Sheet Portion

Concerning the sheet portion, two major quantities must be determined: the shape of the sheet and its breakup length. Up to the breakup point, the shape of the water sheet can be calculated by the model developed in Chapter II. For this purpose, the calculation and experiments are performed on the Nozzle #1, #2, #3 which are described in Chapter III (Table III-1). A program for the numerical calculation is listed in Appendix 4. Figures IV-13,14,15 show the typical photographs of these sprays. Figures IV-16,17 show the comparison between calculated and measured results for the sheet portion of Nozzles #1, #2 in air and steam environment. Each rippled line is an outline shape of the water sheet obtained by a tracing from a photograph of the spray. The pulsed laser was used as a light source and shutter. The duration of the pulsed light is 10^{-8} sec and the shape of the spray is not smooth as in the ideal cases. Five or six photographs are taken for each set of conditions and the rippled lines are these traces. For Nozzles #1 and #2, expansion of spray sheet is caused by the tangential velocity since there are slots for swirling inside the nozzle. It is difficult to decide the tangential velocity at the nozzle exit by the angle and size of the slots inside the nozzle because of large pressure drop within the nozzle itself. Therefore, the ratio of tangential velocity and axial

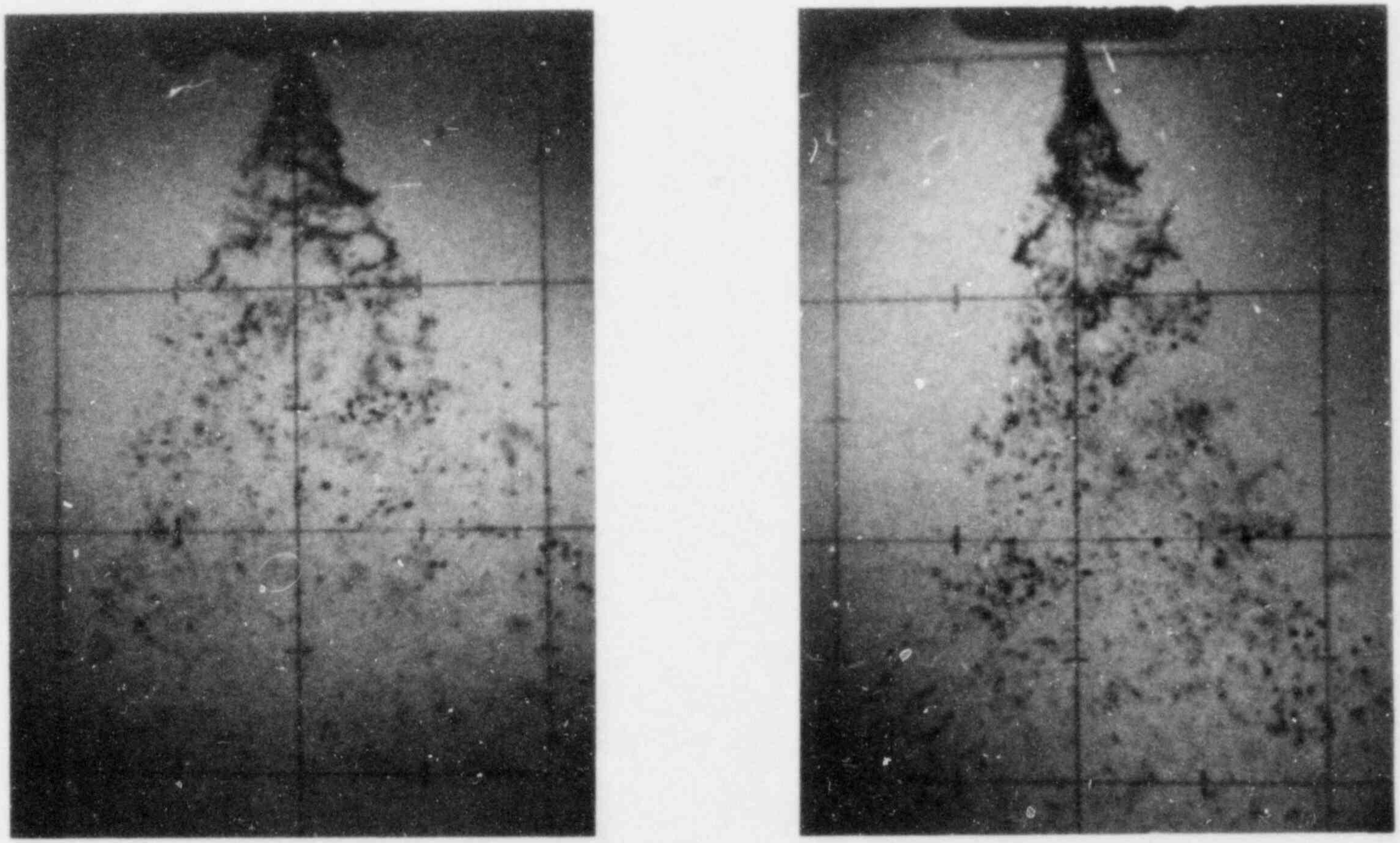

Air 1 atm, Q = 3.52 ml/sec, T_{Lo} = 20°C

Steam 1 atm, Q = 3.52 ml/sec, T_{Lo} = 20°C

Fig.IV-13 Typical photograph of the spray (Nozzle #1)

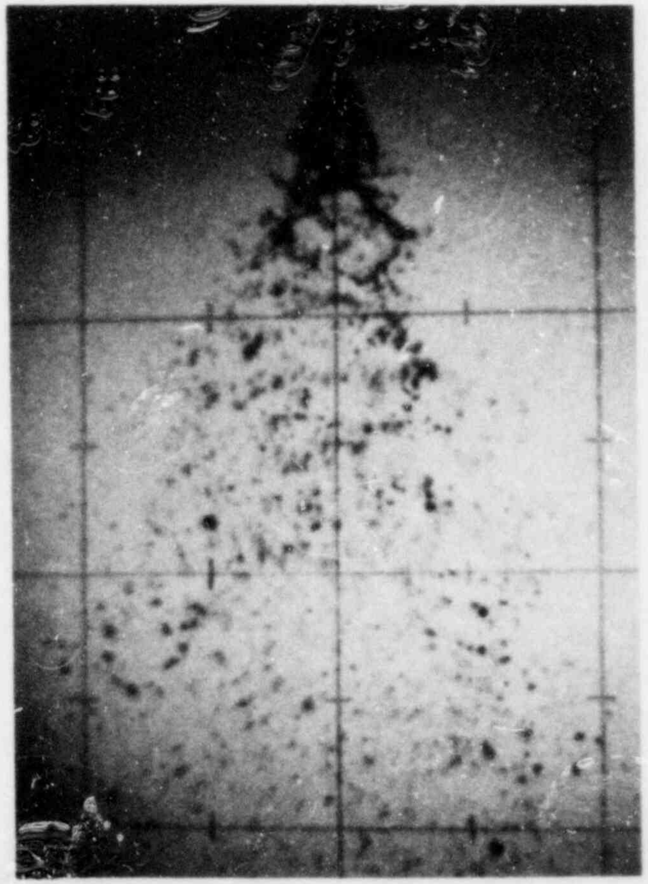

Air 1 atm, $Q = 3.52$ ml/sec, $T_{Lo} = 20°C$

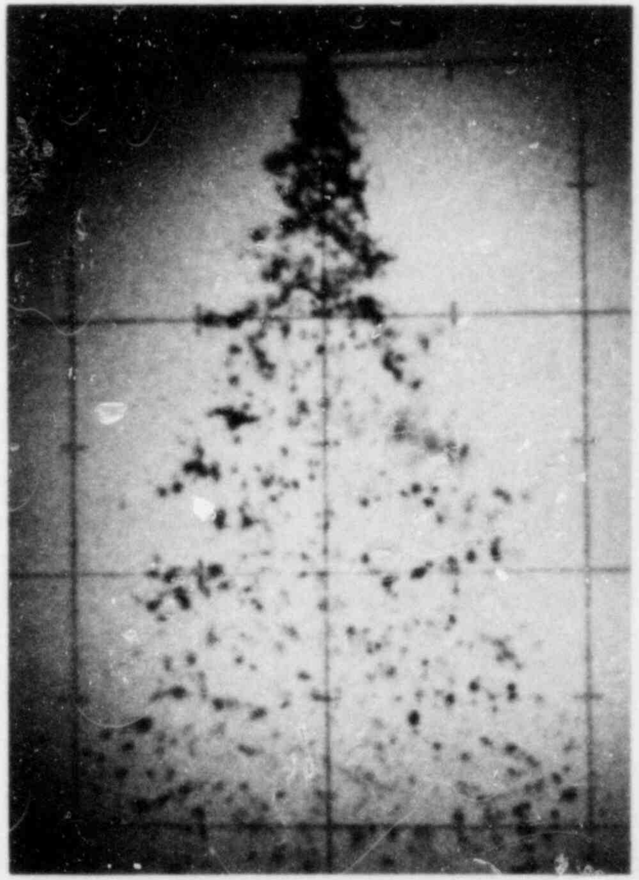

Steam 1 atm, $Q = 3.52$ ml/sec, $T_{Lo} = 20°C$

Fig.IV-14 Typical photograph of the spray (Nozzle #2)

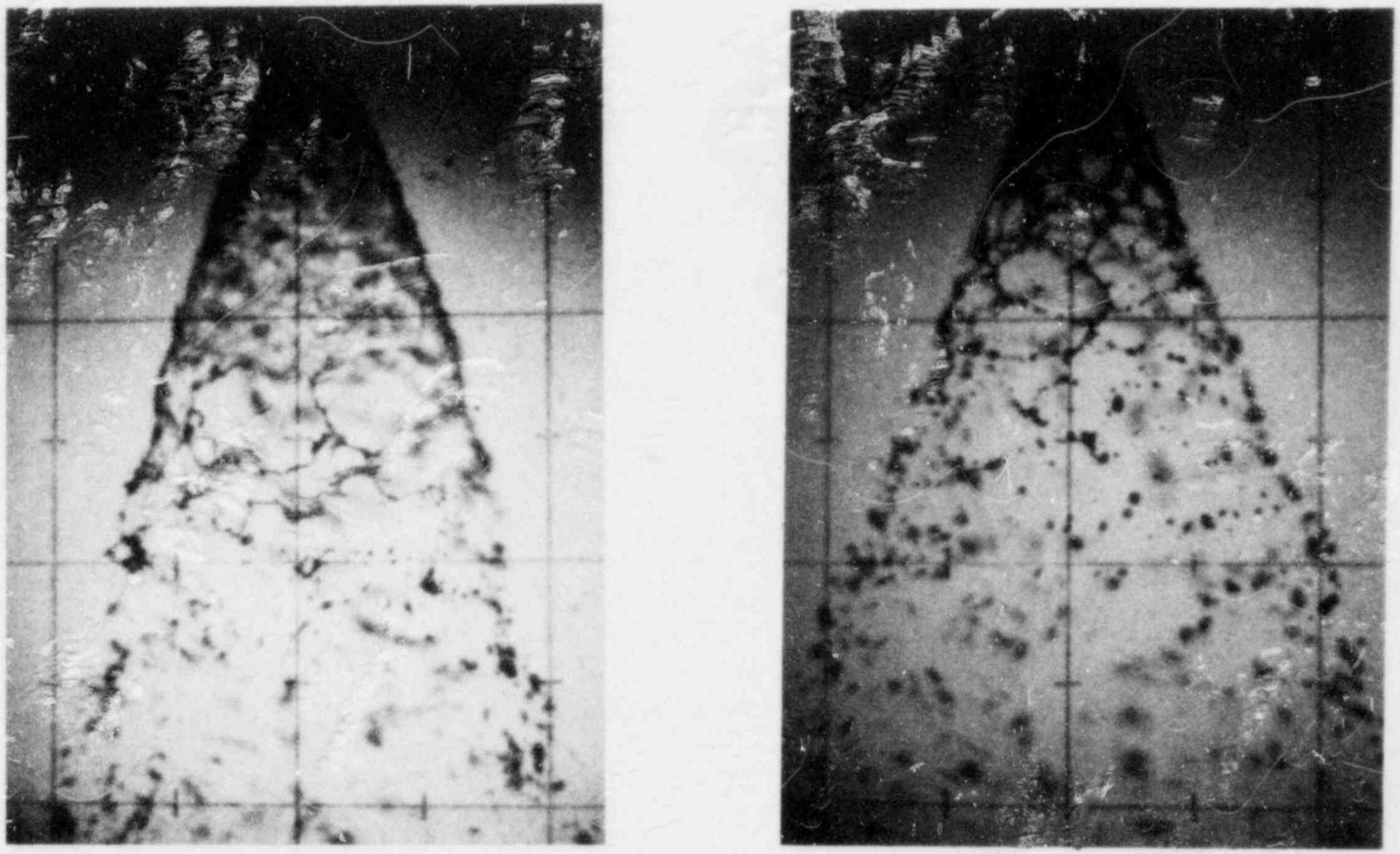

Air 1 atm, Q = 6.30 ml/sec, T_{Lo} = 20°C   Steam 1 atm, Q = 6.30 ml/sec, T_{Lo} = 20°C

Fig. IV-15 Typical photograph of the spray (Nozzle #3) velocity (V_t/V_{Lo}) at nozzle exit was found for each nozzle by a best fit of computed value and experimental value (from a photograph of spray) at a certain test condition. The ratios of V_t/V_{Lo} at nozzle exit turned out to be 0.4 and 0.45 for Nozzle #1 and #2 respectively. Once the ratio, V_t/V_{Lo}, at the nozzle exit was found, then this was used for calculation at the other experimental conditions. That is, the ratio of tangential velocity and axial velocity at nozzle exit depends primarily on the nozzle design and not on the ambient condition after the injection. In case of the poppet type nozzle, the deflector plate spreads the water sheet instead of swirling motion, and initial spray angle is determined by the nozzle geometry. Figures IV-16,17 are replotted in Fig. IV-18 with the average value of measured shape. Also, the measured and calculated shapes for Nozzle #3 were plotted in Fig. IV-19. The lines were obtained from computation and the solid dots were averaged values obtained from the photographs of the spray. For the nozzles tested, the experimentally obtained results show good agreement with the calculated shape. As seen in Fig. IV-19, the difference of breakup length between the cases of condensation and non-condensation is well observed with Nozzle #3, which is designed to have a relatively long sheet portion. It is noted that, the breakup occurs earlier in case of condensation. This effect is not as clearly defined with Nozzle #1, #2, because both of these nozzles have very short sheet portion due to high water velocity and small orifice size compared with Nozzle #3. The surface tension of water listed in the published tables is for pure water. In our case, we used tap water which has a lower value. For the spray shape computations, the surface tension of tap water was measured as

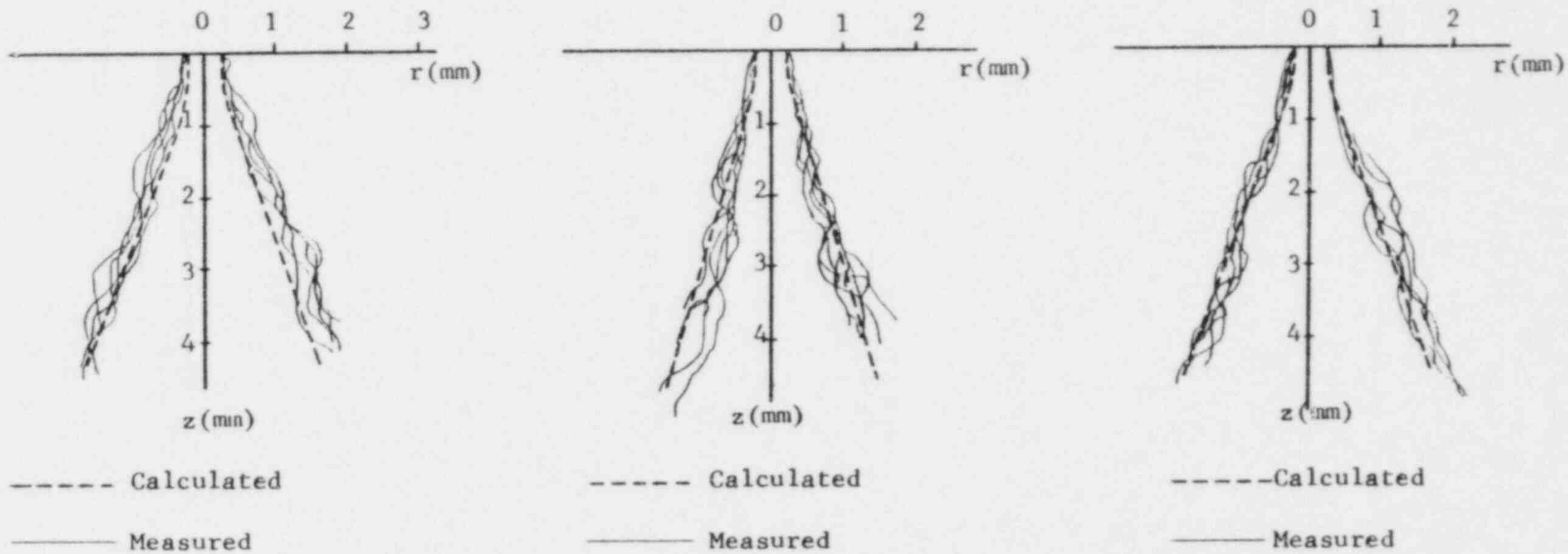

Steam 1 atm
$Q = 3.52$ ml/sec, $T_{Lo} = 73°C$

Steam 1 atm
$Q = 3.52$ ml/sec, $T_{Lo} = 20°C$

Air 1 atm
$Q = 3.52$ ml/sec, $T_{Lo} = 20°C$

Fig. IV-16 Calculated and measured shape of sheet portion (Nozzle #1)
($V_t/V_{Lo} = 0.4$ at nozzle exit)

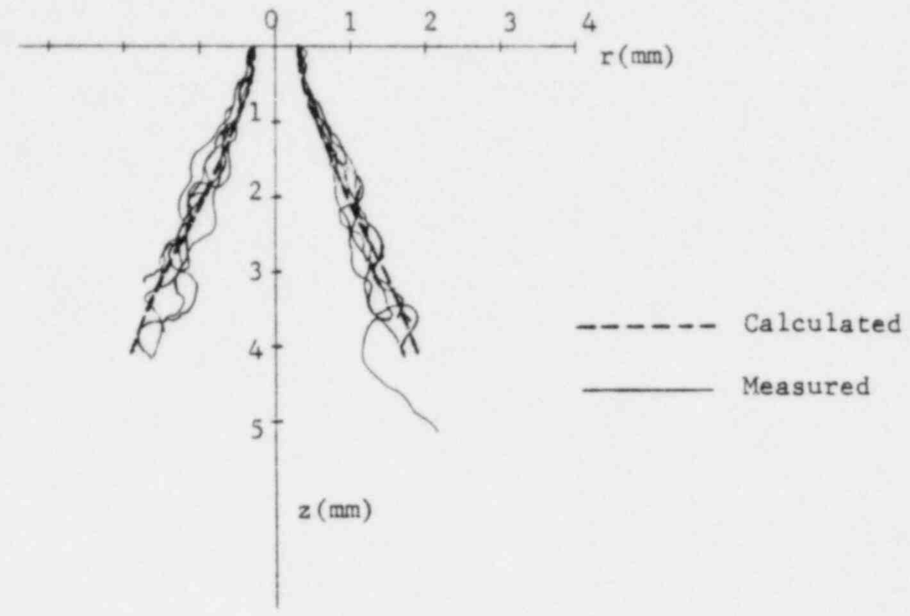

Air 1 atm, Q = 3.52 ml/sec, T_{Lo} = 20°C

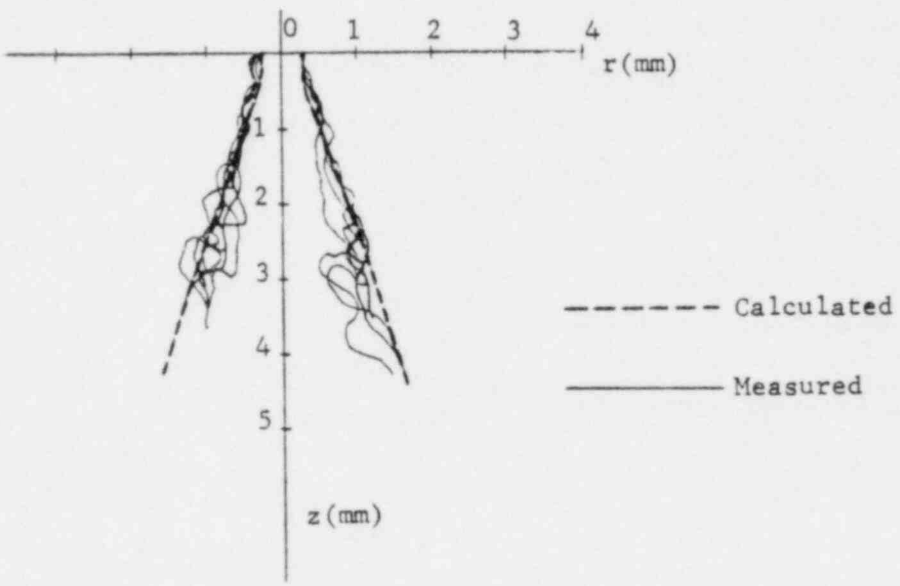

Steam 1 atm, Q = 3.52 ml/sec, T_{Lo} = 20°C

Fig.IV-17 Calculated and measured shape of sheet portion (Nozzle #2) (V_t/V_{Lo}= 0.45 at nozzle exit)

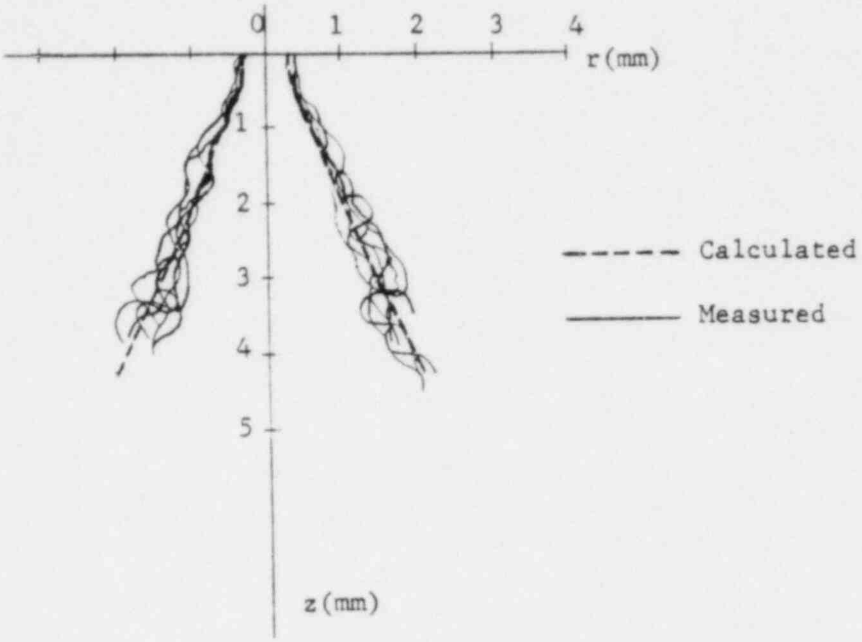

Air 1 atm, Q = 4.40 ml/sec, T_{Lo} = 20°C

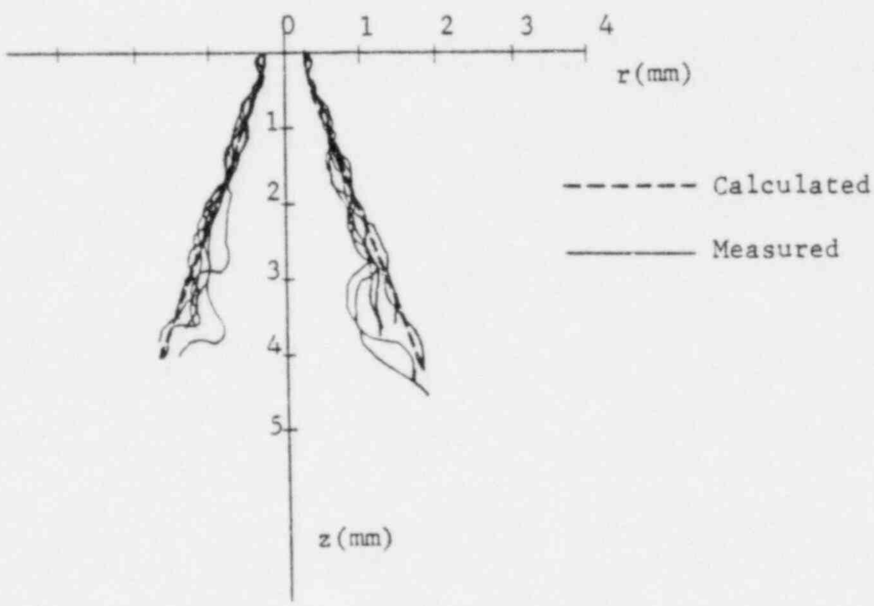

Steam 1 atm, Q = 4.40 ml/sec, T_{Lo} = 30°C

Fig. IV-17 (Cont'd)

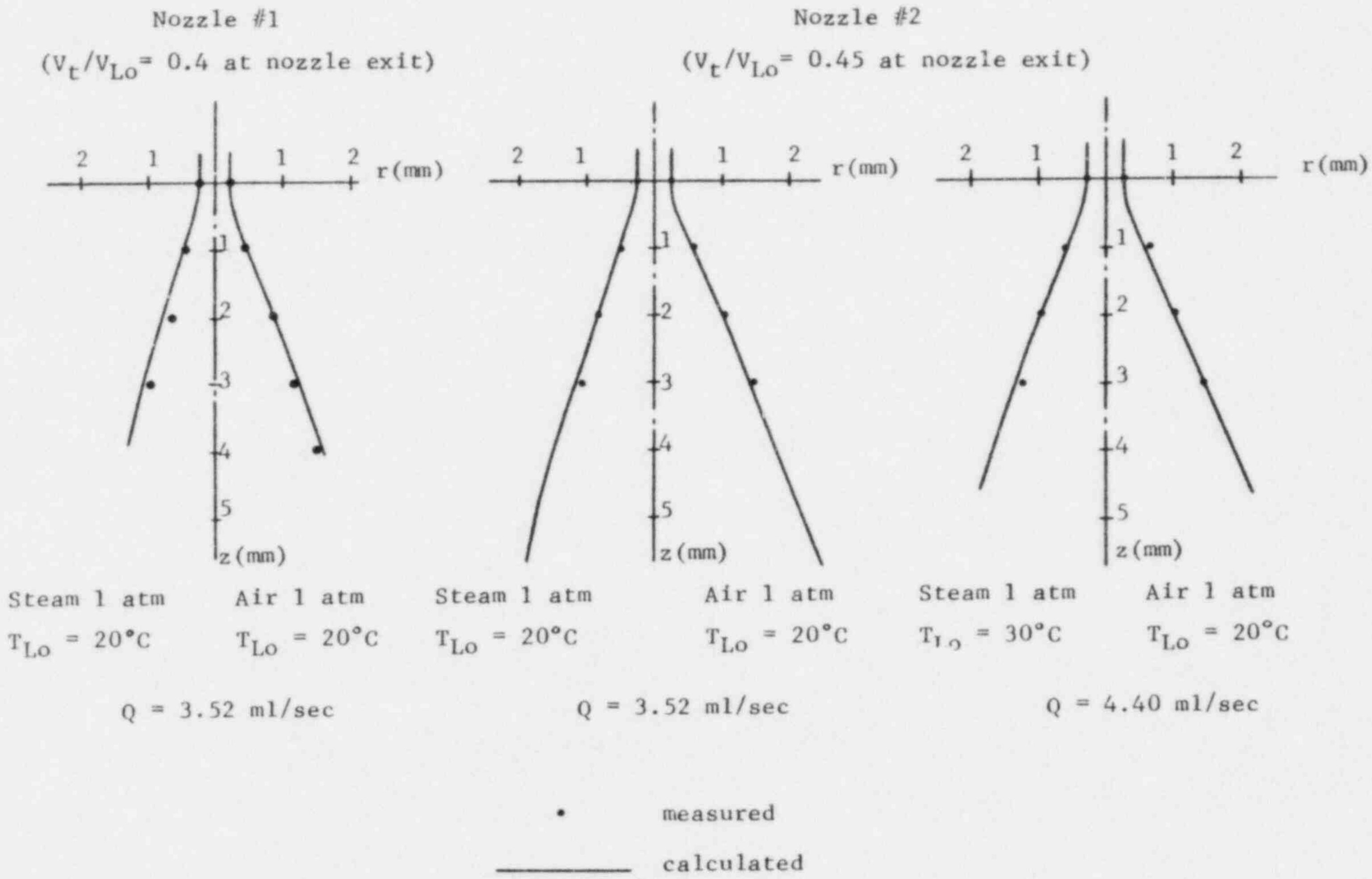

Fig. IV-18 Calculated and measured shape of sheet portion (nozzle #1,#2) described in Appendix 2. The results show the surface tenison of tap water varies from 50 to 60 dyne/cm depending on the temperature. For large initial spray angle and/or radius (Nozzle #3, Fig. IV-19), the calculated results show that the outline shape of sheet portion is not changed significantly by condensation. The outline shape does change significantly for a spray having a small initial spray angle and/or radius. Accordingly, the contraction of spray angle is well observed in the case of Nozzles #1, #2 as in Fig. IV-13, 14 (or Fig. IV-18). Similar results are reported by Sandoz et al. [30] as seen in Fig. IV-20. In both figures (Sandoz's and ours), the spray angle contracts in case of steam environment prior to breakup. However, after breakup, the spray expansion is greater in the case of a steam environment as compared with the case of an air environment (non-condensation). This can be explained as follows: With a small angle and assuming a vortex type flow (for a swirl nozzle), the centrifugal force is greater at breakup because of higher tangential velocity (smaller radius). Thus, with contraction of the cone angle in the sheet portion along with shorter breakup length (for condensation) one would expect the droplets to have a greater tangential velocity at the breakup point. This in turn would result in a greater centrifugal force on the droplet and thus forms a greater expansion angle of the spray after breakup. One would not expect this for the poppet type nozzle.

As mentioned earlier, the shape of the water sheet is not the only factor that governs the spray shape, but also the breakup length. Figure IV-21 shows the sample calculation of the outline shape of the two sprays with all same initial conditions but different breakup

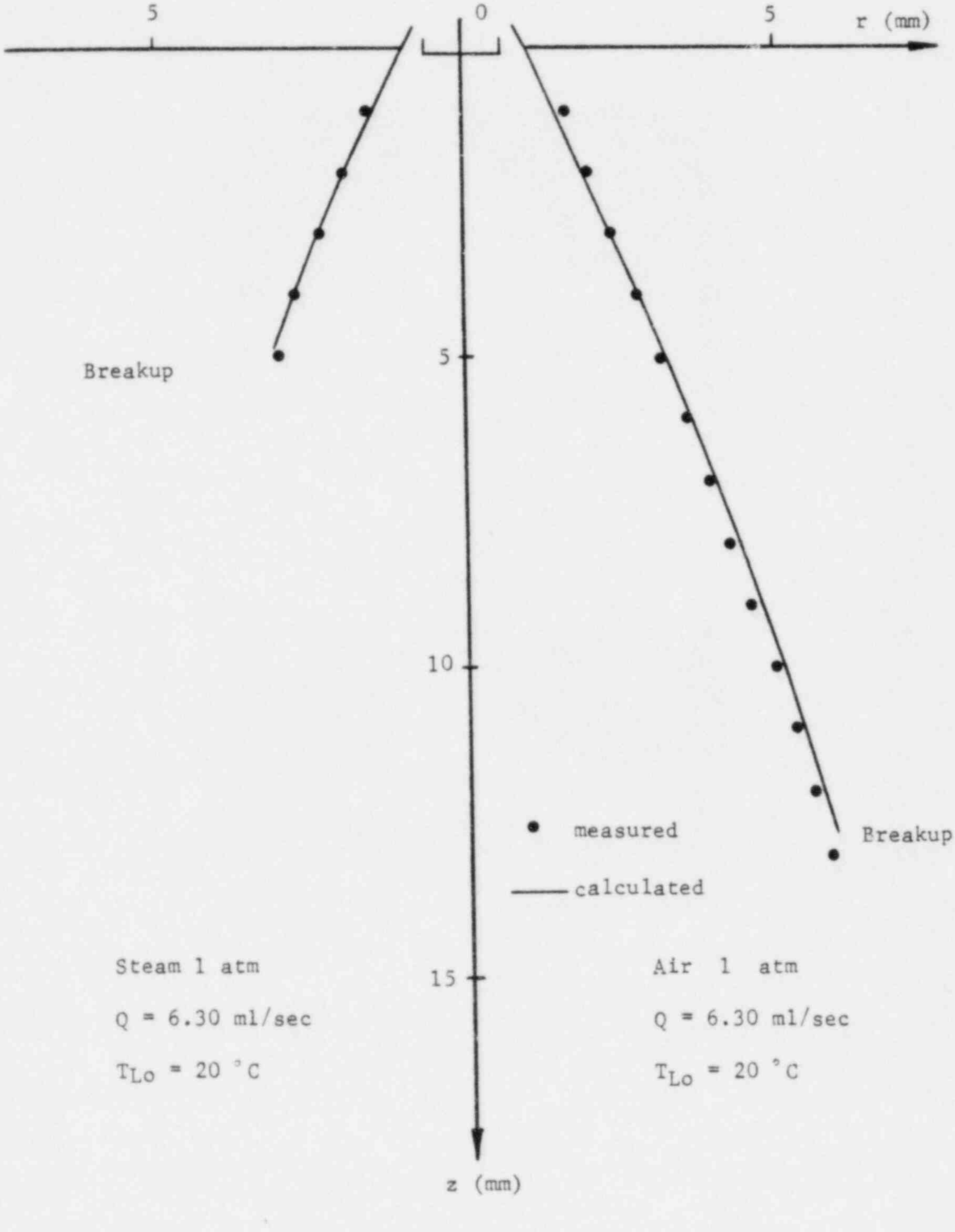

Fig.IV-19 Calculated and measured shape of sheet portion (Nozzle #3)

(a) No condensation (Nozzle: Spraying Systems, 1HH12)

(b) Significant condensation (Nozzle: Spraying Systems, 1HH12)

Fig.IV-20 Full cone swirl nozzle spray with and without condensation (Results of Sandoz et.al.[31])

lengths are assumed. The lengths of the sheet portion are assumed to be 5 and 10 mm respectively for Nozzle #3. The straight lines were drawn after the breakup assuming that the velocity and direction of the large drop-lets will be the same as the sheet value at the breakup point. It can be seen from Fig. IV-21 that the breakup length plays an important role on the final shape of the spray. This is why, in Fig. IV-15, the water spray with condensation has a larger area of coverage compared to the case of non-condensation. The breakup length is an important parameter in determining the spray shape.

Although, breakup of liquid sheets have been studied by numerious researchers [11-17, 51-53], the breakup length cannot be predicted analytically. It depends on the flow conditions for a given nozzle as well as the type of the nozzle. In the present research, a number of experiments were performed under experimental conditions listed in Table IV-3 to determine if a correlation can be obtained from the experimental data in nondimensional form. The results obtained by examining 425 frames of pictures with 5 different types of nozzles are shown in Fig. IV-22. A correlation is obtained with the three non-dimensional groupings, i.e., the Weber number, the Jakob number and $L/\sqrt{A_o}$. The following equation was fitted to the experimental data:

$$\frac{L}{\sqrt{A_o}}\left[1 + C_1 Ja^{C_2} e^{-C_3(We - C_4)^2}\right] = C_5 We^{C_6} \qquad (39)$$

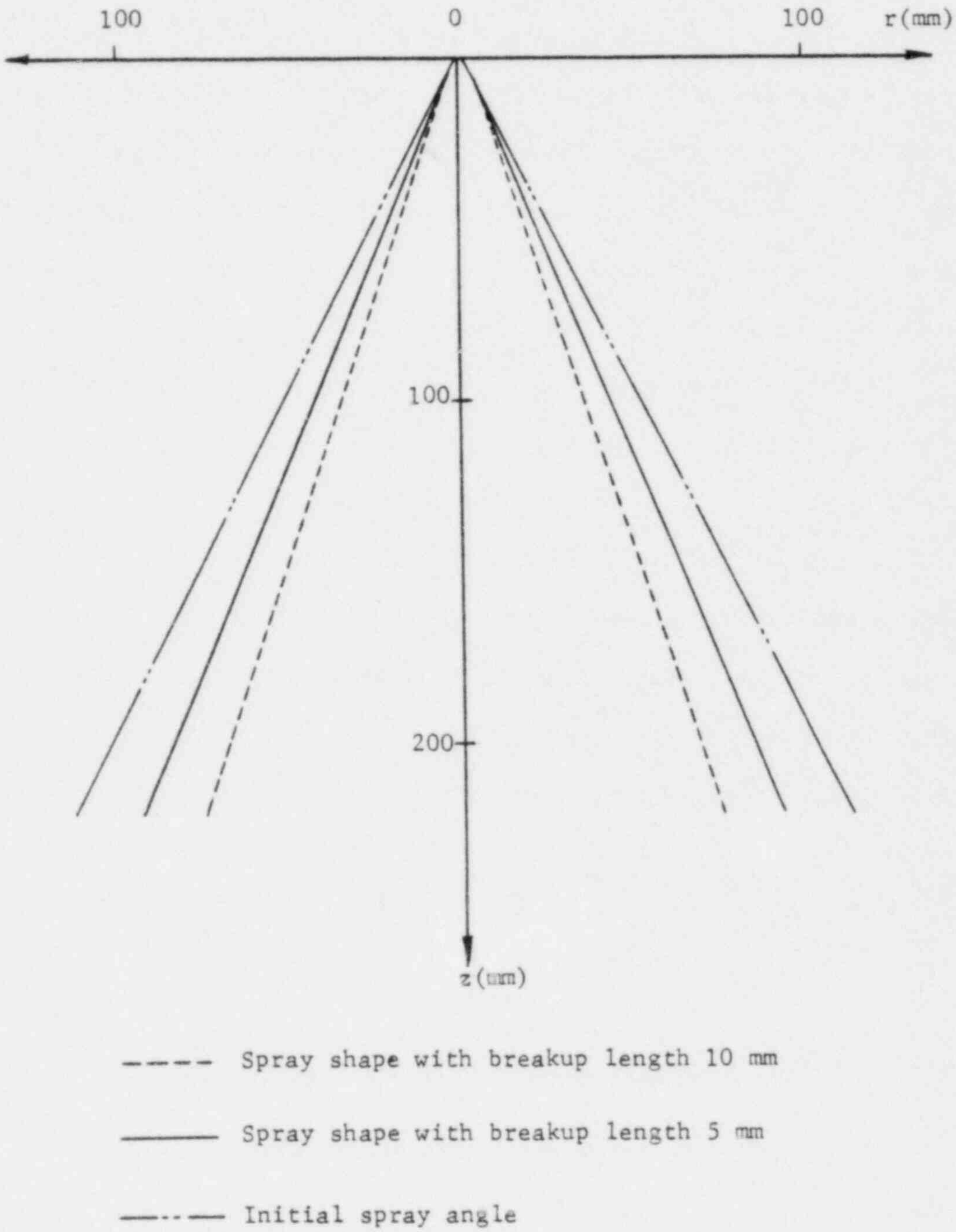

Fig.IV-21 Effect of sheet length on the spray shape (Nozzle #3, Q = 6.3 ml/sec)

Nozzle #	Environment (1 atm)	Flow rate (ml/sec)	Initial water temperature, T_{Lo} (°C)					
			10	20	35	50	65	80
1	Air	3.52		x				
	Steam	3.52		x				x
2	Air	3.52		x				
		4.40		x				
		6.30		x				
	Steam	3.52		x				x
		4.40			x		x	
3	Air	2.67	x	x*	x*	x*	x*	x*
		3.52	x	x	x*	x*	x*	
		4.00		x				
		4.40	x	x	x*	x*		
		5.25	x					
		6.30	x	x				
		7.83	x	x				
		9.40	x	x	x			
		11.10	x	x				
		12.50	x	x				
		13.40	x					
		14.90	x	x				
	Steam	2.23		x		x		x
		2.67		x		x		x
		3.10		x	x	x	x	x
		3.52		x		x		x
		4.00		x	x	x	x	
		4.40		x	x	x	x	
		5.25		x		x		
		6.30		x	x	x		
		9.40			x			
4	Air	5.25	x					
		6.00	x					
		6.60	x					
		7.20	x					
		7.83	x					
		8.50	x					
	Steam	4.40	x					
		5.25	x			x		
5	Air	7.20	x					
		7.80	x					
		8.20	x					
		8.60	x					
		8.80	x					
		9.10	x					
		9.40	x					

* Formation of water bell

Table IV-3. Test conditions for experiments on breakup and spray shape (2 - dimensional photographs taken with pulsed laser)

where,

$C_1 = 6.55$

$C_2 = 0.714$

$C_3 = 3.02 \times 10^{-6}$

$C_4 = 475$

and if $W_e < 750$ $C_5 = 2.47$

$C_6 = 0.29$

$W_e > 750$ $C_5 = 820$

$C_6 = -0.58$

The constants were chosen for the best-fit curve to the data points by nonlinear least square method. For the poppet type of nozzle, the Weber number is based on the equivalent diameter (or hydraulic diameter). The subcooling effects between spray water and steam are expressed as Jakob Number, $C_p \Delta T/\lambda$, and the breakup length is divided by the square root of the flow area for non-dimensionalization. In the case of poppet type nozzle, the size of the poppet must be taken into account as well as the gap between the poppet and the orifice. For the single hole nozzle, without the poppet, this dimension is directly proportional to the orifice diameter. The results, seen in Fig. IV-22, were obtained for the Weber number ranging from 30 to about 5000 and initial spray angle of 40-60°. One finds that the breakup occurs earlier in steam environment than in an air environment, which means the condensation plays an important role on the breakup of water sheet. In Fig. IV-15 there are two photographs which clearly shows the effect of condensation on the breakup length. However, if the liquid velocity (or Weber number) is large, the breakup length in air also is very short and it is difficult to measure the difference between air and steam environment. In Fig. IV-23, observations of breakup length by Sandoz [54] and modified results of Huang [52] are plotted for comparison. In case of Huang, the water sheet was formed by two jets impinging from opposite directions. Thus, in Fig. IV-23, his original results were reduced in half since the water flow rate (and water sheet thickness) is twice as large as for a single liquid jet. Huang's experiments covered the Weber number range of 100 to 40000. His results show the maximum valve of breakup length to occur at Weber number between 800 to 1000 - which agree with our maximum value. However his results differ from ours by a factor of about 2. This difference, we think, may be due to the entirely different way the water sheet is formed. According to Sandoz, the breakup length of water spray observed is 5 ~ 10 orifice diameters with Weber numbers ranging between 4000 ~ 160000. Her observations are in agreement with the extrapolation of our data within a factor of 2. Her sheets are probably in turbulent range whereas ours are laminar, which may explain the factor of 2 difference. If Weber number is taken as defined by Taylor [51], $We_T = 2\sigma/\rho_L V_{Lo}^2 d$, the We_T in our experiments

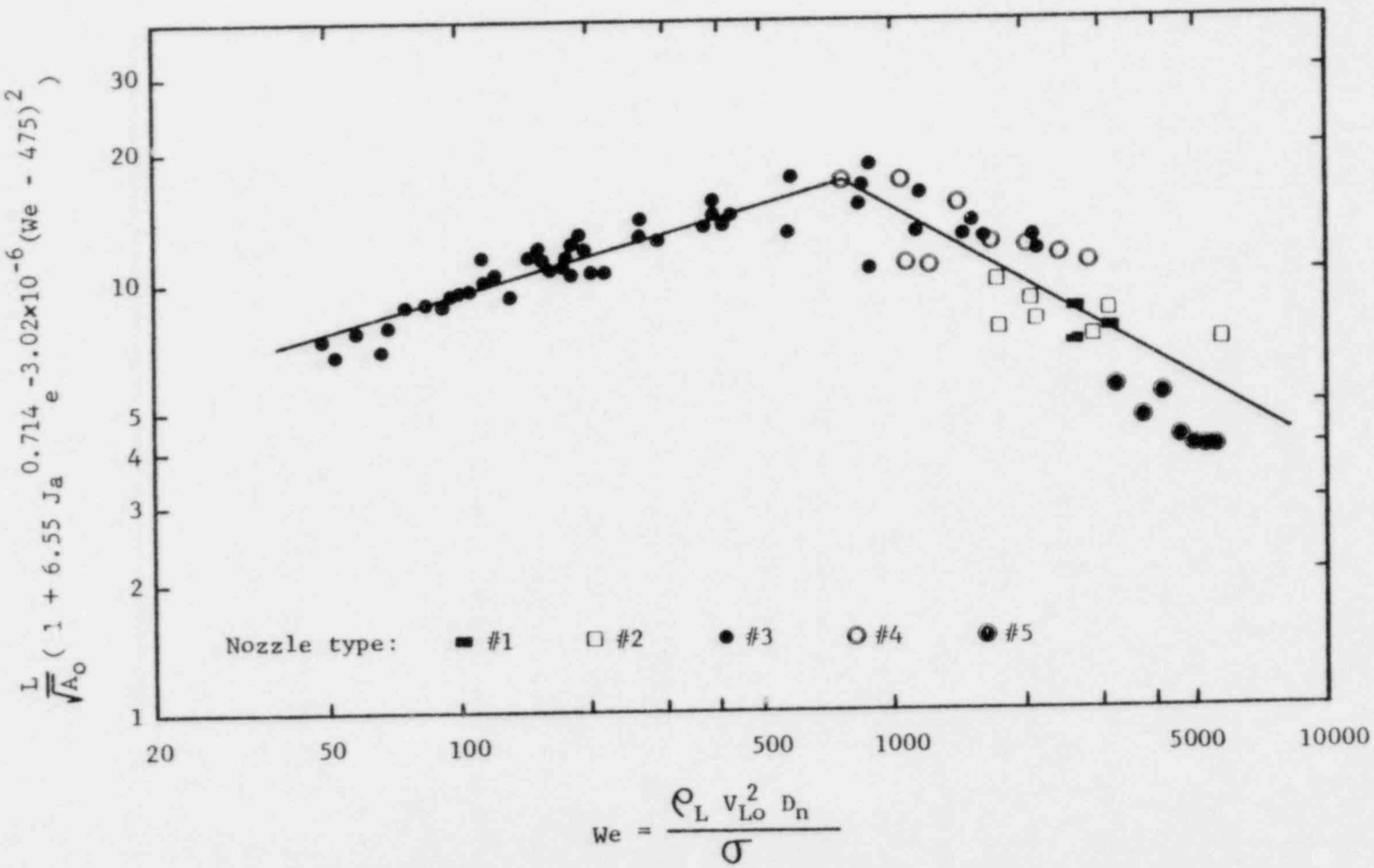

Fig.IV-22 Breakup length of the liquid sheet as function of Weber number and Jakob number ranges from 0.01 to 0.26. Taylor gives an upper limit on the sheet length which is $We_T = 1$. This is certainly true for our experiments. Knowing the breakup length, the shape of the spray can be obtained using the analytical model presented in Chapter II. Figures IV-24,25 show the calculated shape of the spray - both sheet and droplets taken into account. Plots were made for a wedge shaped volume having a 5 degree angle (in the azimuthal direction) and drop size of 50 micron increments. The method of plotting is the same as described in Fig. IV-11,12. That is, one side of the figure (Number distribution) shows the position of each droplet in space and the other side (Volume distribution) shows the relative volume distributions in space. The droplet velocity and temperature at breakup point are taken from the values of water sheet at breakup. As can be seen from Fig. IV-24, larger droplets remain at the edge portion of the spray outline; whereas the smaller droplets deflect inwards. This can be judged by the relative density of points in Number distribution and Volume distribution of Fig. IV-24. It is important to note that the outline shape does not change significantly after breakup. Therefore, as seen in Figs. IV-24,25, the shape of the spray is primarily determined by the sheet portion of the spray. Figure IV-26, shows the water spray injected into saturated steam environment with small subcooling. The outline of its shape is very similar to the case of water sprayed into an air environment (Fig. IV-24). In order to substantiate the space distribution of droplets as in Figs. IV-24,25,26, a simple experiment was conducted. Figure IV-27 shows the schematic picture of experimental set up. Nozzle #3 was installed in open space (not the test chamber), and droplets were

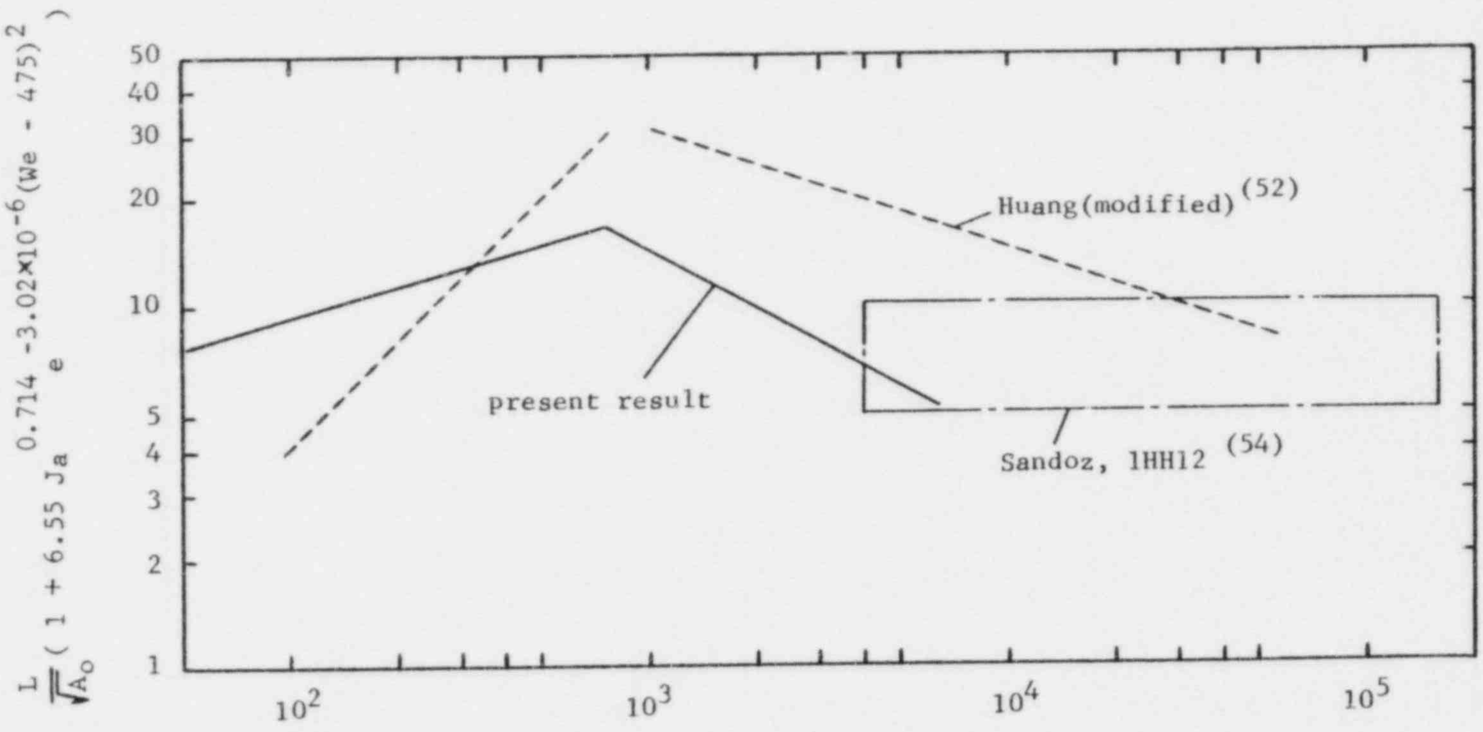

$$We = \frac{\rho_L V_{Lo}^2 D_n}{\sigma}$$

Fig.IV-23 Comparison of breakup length with other data

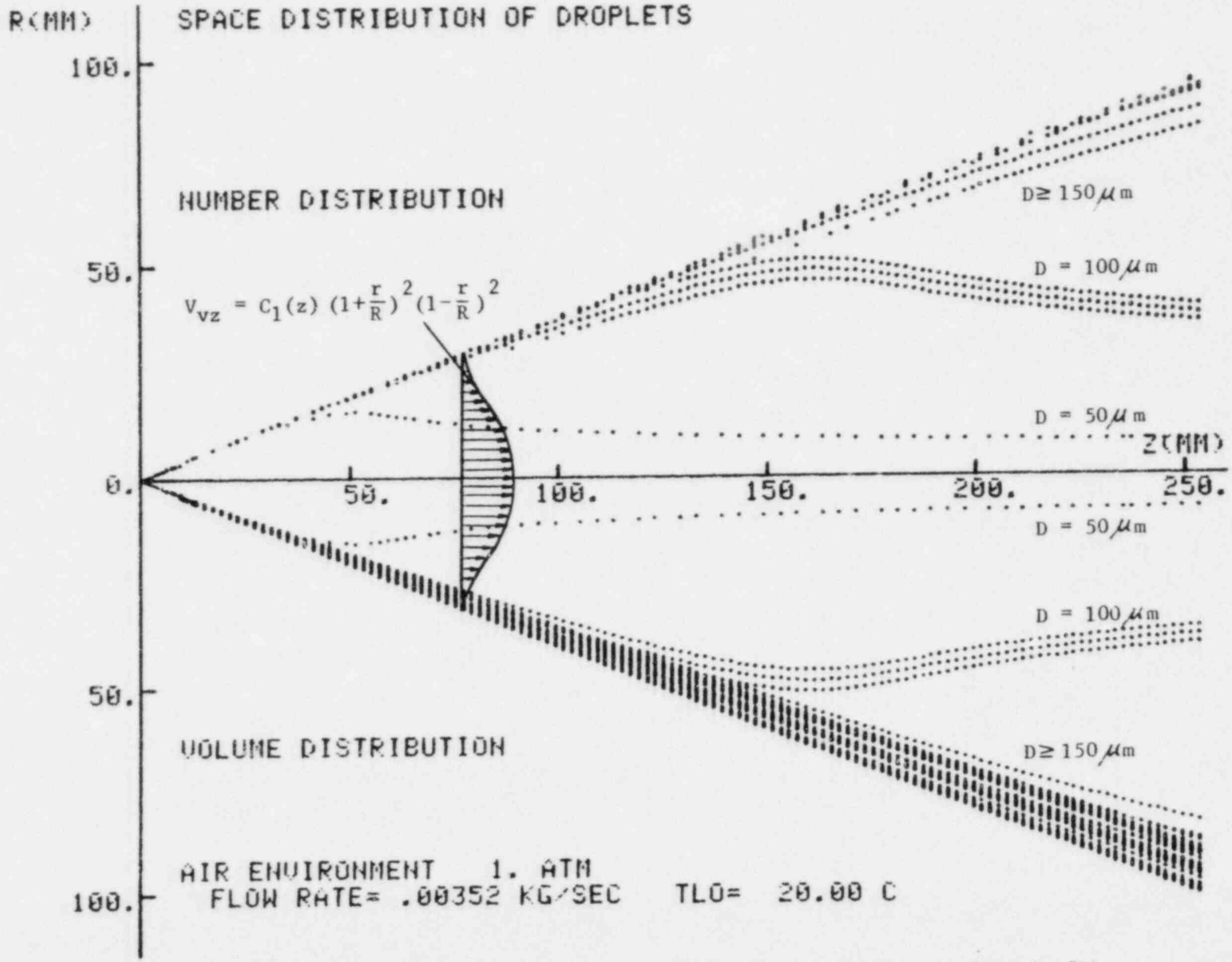

Fig.IV-24 Shape of the spray both sheet and drop taken into account (Nozzle #1)

06

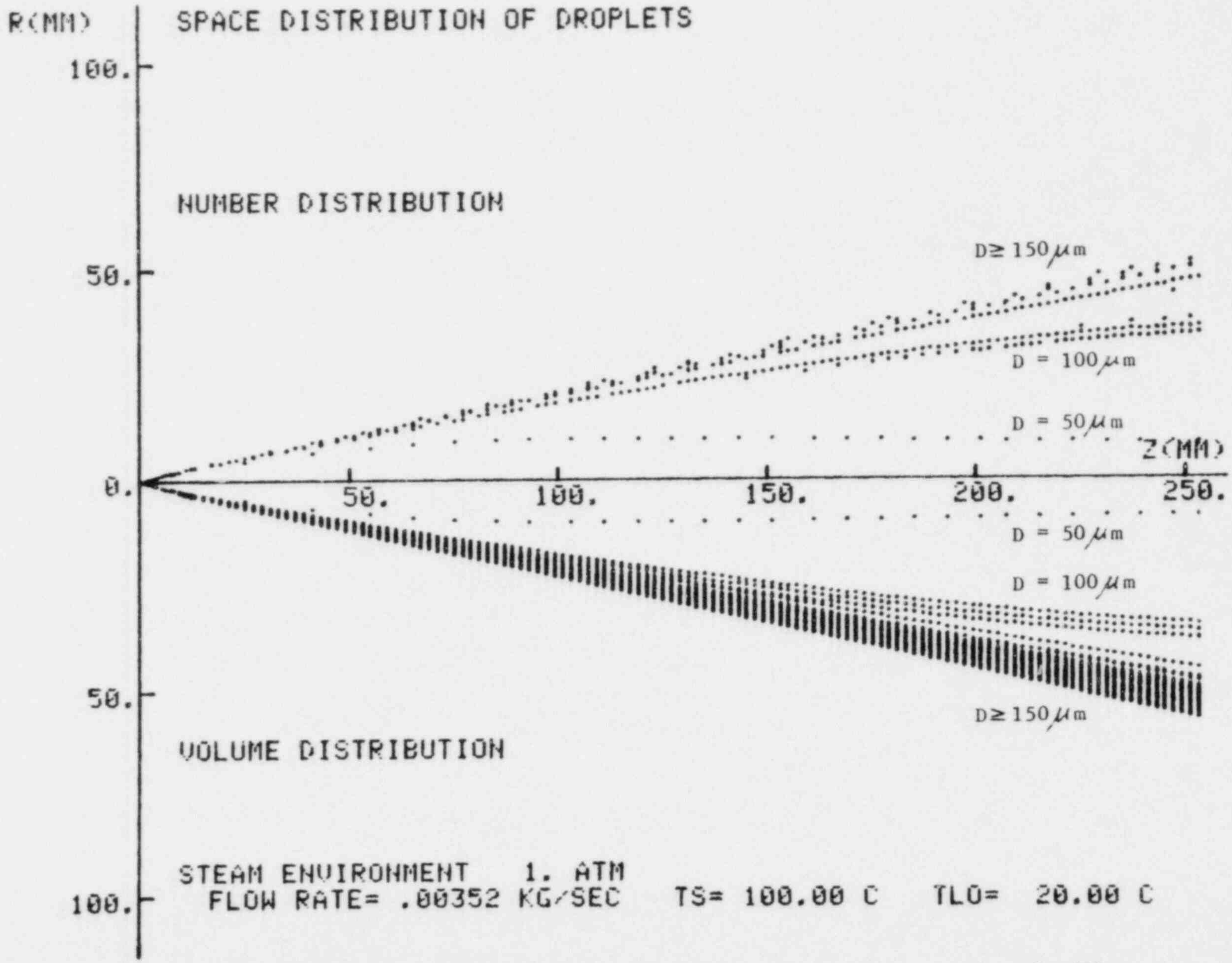

Fig. IV-25 Shape of the spray both sheet and drop taken into account (Nozzle #1)

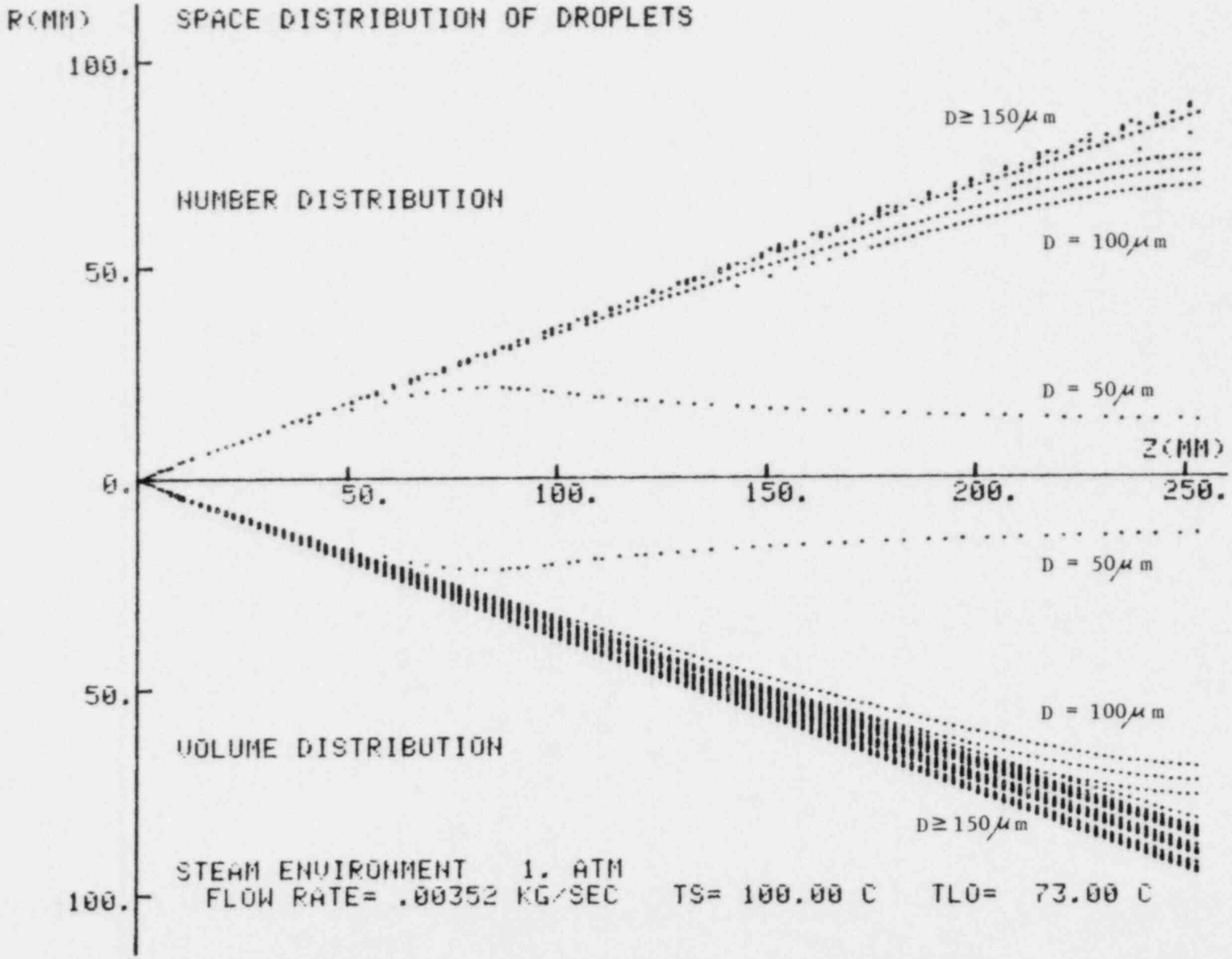

Fig. IV-26 Shape of the spray both sheet and drop taken into account (Nozzle #1) collected by oil bath located at downstream. A shield is placed to collect the droplets at the desired portion of the spray. The axial position of the shield from the nozzle is 160 mm, and it is doubtful that it affects the spray pattern upstream. The cover to the shield was removed for about 1 second when the shield was near the edge of the spray. When the shield was along the centerline the cover was removed for about 10 seconds. With these collection times, a proper number of droplets were collected with the oil bath at the center and edge portion of the spray. Photo-graphs of the oil bath were taken - see Fig. IV-28. As predicted, the droplets collected at the center portion are much smaller than the droplets collected at the edge portion. This droplet collecting experi-ment was not done for the water spray in steam environment; because of limitations on the size of the test section. In addition, it would be difficult to remove and cover the shield inside the test chamber. There is no reason to suspect the droplets in a steam environment would act substantially different than in an air environment. Thus, the space distribution of droplets confirmed in an open air environment substan-tiates, at least qualitatively, the motion of the droplets predicted by the analytical model.

Figure IV-29 shows the calculated results of temperature rise of spray water along the axial direction. As is seen, a major portion of the heat transfer occurs in the sheet portion (the slope of the temperature rise is much steeper in sheet portion). Weinberg [28] and Takahashi et al. [33] measured the spray water temperature by experiments, and their results are also plotted in Fig. IV-29. Their results show much sharper increase in temperature of water spray compared with

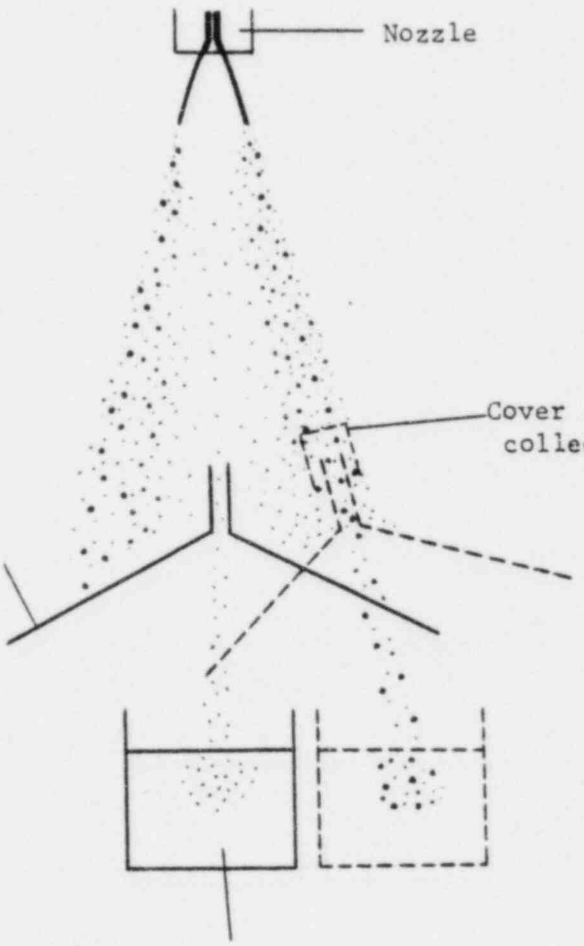

Fig. IV-27 Schematic configuration of droplet collecting system

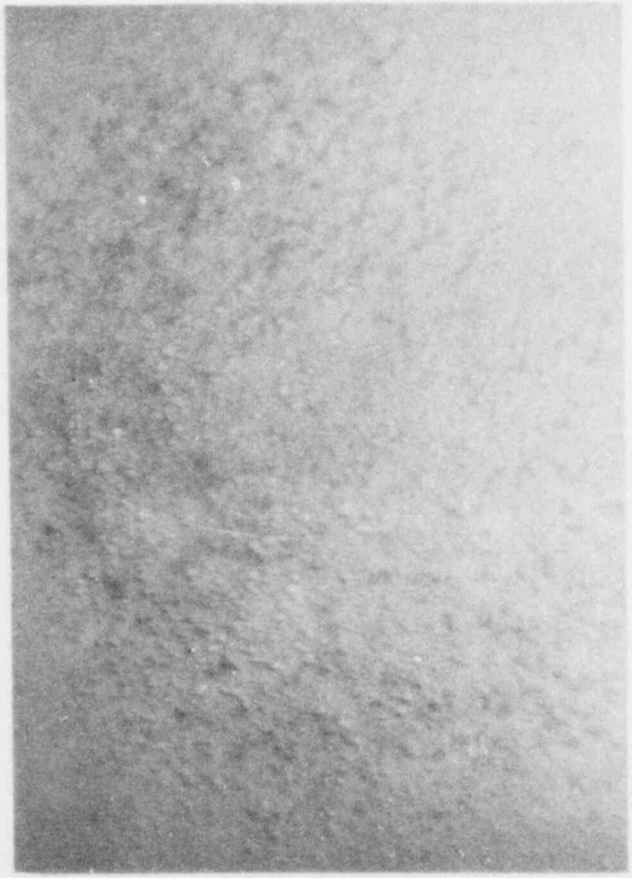

Center portion

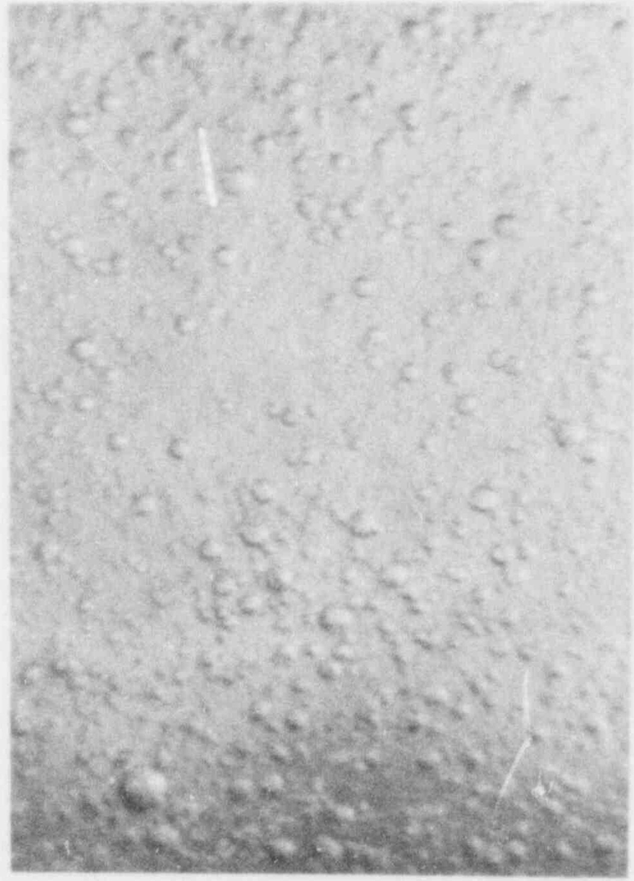

Edge portion

Fig.IV-28 Typical photograph of the droplets collected at center and edge portion of the spray our calculated results. The spray angle of Weinberg and Takahashi sprays were much greater (85-90°) than the spray angles for nozzles #1, #2, #3 (40-60°). If we carry out the temperature calculations for 90° angle spray and use Eq. (39) to determine the breakup length, the results shown in Fig. IV-29 are in agreement with Weinberg and Takahashi. In addition, there are some comments concerning the measurements of Weinberg and Takahashi-Masuda that seem appropriate. Weinberg used a thermocouple to measure the spray water temperature. From our sprays, the water sheet thickness is so thin, that it would be difficult to immerse the thermocouple tip in the water. In addition, as seen in Figs. IV-16, 17, the spray sheet is rippled; thus the thermocouple would be frequently exposed to the steam environment. Takahashi collects the water in a pool and then measures the temperature of the water flowing from the bottom of the pool. An adiabatic screen is floated on the surface of the water pool to prevent direct heat transfer between the steam and the pool water. It is assumed that the temperature of the outflow of water from the pool is the spray water temperature. By varying the pool level, the temperature of the spray at various distances from nozzle exit is measured. This method seems questionable, because of the assumption of an adiabatic screen on the pool surface. In both the thermocouple measurements and the pool measurements, the experimental values may give high readings. Also, in case of Weinberg and Takahashi, the flow regime may be turbulent; thus the heat transfer will be greater, leading to a higher temperature rise than our computed values. Indeed, their values lie above the computed curve in Fig. IV-29.

3. Air/Vapor Flow Pattern

It is important to confirm the validity of air (or vapor) flow pattern that was assumed in the proposed model (Fig. II-1,2). It is difficult to measure the pressure or velocity of vapor inside the spray by conventional pitot tubes because of the limited space and the formation of condensate in the probe. It was noted, however, that when a small wire was inserted inside the sheet region, a droplet of water is formed on the wire from the surrounding fog. This droplet is located at a fixed point relative to the breakup region. A typical picture of this phenomena is shown in Fig. IV-30. If the wire is moved vertically downward below the breakup zone, the existing droplets run down the wire. This is shown schematically in Fig. IV-31. Further evidence of the flow pattern is obtained when a small wire with a 90° bend is inserted in the sheet region of the spray (above the breakup region). A droplet forms on the horizontal portion of the wire, with the droplet resting on the top surface of the wire. If the wire is lowered below the breakup zone, the droplet rests on the bottom surface of the wire. This is also shown schematically in Fig. IV-31. These results indicate that the gas flow along the central portion above the breakup zone is upwards; below the breakup zone is downwards. Photographs were taken of the droplet for the various experimental conditions. Experimental result shows, as in Fig. IV-31, the higher the flow rate the larger the droplet size and close to the nozzle exit. This means the internal air (or vapor) flow is faster and sheet length is shorter at higher flow rate. Figure IV-32 shows certain relation between the position of the droplet and breakup point for Nozzle #3 (poppet nozzle). It was difficult to obtain the

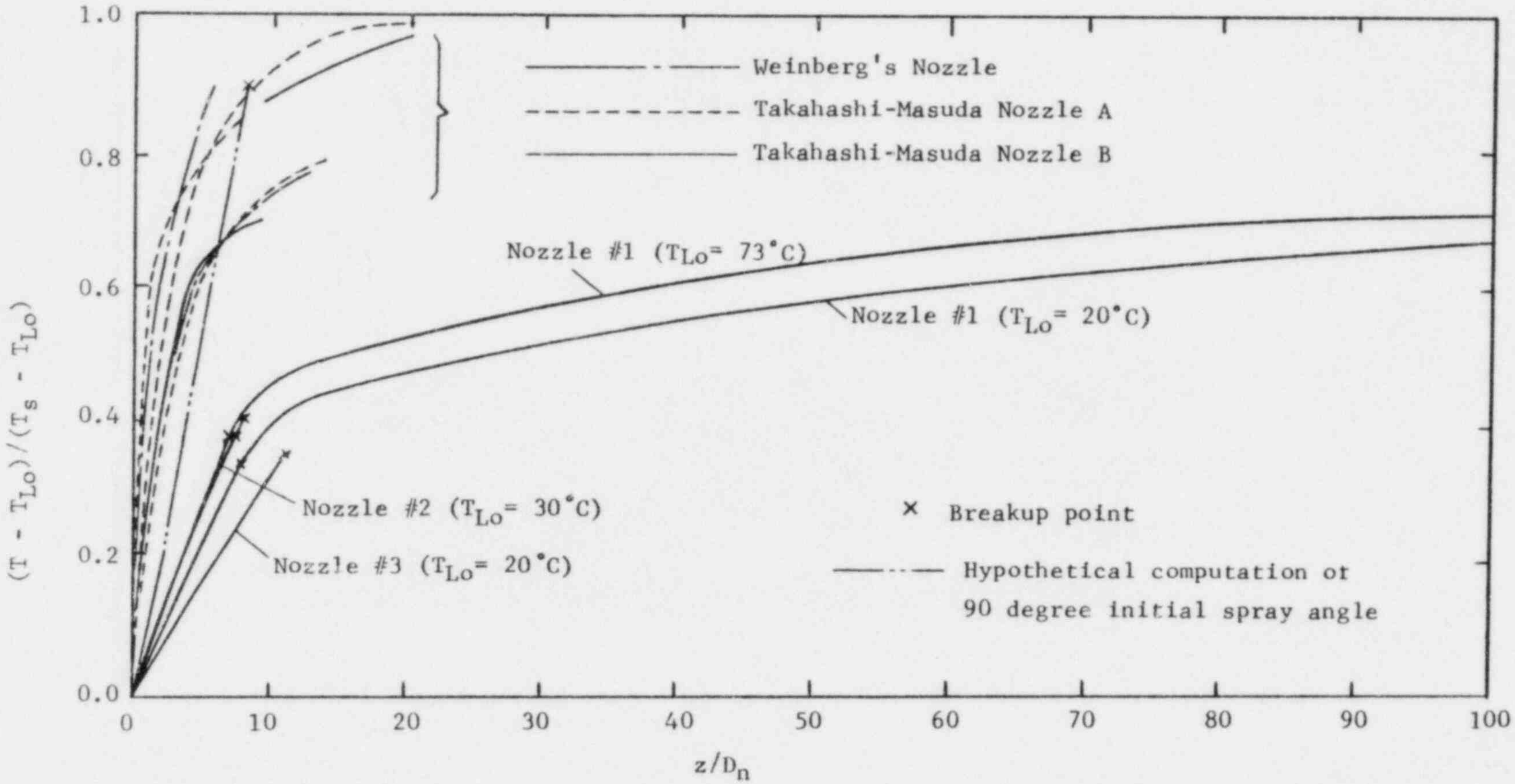

Fig. IV-29 Temperature variation of water spray along axial direction

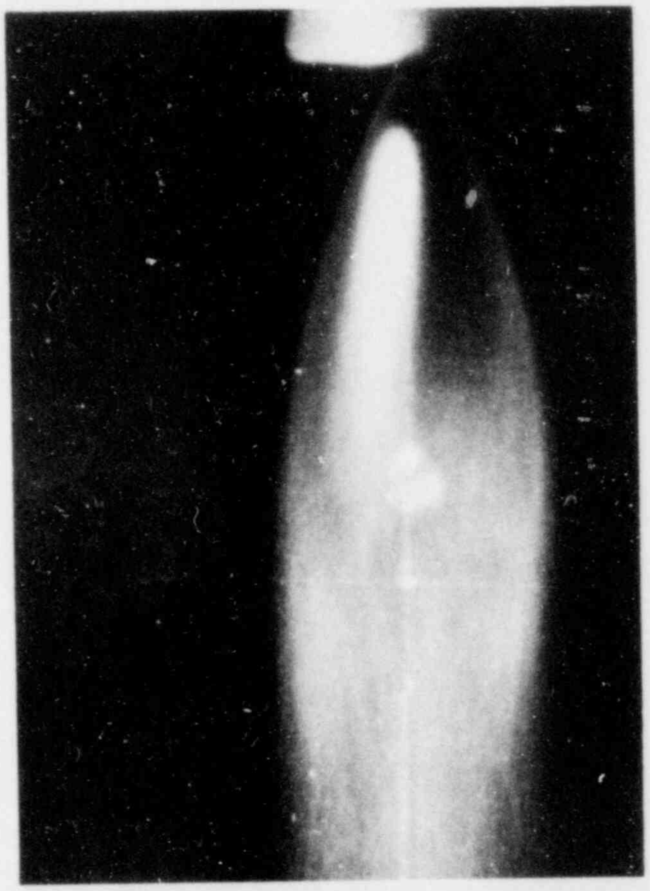

Q = 7.0 ml/sec, Air 1 atm
(Nozzle #3)

Fig.IV-30 Formation of a droplet on a vertical wire inserted inside the spray sheet quantitative position of the droplet as Fig. IV-32 for all ranges of experimental conditions. At the very low flow rates, wetting of the wire reduces the stable formation of the droplet on the wire, and at the very high flow rates, the sheet length becomes very short, making it difficult to form a stable droplet. In addition, oscillation of the droplet makes the measurement of its position difficult. However, at least qualitatively, the experimental results give evidence that supports the flow pattern assumed in Figs. II-1 and 2.

4. Effect of Assumed Vapor Velocity Profile

It was stated earlier that the vapor velocity profile assumed in the droplet region had little effect on the spray outline shape. Figures IV-24,33,34 show the results for 3 different assumed vapor velocity profiles. In Fig. IV-33, a vapor velocity profile is assumed which is zero in the center and maximum near the outer radius of the spray; in Fig. IV-34, a uniform vapor velocity profile is assumed; and in Fig. IV-24, a velocity profile that is maximum in the center is assumed (Eq. (28)). As is seen, these different vapor velocity profiles have a negligible effect on the spray outline shapes.

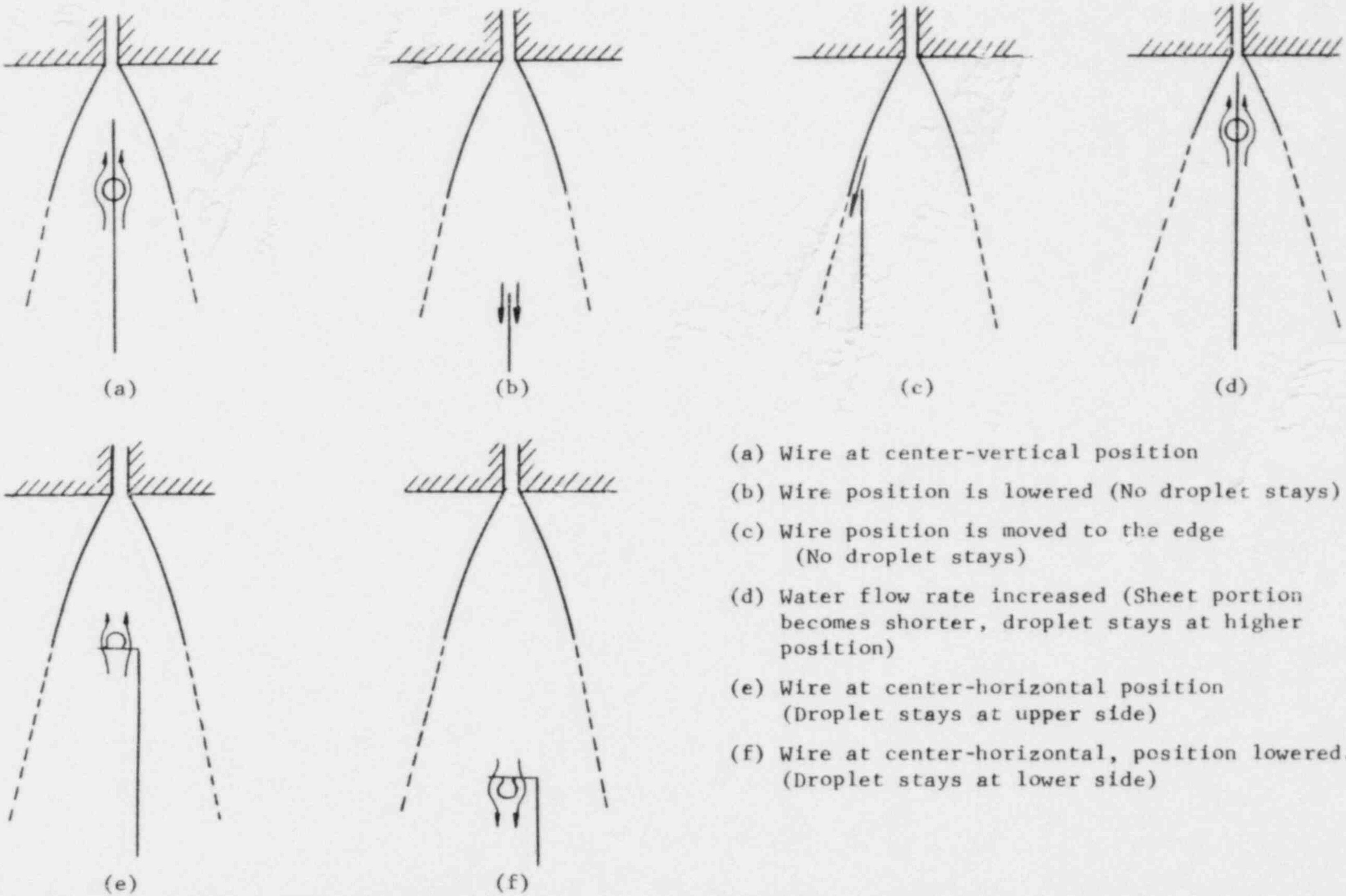

(a) Wire at center-vertical position

(b) Wire position is lowered (No droplet stays)

(c) Wire position is moved to the edge (No droplet stays)

(d) Water flow rate increased (Sheet portion becomes shorter, droplet stays at higher position)

(e) Wire at center-horizontal position (Droplet stays at upper side)

(f) Wire at center-horizontal, position lowered. (Droplet stays at lower side)

Fig. IV-31 Schematic diagram of experiments on Air/steam flow pattern

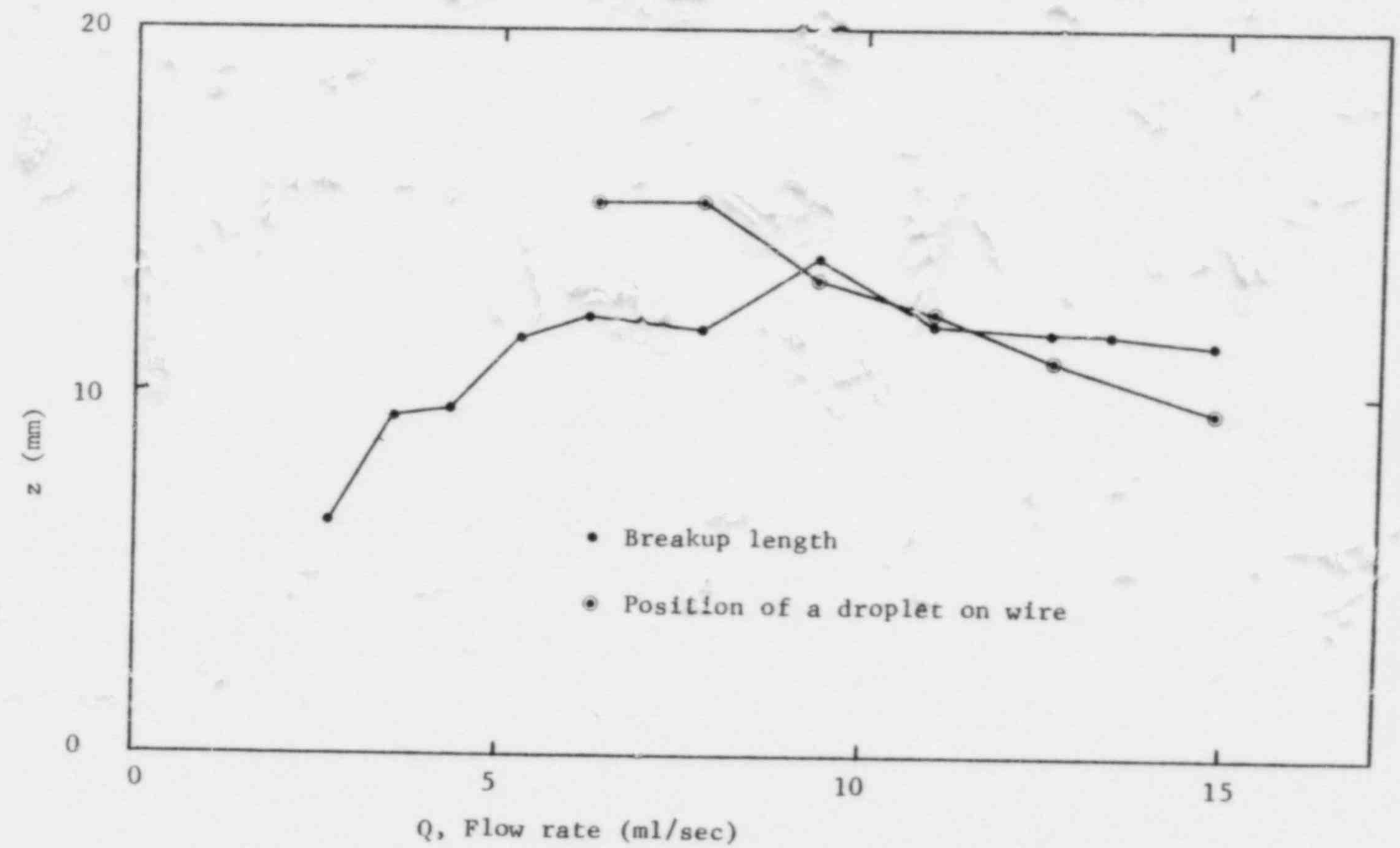

Fig.IV-32 Position of a droplet on the wire inserted inside of water sheet as function of flow rate (Nozzle #3, air 1 atm)

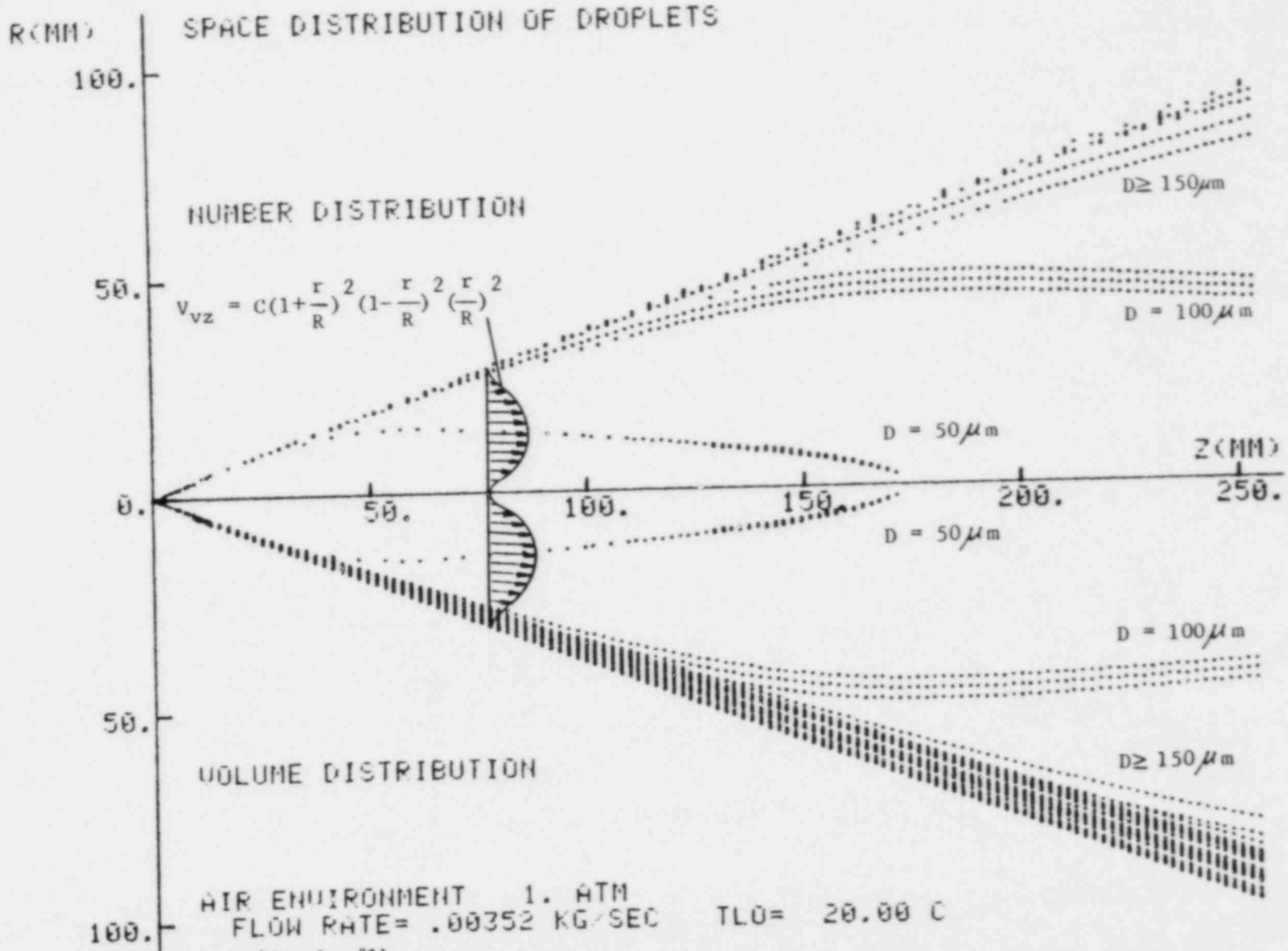

(Nozzle #1)

Fig.IV-33 Effect of assumed vapor velocity profile on the spray outline shape

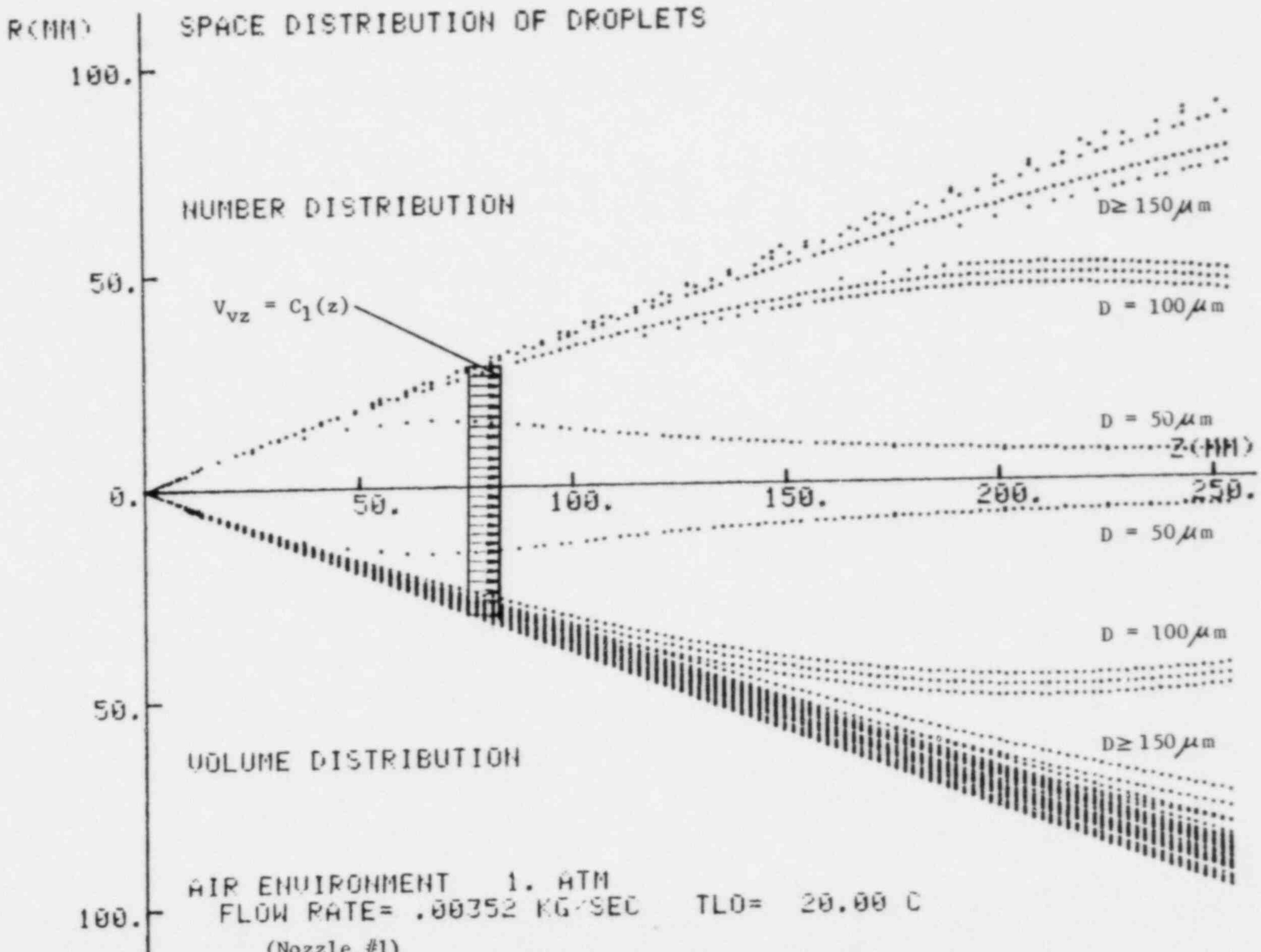

(Nozzle #1)

Fig. IV-34 Effect of assumed vapor velocity profile on the spray outline shape

V. CONCLUSION

From proposed model and experiments, it can be concluded that:

1. The spray outline-shape (or spray angle) is primarily determined by the shape of sheet portion and breakup length.
2. For our size sprays, most of the heat transfer occurs in the sheet portion of the spray. The spray angle contraction is mainly due to the lower pressure by condensation of steam within the sheet portion of the spray.
3. Breakup occurs earlier in case of condensation.
4. A correlation is obtained experimentally for breakup length in terms of the Weber number and the Jakob number.
5. In droplet portion, the small droplets tend to deflect inwards because of the entrainment of the vapor (or air).
6. Drop sizes become more uniform and smaller when ambient pressure and injection pressure increases.
7. Drop sizes are larger in a steam environment than in an air environment at same pressure and flow rate.
8. The outline shape of water spray injected into the steam environment with small subcooling temperature is similar to water spray injected into the air environment.

APPENDIX 1.

CALCULATION OF THE PRESSURE DIFFERENCE DUE TO CIRCULATION OF AIR

Here, the procedure follows the method of Parlange [44] to find out the air flow pattern inside the water sheet.

The shape of the water sheet can be obtained as

$$\frac{2\sigma}{\zeta} + \frac{2\sigma \cos \eta}{r} + \Delta P + g\rho_L d \sin \eta = \frac{V_{Lo}^2 \rho_L d}{\zeta} \qquad \text{(A-1)}$$

By definition of streamline for axisymmetric flow,

$$V_{vr} = \frac{1}{r}\frac{\partial \psi}{\partial z} \;, \quad V_{vz} = -\frac{1}{r}\frac{\partial \psi}{\partial r} \qquad \text{(A-2)}$$

where, ψ represents the stream function.

Also, from the definition of vorticity, ξ,

$$\begin{aligned} \xi &= \frac{1}{r}\left[\frac{\partial V_{vr}}{\partial z} - \frac{\partial V_{vz}}{\partial r}\right] \\ &= \frac{1}{r}\left[\frac{\partial^2 \psi}{\partial z^2} + \frac{\partial^2 \psi}{\partial r^2} - \frac{1}{r}\frac{\partial \psi}{\partial r}\right] \end{aligned} \qquad \text{(A-3)}$$

From the equation of motion, if the pressure term is eliminated,

$$V_{vr}\frac{\partial \xi/r}{\partial r} + V_{vz}\frac{\partial \xi/r}{\partial z} = \nu_a\left[\frac{\partial^2 \xi/r}{\partial z^2} + \frac{\partial^2 \xi/r}{\partial r^2} + \frac{3}{r}\frac{\partial \xi/r}{\partial r}\right] \qquad \text{(A-4)}$$

By Batchelor's theorem, if the streamline is closed, then the solution of (A-4) will be the constant, A. Moreover, the boundary layer thickness is usually very thin and most of the air flow can be considered as inviscid. Then from (A-3),

$$\frac{\xi}{r} = A = \frac{1}{r^2}\left[\frac{\partial^2\psi}{\partial z^2} + \frac{\partial^2\psi}{\partial r^2} - \frac{1}{r}\frac{\partial\psi}{\partial r}\right] \tag{A-5}$$

and the solution ψ for (A-5) should be obtained with the constant A obtained from boundary conditions.

No other conditions were imposed to obtain (A-5) except the condition of axisymmetry and closed streamline, and there can be numbers of analytical function forms available. Among them, the appropriate function form can be found out as,

$$\psi = \frac{Ar^2}{8 + 16ab/3}\left[r^2(1 + ab - za) - \frac{4}{3}az^2(b - z)\right] \tag{A-6}$$

with A, a, b chosen appropriately. Here, ψ=0 denotes the shape of the water sheet. Once ψ is obtained, the velocity of air can be obtained from (A-2) and the pressure inside the water sheet can be calculated as,

$$\begin{aligned}\Delta P &= P_\infty - P_z \\ &= \frac{1}{2}\rho_a V_a^2\end{aligned} \tag{A-7}$$

where, at ψ=0,

$$V_a^2 = V_{vr}^2 + V_{vz}^2$$

Then with Eq. (A-1), the shape of the water sheet can be calculated iteratively.

As a sample calculation for the poppet type nozzle (Nozzle #3) with the flow rate 6.3 ml/sec and surface tension 57.0 dyne/cm (from measurement as in Appendix 2), the constant b (stagnation point) and the velocity of air were determined from the experiment as,

$$b = 0.025 \text{ m}$$

$$V_{vz} = \frac{Aa}{3 + 2ab} z^2(b-z) \cong -4.0 \text{ m/sec at} \quad \begin{matrix} z=0.0153\text{m} \\ r=0 \end{matrix}$$

Then with iteration from (A-1) to (A-7), the other constants a and A is determined as

$$a = 12.72$$

and

$$A = -5.04 \times 10^5$$

where, the gravity effect neglected. Therefore,

$$\psi = -5.2 \times 10^4 \, r^2[r^2(1.318 - 12.72z) - 16.96z^2 \, (0.025 - z)]$$

In Fig. A-1, the outermost line indicates the calculated results from Eq. (A-1) with $\Delta P=0$, and also the experimental results show good agreement. The maximum pressure difference occurs at about the maximum point of r of the streamline $\psi=0$, which is about 4 m/sec, and the pressure difference will be

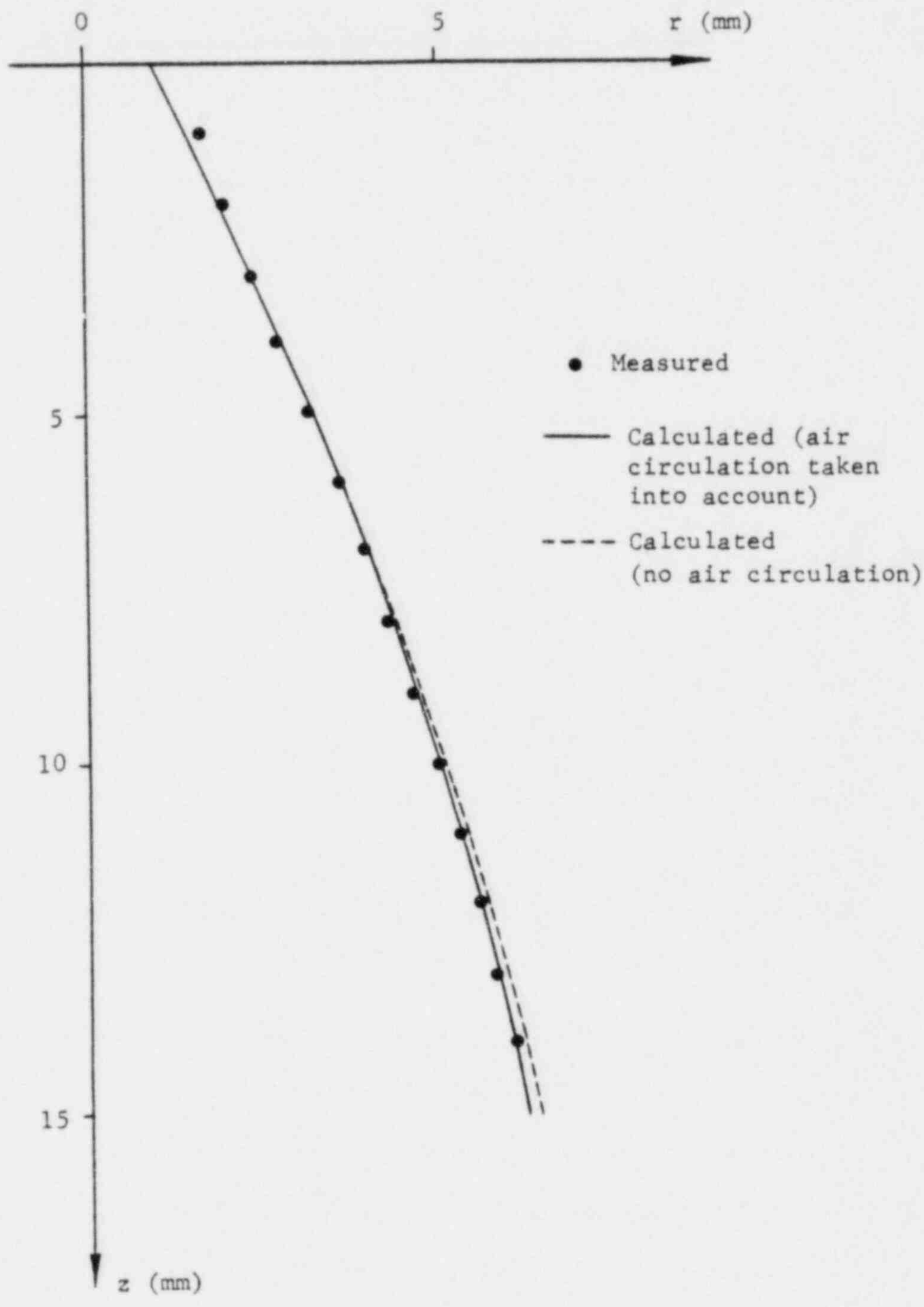

Fig.A-1 Effect of internal air flow on the shape of water sheet

$$\Delta P = \frac{1}{2}\rho_a V_a^2 = \frac{1}{2} \times 1.22 \times 4^2 = 10 \text{ N/m}^2 \sim 1.0 \text{ mm } H_2O$$

which is very small. Hence, for this case, the shape of water sheet calculated from Eq. (A-1) with pressure difference neglected gives very good agreement with the case of internal air circulation and experimental results.

APPENDIX 2

DETERMINATION OF THE SURFACE TENSION

In present experiments in Chapter III, tap water is used. Usually, it is known that the surface tension of the tap water is much lower than the pure water and there might be error if the surface tension data taken from the tables in most texts of fluid mechanics. Therefore, it was decided to measure the surface tension of the tap water which was used for the experiments. Basically, the surface tension were decided by measuring the dimensions of water bell made by poppet type nozzle (Nozzle #3). The method of Parlange [44] was used as Appendix 1 to determine the surface tension. Equations (A-1) - (A-5) is also directly applicable here. However, because of different geometry by closing up of water sheet to form a water bell, the boundary condition should be different. By Parlange, the boundary condition will be

$$\int_{\psi=0} r^2 V_a V_{Lo}^2 dS = \int_{\psi=0} r^2 V_{Lo}^3 dS \qquad \text{(A-9)}$$

and integration is done along the $\psi=0$ of Eq. (A-5), which includes the axis and outer shape of the water bell. Here, the gravitational force is going to be neglected in Eq. (A-1). Actually, Eq. (A-5) and (A-1) are coupled with boundary condition (A-9), and it is not easy to solve. Therefore, an approximate shape of the water bell which satisfies Eq. (A-5) to get the air flow pattern inside was chosen, and decoupled from Eq. (A-1). This gives also a good accuracy. The shape of the ellipsoid was chosen as an approximate solution of Eq. (A-1) as follows:

$$\psi = \frac{Ar^2}{8/a^2 + 2/b^2}\left[\left(\frac{r}{a}\right)^2 + \left(\frac{z}{b}\right)^2 - 1\right] \tag{A-10}$$

where, a corresponds to the maximum radius of water bell and b corresponds to the half length of the water bell, which can be mesured directly from the photographs of the water bell (Fig. A-2). If the water sheet velocity, V_{Lo}, is taken as constant, the constant A is decided by the boundary condition (A-9) as follows:

$$\begin{aligned} V_{vr} &= \frac{1}{r}\frac{\partial\psi}{\partial z} \\ &= \frac{Arz}{4(b/a)^2 + 1} \end{aligned} \tag{A-11}$$

$$\begin{aligned} V_{vz} &= -\frac{1}{r}\frac{\partial\psi}{\partial r} \\ &= -\frac{A}{4/a^2 + 1/b^2}\left[2\left(\frac{r}{a}\right)^2 + \left(\frac{z}{b}\right)^2 - 1\right] \end{aligned} \tag{A-12}$$

and if we put

$$U_r = \frac{rz}{4(b/a)^2 + 1}$$

$$U_z = -\frac{1}{4/a^2 + 1/b^2}\left[2\left(\frac{r}{a}\right)^2 + \left(\frac{z}{b}\right)^2 - 1\right]$$

then, (A-11) and (A-12) will be

$$V_{vr} = A\,U_r \tag{A-13}$$

$$V_{vz} = A\,U_z \tag{A-14}$$

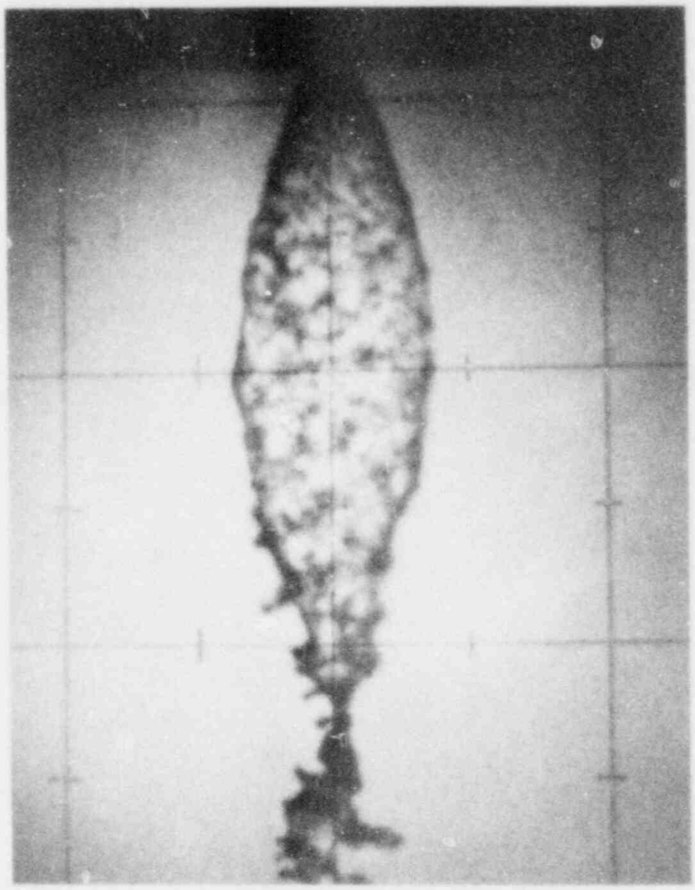

Fig. A-2   Typical shape of the water bell (Nozzle #3) and from (A-9), (A-13), (A-14),

$$A = \frac{V_{Lo} \int_{\psi=0} r^2 dS}{\int_{\psi=0} r^2 \sqrt{U_r^2 + U_z^2}\, dS} \qquad \text{(A-15)}$$

Once A, a, b are obtained, then it is possible to get the pressure difference by the circulation with Eq. (A-7), (A-11), (A-12). Then Eq. (A-1) can be solved with the flow condition given to obtain the surface tension. The surface tension was determined as in Fig. A-3 by examining 36 frames of photographs of the water bell, and a straight line was drawn by the least square method. The dotted line at the upper part of data points is the surface tension for the pure water. Therefore, the surface tension of air/water can be expressed as a function of water temperature as:

$$\sigma = 60.28 - 0.1657\, T_{Lo} \qquad \text{(A-16)}$$

where, σ is surface tension in dyne/cm and T_{Lo} is water temperature in ^{o}C. In order to check the correctness of this relation, the other measurements were done. That is, by measuring the meniscus shape (height and width) of the water surface at the vertical wall partly immersed in water bath, the surface tension can be obtained. These results are also plotted in Fig. A-3, and are also shown in good agreement with the data obtained by the water bell.

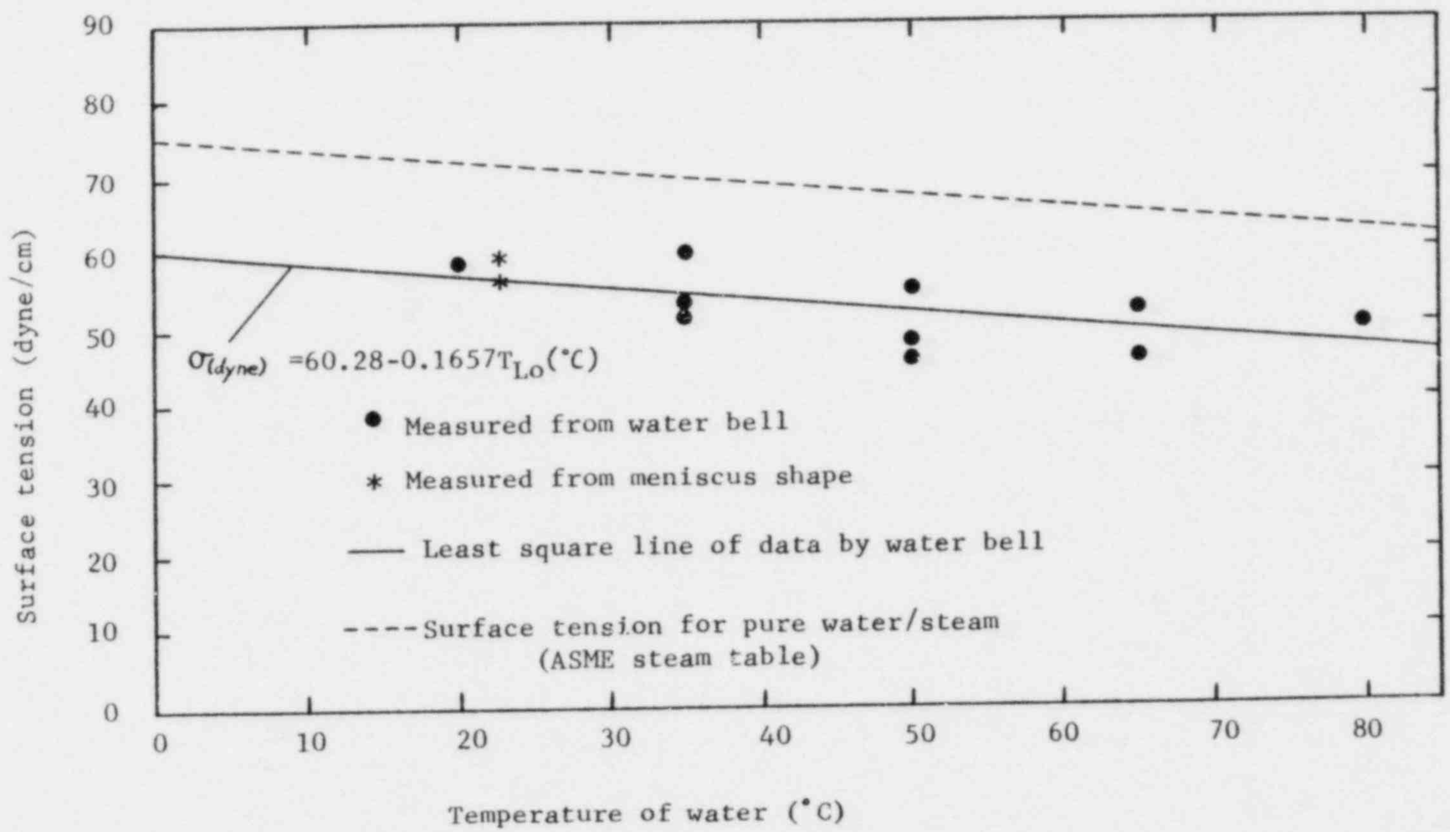

Fig. A-3 Surface tension of Air/Tap-water as function of temperature

APPENDIX 3

DERIVATION AND SOLUTION OF HEAT BALANCE EQUATION OF WATER SHEET

As seen in Fig. II-5, a energy balance over an element of length dS in the flow direction and width $d\phi$ normal to the flow direction gives, with d << r,

$$\dot{m}C_pT - k\frac{\partial T}{\partial \phi} 2\pi r\, dS = \dot{m}C_pT + \frac{\partial}{\partial S}\left(\dot{m}C_pT\right)dS - k\frac{\partial T}{\partial \phi} 2\pi r\, dS - \frac{\partial}{\partial \phi}\left(k\frac{\partial T}{\partial \phi} 2\pi r\, dS\right)d\phi \qquad \text{(A-17)}$$

then Eq. (A-17) will be

$$\frac{\partial}{\partial S}\left(\dot{m}C_pT\right)dS = \frac{\partial}{\partial \phi}\left(k\frac{\partial T}{\partial \phi}\right)2\pi r\, dS\, d\phi \qquad \text{(A-18)}$$

The major advantage of choosing the element as above is that we can have a convection term only in flow direction and only conduction has to be taken into account in normal direction. Here,

$$\dot{m} = 2\pi r\, d\phi\, V_{Lo} = \text{const}$$

since no flow crossing the streamline boundary. Therefore (A-18) will be

$$\dot{m}\, C_p \frac{\partial T}{\partial S} = 2\pi r\, d\phi\, k \frac{\partial^2 T}{\partial \phi^2}$$

or

$$2\pi r\, d\phi\, V_{Lo}\, \rho_L C_p \frac{\partial T}{\partial S} = 2\pi r\, d\phi\, k \frac{\partial^2 T}{\partial \phi^2}$$

This can be simplified as

$$V_{Lo}\frac{\partial T}{\partial S} = \alpha \frac{\partial^2 T}{\partial \phi^2} \qquad \text{(A-19)}$$

and boundary conditions will be

$$\begin{aligned} T(S,0) &= T_s \\ T(S,d) &= T_s \\ T(0,\phi) &= T_{Lo} \end{aligned} \quad (A\text{-}20)$$

which are Eq. (6) and boundary condition (7) in Chapter II.

Since V_{Lo} is assumed to be constant, (A-19), (A-20) can be rewritten as

$$\frac{\partial T}{\partial t} = \alpha \frac{\partial^2 T}{\partial \phi^2} \quad (A\text{-}21)$$

with

$$\begin{aligned} T(t,0) &= T_s \\ T(t,d) &= T_s \\ T(0,\phi) &= T_{Lo} \end{aligned} \quad (A\text{-}22)$$

The primary advantage of (A-21), (A-22) over (A-19), (A-20) is, we can handle the problem as non-steady one-dimensional conduction equation. Here, it should be mentioned that the water sheet thickness, d, and the distances between the streamlines, $d\phi$, are physically changing as S increases. Therefore, the solution of (A-21), (A-22) should be obtained numerically as follows. (If the water sheet thickness, d, is given as a function of S or t, the analytical solution can be obtained by coordinate transformation [27].)

Without loss of generality, d (and $d\phi$) is assumed to be constant for the short time segment, Δt. For the ith segment (Fig. A-4), Eq. (A-21), (A-22) will be, by normalizing,

$$\frac{\partial \bar{T}_i}{\partial \bar{t}_i} = \frac{\partial^2 \bar{T}_i}{\partial \bar{\phi}_i^2} \quad (A\text{-}23)$$

$$\bar{T}_i(\bar{t}_i, 0) = 0$$

$$\bar{T}_i(\bar{t}_i, 1) = 0 \qquad \text{(A-24)}$$

$$\bar{T}_i(0, \bar{\phi}_i) = \bar{T}_{i-1}(\bar{\theta}_{i-1}, \bar{\phi}_{i-1})$$

where,

$$\bar{T}_i = \frac{T_i - T_s}{T_{Lo} - T_s}$$

$$\bar{\phi}_i = \phi_i/d \qquad \text{(A-25)}$$

$$\bar{t}_i = \alpha t_i/d_i^2$$

$$\bar{\theta}_i = \alpha \Delta t/d_i^2$$

Here, t_i stands for the small time scale between t and t + Δt, and d_i stands for the thickness of the water sheet at ith segment. The non-dimensionalized length scale $\bar{\phi}_i$ ranges from 0 to 1 for all segments and it will be

$$\bar{\phi}_1 = \bar{\phi}_2 = \dots = \bar{\phi}_i = \bar{\phi} \;;$$

thus, the subscript i will be eliminated from the non-dimensionalized length scale, and (A-23), (A-24) will be

$$\frac{\partial \bar{T}_i}{\partial \bar{t}_i} = \frac{\partial^2 \bar{T}_i}{\partial \bar{\phi}^2} \qquad \text{(A-26)}$$

$$\bar{T}_i(\bar{t}_i, 0) = 0$$

$$\bar{T}_i(\bar{t}_i, 1) = 0 \qquad \text{(A-27)}$$

$$\bar{T}_i(0, \bar{\phi}) = \bar{T}_{i-1}(\bar{\theta}_{i-1}, \bar{\phi})$$

The first two boundary conditions of (A-27) implies the saturation temperature at the interface, and third condition implies the initial temperature profile at ith segment is the same as the final temperature profile at i-1th segment. Therefore, the temperature profile of the whole flow field can be obtained by computing from the beginning of the 1st segment, where the temperature is T_{Lo}. As mentioned above, the water sheet thickness is assumed to be constant over the short time segment Δt, and the solution of (A-26), (A-27) can be obtained as follows:

$$\bar{T}_i(\bar{t}_i,\bar{\phi}) = 2 \sum_{n=1}^{\infty} \left[\int_o^1 \bar{T}_i(0,\bar{\phi}) \sin n\pi\bar{\phi} \, d\bar{\phi}\right] \sin n\pi\bar{\phi} \; e^{-n^2\pi^2\bar{t}_i} \qquad \text{(A-28)}$$

For the 1st segment, i=1,

$$\bar{T}_1(0,\bar{\phi}) = 1 \quad (\text{since, } T_1 = T_{Lo})$$

Therefore, (A-28) will be

$$\bar{T}_1(\bar{t}_1,\bar{\phi}) = 2 \sum_{n=1}^{\infty} \frac{1}{n\pi} (1 - \cos n\pi) \sin n\pi\bar{\phi} \; e^{-n^2\pi^2\bar{t}_1}$$

and the final temperature of the 1st segment will be, at $t_1 = \Delta t$,

$$\bar{T}_1(\bar{\theta}_1,\bar{\phi}) = 2 \sum_{n=1}^{\infty} \frac{1}{n\pi} (1 - \cos n\pi) \sin n\pi\bar{\phi} \; e^{-n^2\pi^2\bar{\theta}_1} \qquad \text{(A-29)}$$

which will be the initial condition for the 2nd segment.

For the 2nd segment, i=2, from (A-28), (A-29),

$$\bar{T}_2(\bar{t}_2,\bar{\phi}) = 2 \sum_{n=1}^{\infty} \left[\int_o^1 2 \sum_{k=1}^{\infty} \frac{1}{k\pi} (1 - \cos k\pi)\, e^{-k^2\pi^2\bar{\theta}_1} \cdot \sin k\pi\bar{\phi} \cdot \sin n\pi\bar{\phi}\, d\bar{\phi}\right] \cdot \sin n\pi\bar{\phi}\, e^{-n^2\pi^2\bar{t}_2}$$

$$= 2 \sum_{n=1}^{\infty} \left[\frac{2}{n\pi} (1 - \cos n\pi) e^{-n^2\pi^2\bar{\theta}_1} \int_o^1 \sin^2 n\pi\bar{\phi}\, d\bar{\phi}\right] \sin n\pi\bar{\phi}\, e^{-n^2\pi^2\bar{t}_2}$$

$$= 2 \sum_{n=1}^{\infty} \frac{1}{n\pi} (1 - \cos n\pi) \sin n\pi\bar{\phi}\, e^{-n^2\pi^2(\bar{\theta}_1 + \bar{t}_2)}$$

and the final temperature of the 2nd segment will be, at $t_2 = \Delta t$,

$$\bar{T}_2(\bar{\theta}_2,\bar{\phi}) = 2 \sum_{n=1}^{\infty} \frac{1}{n\pi} (1 - \cos n\pi) \sin n\pi\bar{\phi}\, e^{-n^2\pi^2(\bar{\theta}_1 + \bar{\theta}_2)}$$

Generally, at the end of the mth segment,

$$\bar{T}_m(\bar{\theta}_m,\bar{\phi}) = 2 \sum_{n=1}^{\infty} \frac{1}{n\pi} (1 - \cos n\pi) \sin n\pi\bar{\phi}\, e^{-n^2\pi^2 \sum_{i=1}^{m} \bar{\theta}_i} \qquad \text{(A-30)}$$

Since,

$$\frac{1}{n\pi} (1 - \cos n\pi) = 0 \qquad \text{when } n = 2,4,6,\ldots$$

$$\frac{1}{n\pi} (1 - \cos n\pi) = \frac{2}{n\pi} \qquad \text{when } n = 1,3,5,\ldots$$

(A-30) can be rewritten as

$$\bar{T}_m(\bar{\theta}_m,\bar{\phi}) = \frac{4}{\pi} \sum_{\ell=o}^{\infty} \frac{\sin\left[(2\ell + 1)\pi\bar{\phi}\right]}{(2\ell + 1)}\, e^{-(2\ell+1)^2\pi^2 \sum_{i=1}^{m} \bar{\theta}_i} \qquad \text{(A-31)}$$

where,

$$\bar{\theta}_i = \alpha\Delta t/d_i^2$$

As a special case of uniform thickness of water sheet,

$$d_1 = d_2 = d_3 = \ldots\ldots = d = \text{const}$$

and

$$\bar{\theta}_1 = \bar{\theta}_2 = \bar{\theta}_3 = \ldots\ldots = \bar{\theta}_i = \text{const}$$

Therefore, (A-31) will be

$$\bar{T}(\bar{\theta},\bar{\phi}) = \frac{4}{\pi} \sum_{\ell=o}^{\infty} \frac{\sin[(2\ell + 1)\pi\bar{\phi}]}{(2\ell + 1)} e^{-(2\ell+1)^2\pi^2\bar{\theta}}$$

where,

$$\bar{\theta} = \alpha t/d^2$$

which is just the solution of non-steady conduction equation of a parallel sided slab.

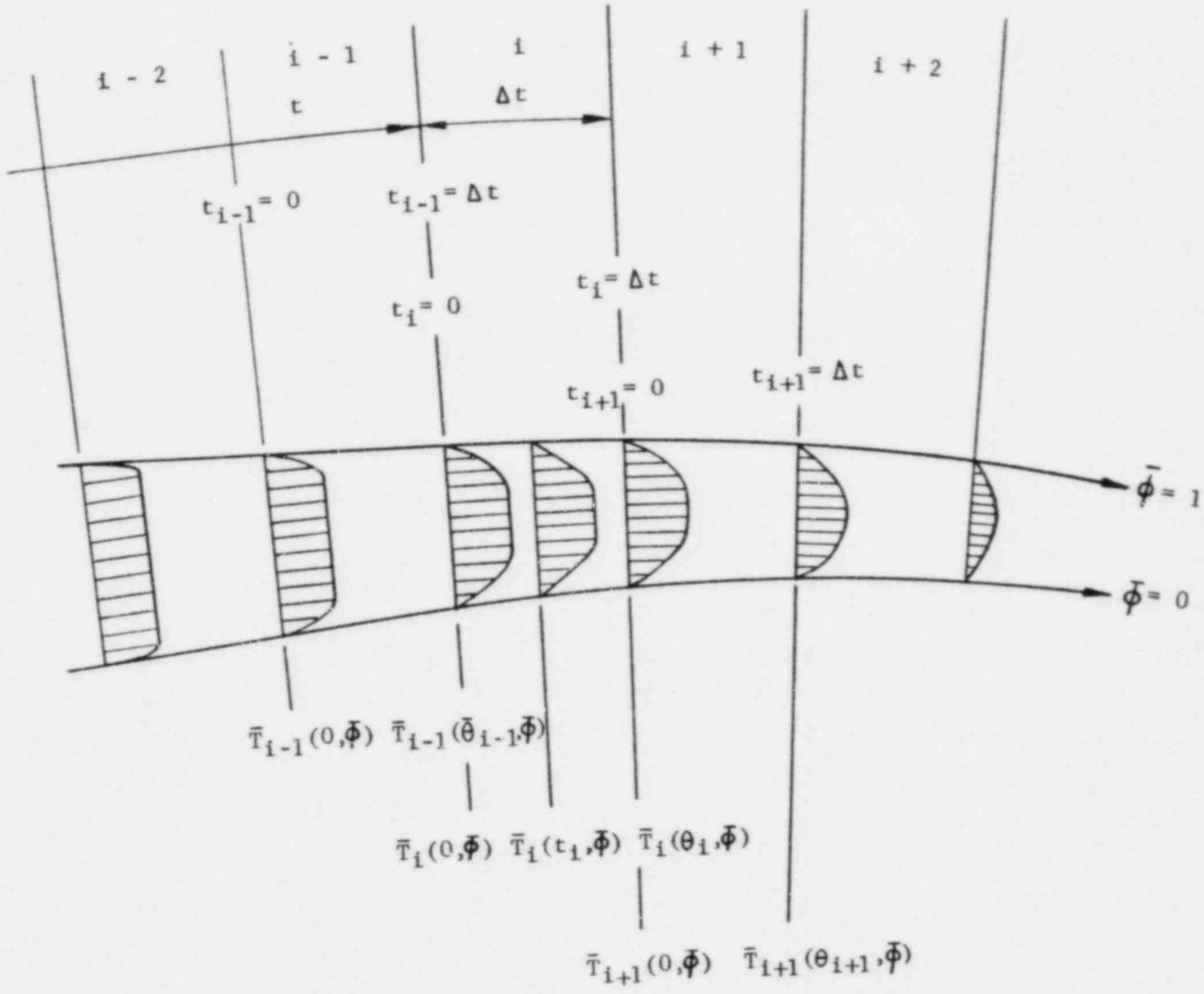

Fig. A-4 Diagram of numerical elements for the calculation of temperature distribution of liquid sheet

APPENDIX 4

COMPUTER PROGRAM FOR NUMERICAL CALCULATION OF WATER SHEET AND DROPLETS

```
C         ************************************************************
C         *                                                          *
C         *  PROGRAM FOR WATER SPRAY INJECTED INTO STEAM ENVIRONMENT *
C         *                                                          *
C         ************************************************************
C
C         This program consistc of two portions - sheet portion and
C         drop portion.  In the sheet portion, the surface tention and
C         swirl motion are taken into account. Gravity force neglected.
C
C         This calculation is performed with the PDP-11/44 MINI COMPUTER.
C         The TEKTRONIX 4052 is used for plotting.
C
C
C
C
C
C
          DIMENSION DELM(150),VLZZ(150),VLRR(150),TT(150),DTT(150),D(150),
     1       DA(150),R(150),EMCC(300),C1(300),C2(300),ANUM(150),AVOL(150),
     2       VT(150),RK(150),RT(150)
C
C
C
C
C         Input data and constants
C         ------------------------
C
          TYPE 12
12        FORMAT(1X,'WHAT IS THE ENVIRONMENT PRESSURE?')
          ACCEPT 13,PR
13        FORMAT(1X,F2.0)
          TYPE 14,PR
14        FORMAT(1X,'ENVIRONMENT PRESSURE=  ',F2.0,' ATM')
          TYPE 15
15        FORMAT(1X,'WHAT ARE THE VALUES OF VIS,RHOV,TS?')
          ACCEPT 20,VIS,RHOV,TS
20        FORMAT(1X,E9.3,1X,F6.4,1X,F6.2)
          TYPE 25
25        FORMAT(1X,'WHAT ARE THE VALUES OF THETO,ALAMD,TLO,EMLO?')
          ACCEPT 30,THETO,ALAMD,TLO,EMLO
30        FORMAT(1X,F4.1,1X,F5.0,1X,F5.1,1X,F6.5)
          TYPE 36
36        FORMAT(1X'WHAT ARE THE VALUES OF AO,RA,DN?')
          ACCEPT 37,AO,RA,DN
37        FORMAT(1X,E9.3,1X,F7.6,1X,F7.6)
          TYPE 38
38        FORMAT(1X,'WHAT IS THE VALUE OF VTAN/VLO ?')
          ACCEPT 39,PO
39        FORMAT(1X,F3.2)
          TYPE 40,AO,RA,DN
40        FORMAT(1X/5X,'AO= ',E9.3,
     1        'M**2.    ','RA= ',F7.6,'M    ','DN= ',F7.6,' M')
          TYPE 41
41        FORMAT(5X,'VIS',6X,'RHOV',3X,'TS',2X,'THETO',1X,'ALAMD',
     1        2X,'TLO',3X,'EMLO')
          TYPE 42,VIS,RHOV,TS,THETO,ALAMD,TLO,EMLO
42        FORMAT(1X,E9.3,1X,F6.4,1X,F6.2,1X,F4.1,
     1        1X,F5.0,1X,F5.1,1X,F6.5)
          TYPE 125,PO
          TYPE 45
45        FORMAT(1X,'TYPE 1 FOR CONTINUE, TYPE 2 FOR STOP')
          ACCEPT 50,II
50        FORMAT(1X,I1)
          IF(II-2) 55,999,999
55        CONTINUE
          PAI=3.14159
          ALPHA=1.5E-07
          CP=4.187
          RHOL=1000.
          DT=1.E-05
```

```
C
C
C       Print of input data
C
C
        PRINT 70
70      FORMAT(10X,'********************** INPUT DATA **************')
        PRINT 100
100     FORMAT(1X/7X,'TS',8X,'TLO',5X,'EMLO',7X,'RHOV',6X,'RHOL',6X,
     1         'ALAMD')
        PRINT 110
110     FORMAT(6X,'(C)',8X,'(C)',3X,'(KG/SEC)',2X,'(KG/CU.M.)',
     1         '(KG/CU.M.)',2X,'(KJ/KG)')
        PRINT 120,TS,TLO,EMLO,RHOV,RHOL,ALAMD
120     FORMAT(1X,2F10.2,2F10.5,2F10.0)
        PRINT 40,AO,RA,DN
        PRINT 125,PO
125     FORMAT(5X,'VTAN/VLO AT THE NOZZLE OUTLET =    ',F3.2)
C
C
C
C
C
C       Determination of surface tension
C
C       (This relation is obtained by measuring the size of water
C        bell in air environment. The surface tension of steam/water
C        is assumed to be same as air/water)
C
C
        SURF=.001*(60.28-.1657*TLO)
        TYPE 150,SURF
        PRINT 150,SURF
150     FORMAT(1X/1X,'SURFACE TENSION=  ',F5.4,' N/M')
C
C
C       Determination of breakup length as a function of:
C               Weber number,WE
C               Jakob number,AJA
C
        VLO=EMLO/(AO*RHOL)
        WE=RHOL*VLO*VLO*DN/SURF
        AJA=CP*(TS-TLO)/ALAMD
        FIT=3.024E-06*(WE-474.8)*(WE-474.8)
        IF(FIT-40.)157,157,156
156     EXPC=0.
        GO TO 158
157     EXPO=EXP(-FIT)
158     CONTINUE
        IF(AJA)159,159,160
159     CONST=1.
        GO TO 161
160     CONST=1.+6.554*AJA**.7135*EXPO
161     IF(WE-750.)162,162,163
162     BREAK=2.469*WE**.2895/CONST
        GO TO 165
163     BREAK=818.8*WE**(-.581)/CONST
165     CONTINUE
```

```
C
C
C
C
C       ****************************
C       PROGRAM FOR SHEET PORTION
C       ****************************
C
C
        PRINT 167
167     FORMAT(1X/1X,'SOLUTION FOR SHEET PORTION')
        PRINT 168
168     FORMAT(1X/3X,'ZZ',10X,'RADIUS',10X,'EMCG',10X,'DELP',10X,
     1        'ANGLE',12X,'TI',13X,'HZ',13X,'VVZ')
        PRINT 170
170     FORMAT(2X,'(MM)',10X,'(MM)',9X,'( G/SEC)',7X,'(N/M**2)',7X,
     1        '(DEG)',12X,'(C)',7X,'(KW/M**2 C)',6X,'(M/SEC)')
        TH=THETO*2.*PAI/360.
        Z=0.
        RR=SIN(TH)/COS(TH)
        EMCG=0.
        ENTHO=CP*EMLO*DT*TLO
        ENTHS=ENTHO
        VORTEX=RA*VLO*PO
C
C
C       Calculation of water sheet temperature
C       (Heat transfer by conduction)
C
        TBAR=0.
        TI=TLO
200     VLZ=VLO/(1.+RR*RR)**.5
        VLR=VLO*RR/(1.+RR*RR)**.5
        DZ=DT*VLZ
        DEL=EMLO/(2.*PAI*RA*RHOL*VLZ)
        DELPR=DEL/(1.+RR*RR)**.5
        IF(TS-TLO) 205,205,206
205     HZ=0.
        ENTH=ENTHO
        GO TO 271
206     TBAR=ALPHA*DT/DELPR**2.+TBAR
        DX=.005
        X=0.
        ENTH=0.
210     SUM=0.
        EN=0.
220     SSIN=SIN((2.*EN+1.)*PAI*X)/(2.*EN+1.)
        SUB=(2.*EN+1.)**2.*PAI**2.*TBAR
        IF(SUB-40.) 240,240,230
230     EXPO=0.
        GO TO 250
240     EXPO=EXP(-SUB)
250     CONTINUE
        SUM=SUM+(4./PAI)*SSIN*EXPO
        EN=EN+1.
        IF(EN-50.) 220,220,260
260     TEMP=TS+(TLO-TS)*SUM
        ENTH=ENTH+2.*CP*TEMP*DX*DELPR*2.*PAI*RA*DZ*RHOL*(1.+RR*RR)**.5
        X=X+DX
        IF(X-.5) 210,270,270
```

```
C
C
C
C       Calculation and print out of:
C               Condensation rate,EMCG
C               Pressure difference by condensation,DELP
C               Spray angle,ANG
C               Spray radius,RA
C               Water temperature,TI
C               Heat transfer coefficient,HZ
C
C
270     EMC=(ENTH-ENTHS)/(ALAMD*DT)
        HZ=EMC*ALAMD*.25/((TS-TI)*PAI*RA*DZ*(1.+RR*RR)**.5)
271     EMCG=(ENTH-ENTHO)/(ALAMD*DT)
        VVZ=(EMCG/(2.*RHOV))/(PAI*RA*RA)
        DELP=(RHOV*VVZ*VVZ)/2.
        ANG=ATAN(RR)*360./(2.*PAI)
        RRR=-(1.+RR*RR)**(3./2.)*(DELP+2.*SURF/(RA*(1.+RR*RR)**.5)-
     1      RHOL*DELPR*VORTEX*VORTEX/(RA*RA*RA*(1.+RR*RR)**.5))
     2      /(RHOL*DELPR*VLO*VLO-2.*SURF)
        RR=RR+RRR*DZ
        TYPE 280,Z*1000.,(RA+DEL/2.)*1000.,EMCG*1000.
280     FORMAT(1X,F15.3,2F20.7)
        PRINT 290,Z*1000.,(RA+DEL/2.)*1000.,EMCG*1000.,DELP,ANG,TI,HZ,
     1          VVZ
290     FORMAT(1X,F6.3,7F15.7)
        RA=RA+RR*DZ
        Z=Z+DZ
        TI=ENTH/(EMLO*DT*CP)
        ENTHS=ENTH
        IF(RA)293,293,295
293     TYPE 294
294     FORMAT(1X,'SPRAY COLLAPSED')
        GO TO 999
295     IF(Z-BREAK*AO**.5) 200,300,300
C
C
C
300     TYPE 310
310     FORMAT(1X,'ENTER 1 FOR CALCULATION OF DROP PORTION, TYPE 2 FOR
     1  STOP')
        ACCEPT 320,KIJ
320     FORMAT(1X,I1)
        IF(KIJ-2) 330,999,999
330     CONTINUE
```

```
C
C
C
C       ************************
C       PROGRAM FOR DROP PORTION
C       ************************
C
C
C
C       Additional data input for drop portion
C       50 micron increments for drop sizes
C
C
        TYPE 350
350     FORMAT(1X,'WHAT ARE THE VALUES OF A,DELTA,DDM?')
        ACCEPT 360,A,DELTA,DDM
360     FORMAT(1X,F6.4,1X,F6.4,1X,F8.3)
        DM=DDM/1.E+06
        DDI=5.E-05
        DZ=.001
        ZA=BREAK*AO**.5
        EL=ZA
        TYPE 370
        PRINT 370
370     FORMAT(1X/1X,'PARAMETERS FOR DROP SIZE DISTRIBUTION')
        TYPE 380,A,DELTA,DDM
        PRINT 380,A,DELTA,DDM
380     FORMAT(1X,'A=  ',F6.4,10X,'DELTA=  ',F6.4,10X,'DDM=  ',F8.3,
     1        ' MICRONS')
        TYPE 390
390     FORMAT(1X,'ENTER 1 FOR CONTINUE, ENTER 2 FOR STOP')
        ACCEPT 393,LI
393     FORMAT(1X,I1)
        IF(LI-2)395,999,999
395     CONTINUE
C
C
C       Number distribution of spray droplets
C       -------------------------------------
C
        J=1
        DI=DDI
410     Y=ALOG(A*DI/(DM-DI))
        DELN(J)=(EMLO/RHOL)*(DELTA/PAI**.5)*(DM/(DI*(DM-DI)))
     1        *(6./(PAI*DI**3.))*EXP(-DELTA**2.*Y*Y)*DDI
        DI=DI+DDI
        IF(DI-DM) 420,430,430
420     J=J+1
        GO TO 410
430     CONTINUE
C
C
C
C
C       Boundary condition for calculation of drop portion
C       --------------------------------------------------
C       (Obtained from the sheet portion)
C
C
        JI=J
        TYPE 440,TI,ZA*1000.,RA*1000.,VLZ,VLR
440     FORMAT(1X,F10.2,4F15.4)
        PRINT 445
445     FORMAT(1X/1X,'BOUNDARY CONDITION FOR DROP PORTION'/1X,
     1        'OBTAINED FROM SHEET PORTION')
        PRINT 450,TI,ZA*1000.,RA*1000.,VLZ,VLR,EL*1000.
450     FORMAT(1X,'TI=',F6.1,1X,'C',3X,'Z=',F10.4,1X,'MM',3X,'R=',
     1        F10.4,1X,'MM',3X,'VLZ=',F10.4,1X,'M/SEC',3X,'VLR=',
     2        F10.4,1X,'M/SEC',3X,'EL=',F10.4,1X,'MM')
        VVZO=0.
        TEMP=TI
C
```

```
C
C
460     VVZ=VVZO
        Z=ZA
        DO 465 J=1,JI
        TT(J)=0.
        RK(J)=RA
        RT(J)=0.
        VT(J)=VORTEX/RA
        VLZZ(J)=VLZ
465     VLRR(J)=VLR
        M=1
        MM=10
        MMM=2
        PRINT 467
467     FORMAT(1X/1X,'SOLUTION FOR DROP PORTION')
C
C
C
C       Initiation of plotting
C       ----------------------
C
C
C       Outline drawing
C
        CALL TKINIT(240)
        CALL DWINDO(-40.,260.,-114.,114.)
        CALL MOVEA(0.,114.)
        CALL DRAWA(0.,-114.)
        CALL MOVEA(300.,0.)
        CALL DRAWA(0.,0.)
C
C       Insert scales
C
        ZX=50.
        DO 472 J=1,5
        CALL MOVEA(ZX,3.)
        CALL DRAWA(ZX,0.)
        CALL MOVEA(ZX-5.,0.)
        CALL ANMODE
        WRITE(10,471)ZX
471     FORMAT(1X,F4.0)
472     ZX=ZX+50.
        RY=100.
        DO 475 J=1,5
        CALL MOVEA(0.,RY)
        CALL DRAWA(3.,RY)
        CALL MOVEA(-20.,RY+3.)
        CALL ANMODE
        WRITE(10,473)ABS(RY)
473     FORMAT(1X,F5.0)
475     RY=RY-50.
C
C       Insert units
C
        CALL MOVEA(-30.,114.)
        CALL ANMODE
        WRITE(10,477)
477     FORMAT(1X,'R(MM)')
        CALL MOVEA(240.,10.)
        CALL ANMODE
        WRITE(10,478)
478     FORMAT(1X,'Z(MM)')
C
C       Draw the spray outline of sheet portion
C       (Straight line is drawn from origin to breakup point)
C
        CALL MOVEA(0.,0.)
        CALL DRAWA(ZA*1000.,RA*1000.)
        CALL MOVEA(ZA*1000.,-RA*1000.)
        CALL DRAWA(0.,0.)
```

```
C
C
C
C       Calculation of matching portion
C       -------------------------------
C
C
C       The length of this portion is assumed to be same as breakup
C       length.
C               EMCC(M)=Condensate rate between z and z+dz
C               DMOM=Momentum of droplets at the end of the matching
C                    portion in axial direction.
C
480     EMCC(M)=0.
        DMOM=0.
        J=1
        DI=DDI
490     DTT(J)=DZ/VLZZ(J)
        CALL DIA(DI,TT(J),DTT(J),TS,TI,ALAMD,ALPHA,PAI,D(J),DA(J),CP)
        EMCC(M)=EMCC(M)+(PAI/6.)*RHOL*(DA(J)**3.-D(J)**3.)*DELN(J)
        DMOM=DMOM+(PAI/6.)*D(J)**3.*RHOL*DELN(J)*VLZZ(J)
        RK(J)=RK(J)+VLRR(J)*DTT(J)
        RT(J)=RT(J)+VT(J)*DTT(J)
        R(J)=(RK(J)*RK(J)+RT(J)*RT(J))**.5
        CALL POINTA((Z+DZ)*1000.,R(J)*1000.)
        CALL POINTA((Z+DZ)*1000.,-R(J)*1000.)
        DI=DI+DDI
        IF(DI-DM) 500,510,510
500     J=J+1
        GO TO 490
510     CONTINUE
C
        TEMP=TEMP+EMCC(M)*ALAMD/(EMLO*CP)
        C2(M)=(EMCC(M)+(EMCG/2.)*(DZ/EL))/(2.*PAI*R(JI)*DZ*RHOV)
        J=1
        DI=DDI
520     CALL DIA(DI,TT(J),DTT(J),TS,TI,ALAMD,ALPHA,PAI,D(J),DA(J),CP)
        DDT=(DA(J)-D(J))/DTT(J)
        VVR=-C2(M)*(R(J)/R(JI))
        V=((VLZZ(J)-VVZ)*(VLZZ(J)-VVZ)+(VLRR(J)-VVR)*(VLRR(J)-VVR)
     1     +VT(J)*VT(J))**.5
        RE=V*D(J)/VIS
        CD=DRAG(RE)
        DVLZ=-(3./D(J))*DDT*(VLZZ(J)-VVZ)-.75*(RHOV/RHOL)*(CD/D(J))
     1      *V*(VLZZ(J)-VVZ)
        DVLR=-(3./D(J))*DDT*(VLRR(J)-VVR)-.75*(RHOV/RHOL)*(CD/D(J))
     1      *V*(VLRR(J)-VVR)
        DVT=-(3./D(J))*DDT*VT(J)-.75*(RHOV/RHOL)*(CD/D(J))*V*VT(J)
        VLZZ(J)=VLZZ(J)+DVLZ*DTT(J)
        VLRR(J)=VLRR(J)+DVLR*DTT(J)
        VT(J)=VT(J)+DVT*DTT(J)
C
        TT(J)=TT(J)+DTT(J)
        DI=DI+DDI
        IF(DI-DM) 530,540,540
530     J=J+1
        GO TO 520
540     Z=Z+DZ
        TYPE 550,Z*1000.,(R(2*J)*1000.,J=1,10)
550     FORMAT(1X,6F10.4/11X,5F10.4)
        TYPE 565, TEMP
        PRINT 560,Z*1000.,(R(2*J)*1000. [illegible] 10)
560     FORMAT(1X/1X,'Z=',F6.1,4X,'R=' [illegible])
        PRINT 565, TEMP
565     FORMAT(1X,'AVERAGE WATER [illegible] F10.5,1X,'C')
        M=M+1
        IF(Z-ZA-EL) 480,480,570
570     CONTINUE
C
```

```
C
C        CALCULATION OF THE MAIN DROP PORTION
C        ----------------------------------
C
C        Determination of:
C                EMCC(M)=Condensation rate between z and z+dz
C                DRMOM=Momentum of droplets at z+dz in axial direction
C
      VZZMA=0.
      DO 575 J=1,JI
      AVOL(J)=0.
575   ANUM(J)=0.
580   C1(M)=VLZ
      C11=C1(M)
      EX=1.
      LL=1
      EMCC(M)=0.
      DRMOM=0.
      J=1
      DI=DDI
590   DTT(J)=DZ/VLZZ(J)
      CALL DIA(DI,TT(J),DTT(J),TS,TI,ALAMD,ALPHA,PAI,D(J),DA(J),CP)
      DRMOM=DRMOM+(PAI/6.)*D(J)**3.*RHOL*DELN(J)*VLZZ(J)
      EMCC(M)=EMCC(M)+(PAI/6.)*RHOL*(DA(J)**3.-D(J)**3.)*DELN(J)
      DI=DI+DDI
      IF(DI-DM) 600,610,610
600   J=J+1
      GO TO 590
610   CONTINUE
      TEMP=TEMP+EMCC(M)*ALAMD/(EMLO*CP)
C
C
C
C        Determination of C1 and C2
C
C        Determine the vapor velocity by confirming the continuity
C        and momentum balance.
C                C1=Axial velocity of vapor at axis
C                C2=Radial velocity of vapor at boundary
C                VMOM=Momentum of vapor in axial direction
C                VZMAS=Mass flow rate of vapor in axial direction
C
620   RB=0.
      DRB=R(JI)/100.
      VMOM=0.
      VZMAS=0.
630   IF(RB-R(JI)) 640,650,650
640   VVZ=C1(M)*(1.-RB/R(JI))**2.*(1.+RB/R(JI))**2.
      VMOM=VMOM+VVZ**2.*(RB+DRB/2.)*2.*PAI*DRB*RHOV
      VZMAS=VZMAS+VVZ*(RB+DRB/2.)*2.*PAI*DRB*RHOV
      RB=RB+DRB
      GO TO 630
650   CONTINUE
      IF(LL-100) 660,970,970
660   VVMOM=(VMOM-(DMOM-DRMOM))/DMOM
      TYPE 670,VVMOM,DMOM,DRMOM,VMOM
670   FORMAT(1X,F20.7,2F15.7,F20.7)
      IF (ABS(VVMOM)-.0001) 710,710,680
680   LL=LL+1
      IF(VMOM-(DMOM-DRMOM)) 700,700,690
690   C1(M)=C1(M)-C11/2.**EX
      EX=EX+1.
      GO TO 620
700   C1(M)=C1(M)+C11/2.**EX
      EX=EX+1.
      GO TO 620
710   VRMAS=EMCC(M)+(VZMAS-VZZMA)
      VZZMA=VZMAS
      C2(M)=VRMAS/(2.*PAI*R(JI)*DZ*RHOV)
      TYPE 720,C1(M),C2(M)
720   FORMAT(1X,2F20.7)
```

```
C
C
C
C       CALCULATION OF DROPLET POSITION IN SPACE
C       ----------------------------------------
C
        J=1
        DI=DDI
730     VVZ=C1(M)*(1.-R(J)/R(JI))*(1.-R(J)/R(JI))*(1.+R(J)/R(JI))*
     1      (1.+R(J)/R(JI))
        VVR=-C2(M)*(R(J)/R(JI))
        DTT(J)=DZ/VLZZ(J)
        V=((VLZZ(J)-VVZ)*(VLZZ(J)-VVZ)+(VLRR(J)-VVR)*(VLRR(J)-VVR)
     1    +VT(J)*VT(J))**.5
        CALL DIA(DI,TT(J),DTT(J),TS,TI,ALAMD,ALPHA,PAI,D(J),DA(J),CP)
        DDT=(DA(J)-D(J))/DTT(J)
        RE=V*D(J)/VIS
        CD=DRAG(RE)
        DVLZ=-(3./D(J))*DDT*(VLZZ(J)-VVZ)-.75*(RHOV/RHOL)*(CD/D(J))*
     1      V*(VLZZ(J)-VVZ)
        DVLR=-(3./D(J))*DDT*(VLRR(J)-VVR)-.75*(RHOV/RHOL)*(CD/D(J))*
     1      V*(VLRR(J)-VVR)
        DVT=-(3./D(J))*DDT*VT(J)-.75*(RHOV/RHOL)*(CD/D(J))*V*VT(J)
        RK(J)=RK(J)+VLRR(J)*DTT(J)
        RT(J)=RT(J)+VT(J)*DTT(J)
        R(J)=(RK(J)*RK(J)+RT(J)*RT(J))**.5
        VLZZ(J)=VLZZ(J)+DVLZ*DTT(J)
        VLRR(J)=VLRR(J)+DVLR*DTT(J)
        VT(J)=VT(J)+DVT*DTT(J)
        IF(R(J)) 740,750,750
740     R(J)=-R(J)
        VLRR(J)=-VLRR(J)
750     TT(J)=TT(J)+DTT(J)
        DI=DI+DDI
        IF(DI-DM) 760,770,770
760     J=J+1
        GO TO 730
770     CONTINUE
C
C
C
C       Plot of space distribution of droplets
C
C       Plot every dz=2mm intervals, within 5 degree range in
C       azimuthal direction.
C
        IF(M-MMM)800,772,772
772     DO 780 J=1,JI
        ANUM(J)=(DELN(J)/(VLZZ(J)*72.))*DZ*2.+ANUM(J)
        IF(ANUM(J)-1.) 780,775,775
775     IF(ANUM(J)-2.)776,777,777
776     CALL POINTA(Z*1000.,R(J)*1000.)
        ANUM(J)=ANUM(J)-1.
        GO TO 780
777     IF(ANUM(J)-3.)778,779,779
778     CALL POINTA(Z*1000.,R(J)*1000.)
        CALL POINTA(Z*1000.,R(J)*1000.*.95)
        ANUM(J)=ANUM(J)-2.
        GO TO 780
779     CALL POINTA(Z*1000.,R(J)*1000.)
        CALL POINTA(Z*1000.,R(J)*1000.*.95)
        CALL POINTA(Z*1000.,R(J)*1000.*1.05)
        ANUM(J)=0.
780     CONTINUE
```

```
      DO 790 J=1,JI
      AVOL(J)=(DELN(J)/(VLZZ(J)*72.))*DZ*2.*(FLOAT(J))**3.
     1       +AVOL(J)
      IF(AVOL(J)-1.)790,785,785
785   IF(AVOL(J)-2.)786,787,787
786   CALL POINTA(Z*1000.,-R(J)*1000.)
      AVOL(J)=AVOL(J)-1.
      GO TO 790
787   IF(AVOL(J)-3.)788,789,789
788   CALL POINTA(Z*1000.,-R(J)*1000.)
      CALL POINTA(Z*1000.,-R(J)*1000.*.95)
      AVOL(J)=AVOL(J)-2.
      GO TO 790
789   CALL POINTA(Z*1000.,-R(J)*1000.)
      CALL POINTA(Z*1000.,-R(J)*1000.*.95)
      CALL POINTA(Z*1000.,-R(J)*1000.*1.05)
      AVOL(J)=0.
790   CONTINUE
      NNN=NNN+2
C
C
C     Print out of the output
C
800   TYPE 550,(Z+DZ)*1000.,(R(2*J)*1000.,J=1,10)
      TYPE 565, TEMP
      IF(M-NN) 950,920,920
920   PRINT 560,(Z+DZ)*1000.,(R(2*J)*1000.,J=1,10)
      PRINT 565, TEMP
      NN=NN+10
950   CONTINUE
      IF(M-250) 960,970,970
960   M=M+1
      Z=Z+DZ
      GO TO 580
970   PRINT 980,(M*10,C1(M*10),C2(M*10),EMCC(M*10),M=1,20)
      PRINT 990,VVZ0
980   FORMAT(1X,I5,10X,'C1=',F10.5,'(M/SEC)',20X,'C2=',F10.5,
     1       '(M/SEC)',20X,'EMC=',E13.6,'(KG/SEC)')
990   FORMAT(1X/1X,'VVZ0=',F20.7,1X,'M/SEC')
      PRINT 991,(DELN(J),J=1,JI)
991   FORMAT(1X,'DELN(J)',5X,10F10.0)
C
C     Label the plot
C     --------------
C
      CALL MOVEA(10.,114.)
      CALL ANMODE
      WRITE(10,992)
992   FORMAT(1X,'SPACE DISTRIBUTION OF DROPLETS')
      CALL MOVEA(10.,70.)
      CALL ANMODE
      WRITE(10,1002)
1002  FORMAT(1X,'NUMBER DISTRIBUTION')
      CALL MOVEA(10.,-60.)
      CALL ANMODE
      WRITE(10,1003)
1003  FORMAT(1X,'VOLUME DISTRIBUTION')
      CALL MOVEA(10.,-90.)
      TYPE 993
993   FORMAT(1X,'ENTER 1 FOR STEAM, ENTER 2 FOR AIR')
      ACCEPT 994,LK
994   FORMAT(1X,I1)
      IF(LK-2)997,995,995
995   CALL ANMODE
      WRITE(10,996)PR,EMLO,TLO
996   FORMAT(1X,'AIR ENVIRONMENT',3X,F2.0,' ATM'/15X,'FLOW RATE= ',
     1       F6.5,' KG/SEC',3X,'TLO= ',F6.2,' C')
      GO TO 999
997   CALL ANMODE
      WRITE(10,998)PR,EMLO,TS,TLO
998   FORMAT(1X,'STEAM ENVIRONMENT',3X,F2.0,' ATM'/15X,'FLOW RATE= ',
     1 F6.5,' KG/SEC',3X,'TS= ',F6.2,' C',3X,'TLO= ',F6.2,' C')
999   STOP
      END
```

```
C
      SUBROUTINE DIA(DI,T,DT,TS,TI,ALAMD,ALPHA,PAI,D,DA,CP)
C
C     ------------------------------------------------------------
C     SUBPROGRAM FOR CALCULATING DROPLET GROWTH BY CONDENSATION
C     ------------------------------------------------------------
C
      PSI=(1.+CP*(TS-TI)/ALAMD)**(1./3.)-1.
      FO=4.*ALPHA*T/DI**2.
      FOO=4.*ALPHA*(T+DT)/DI**2.
      EXPO=PAI**2.*FOO
      IF(EXPO-40.) 20,10,10
10    DA=DI*(1.+PSI)
      D=DA
      GO TO 30
20    CONTINUE
      DA=DI*(1.+PSI*(1.-EXP(-PAI**2.*FOO))**.5)
      D=DI*(1.+PSI*(1.-EXP(-PAI**2.*FO))**.5)
30    RETURN
      END
```

```
C
      FUNCTION DRAG(RE)
C
C     ---------------------------------------------
C     SUBPROGRAM FOR DRAG COEFFICIENT OF DROPLETS
C     ---------------------------------------------
C
C     THIS SUBPROGRAM IS FOR THE REYNOLDS NUMBER UP TO 44,000
C
      W=ALOG10(RE)
      IF(RE-.01) 10,10,20
10    DRAG=3./16.+24./RE
      GO TO 200
20    IF(RE-20.) 30,30,40
30    DRAG=24.*(1.+.1315*RE**(.82-.05*W))/RE
      GO TO 200
40    IF(RE-260.) 50,50,60
50    DRAG=24.*(1.+.1935*RE**.6305)/RE
      GO TO 200
60    IF(RE-1500.) 70,70,80
70    DRAG=10.**(1.6435-1.1242*W+.1558*W*W)
      GO TO 200
80    IF(RE-1.2E+04) 90,90,100
90    DRAG=10.**(-2.4571+2.5558*W-.9295*W*W+.1049*W*W*W)
      GO TO 200
100   DRAG=10.**(-1.9181+.637*W-.0636*W*W)
200   RETURN
      END
```

REFERENCES

[1] Castleman, R. A., "The Mechanism of the Atomization of Liquids," Bureau of Standards, Journal of Research, 1931.

[2] Schweitzer, P. H., "Mechanism of Disintegration of Liquid Jets," Journal of Applied Physics, Vol. 8, 1937.

[3] Tanasawa, Y. and Toyoda, S., "On the Atomization of Liquid Jet Issuing from a Cylindrical Nozzle," The Technology Report of the Tohoku University, Vol. 19, No. 2, 1955.

[4] DeJuhasz, K. J., "Dispersion of Sprays in Solid-Injection Engines," Trans. ASME, OGP-53-5, 1931.

[5] Lee, D. W., "Fuel Spray Formation," Trans. ASME, OGP-54-4, 1932.

[6] Lee, D. W., "A Comparison of Fuel Sprays from Several Types of Injection Nozzles," NACA Technical Report No. 21, 1935.

[7] Ranz, W. E., "Some Experiments on Orifice Sprays," The Canadian Journal of Chemical Engineering, 1958.

[8] Reitz, R. D. and Bracco, F. V., "Ultra-High-Speed Filming of Atomizing Jets," Phys. Fluids, Vol. 22, No. 6, 1979.

[9] Frazer, R. P. and Eisenklam, P., "Liquid Atomization and the Drop Size of Sprays," Trans. Instn. Chem. Engrs., Vol. 34, 1956.

[10] Dombrowski, N. and Wolfsohn, D. L., "The Atomization of Water by Swirl Spray Pressure Nozzles," Trans. Instn. Chem. Engrs., Vol. 50, 1972.

[11] Dombrowski, N. and John, W. R., "The Aerodynamic Instability and Disintegration of Viscous Liquid Sheets," Chemical Engineering Science, Vol. 18, 1963.

[12] Dombrowski, N. and Hooper, P. C., "The Effect of Ambient Density on Drop Formation in Sprays," Chemical Engineering Science, Vol. 17, 1962.

[13] Fraser, R. P., Dombrowski, N. and Eisenklam, P., "Vibration as a Cause of Disintegration of Liquid Sheets," Nature, 1954.

[14] Dombrowski, N. and Fraser, R. P., "A Photographic Investigation into the Disintegration of Liquid Sheets," Phil. Trans., A, Vol. 247, 1953.

[15] Clark, C. J. and Dombrowski, N., "An Experimental Study on the Flow of Thin Liquid Sheets in Hot Atmosphere," J. Fluid Mech., Vol. 64, 1974.

[16] Fraser, R. P., Eisenklam, P., Dombrowski, N. and Hasson, D., "Drop Formation from Rapidly Moving Liquid Sheets," AIChE J., Vol. 8, No. 5, 1962.

[17] Crapper, G. D., Dombrowski, N. and Pyott, G. A. D., "Large Amplitude Kelvin-Helmholtz Waves on Thin Liquid Sheets," Proc. Roy. Soc. London, A., 342, 1975.

[18] DeCorso, S. M. and Kemeny, G. A., "Effect of Ambient and Fuel Pressure on Nozzle Spray Angle," Trans. ASME, 1957.

[19] DeCorso, S. M., "Effect of Ambient and Fuel Pressure on Spray Drop Size," Trans. ASME, 1960.

[20] Giffen, E. and Muraszew, A., "The Atomization of Liquid Fuels," John Wiley and Sons, 1953.

[21] Reitz, R. D., "Breakup Regimes of a Single Liquid Jet," AMS Report No. 1262, Princeton University, 1976.

[22] Rothe, P. H. and Block, J. A., "Aerodynamic Behavior of Liquid Sprays," Int. J. Multi-phase Flow, Vol. 3, 1977.

[23] Brown, G., Ph.D. Thesis, Imperial College of Science and Technology, London, 1948.

[24] Brown, G., "Heat Transmission by Condensation of Steam on a Spray of Water Drops," Proceedings of General Discussion on Heat Transfer, Inst. Mech. Engrs., 1951.

[25] Lim, I. S., Bankoff, S. G., Tankin, R. S. and Yuen, M. C., "Cocurrent Steam/Water Flow in a Horizontal Channel," NUREG/CR-2289, 1981.

[26] Kutateladze, S. S., "Heat Transfer by Condensation and Boiling," 1952, cited by the same author's "Concise Encyclopedia of Heat Transfer," Pergamon Press, 1966.

[27] Hasson, D., Luss, D. and Peck, R., "Theoretical Analysis of Vapor Condensation on Laminar Liquid Jets," Int. J. Heat Mass Transfer, Vol. 7, 1964.

[28] Weinberg, S., "Heat Transfer to Low Pressure Sprays of Water in a Steam Atmosphere," Proc. Instn. Mech. Engrs., 1951.

[29] Hasson, D., Luss, D and Navon, U., "An Experimental Study of Steam Condensation on a Laminar Water Sheet," Int. J. Heat Mass Transfer, Vol. 7, 1964.

[30] Sandoz, S. A. and Sun, K. H., "Modelling Environmental Effects on Nozzle Spray Distribution," ASME Paper 76-WA/FE-39, 1976.

[31] Sandoz, S. A. and Sutherland, W. A., "Core Spray Performance," Experimental and Analytical Model of LWR Safety Experiments, presented at the 19th National Heat Transfer Conference, Orlando Florida, July 1980.

[32] General Electric Company, "General Electric Company Analytical Model for Loss-of-Coolant Analysis in Accordance with 10CFR-50 Appendix K, Amendment No. 3, Effect of Steam Environment on BWR Core Spray Distribution," NEDO-20566-3.

[33] Takahashi, Y., Masuda, M., Aikawa, K. and Tahara, M., "A Basic Study of Mixture-Type Steam Condensers," Mitsubishi Heavy Industries Technical Report, Vol. 9, No. 1, 1972.

[34] Lekic, A., "The Rate of Growth of Drop During Condensation," M.A.Sc., Thesis, University of Waterloo, 1970.

[35] Ford, J. D. and Lekic, A., "Rate of Growth of Drops During Condensation," Int. J. Heat Mass Transfer, Vol. 16, 1973.

[36] Lekic, A., Bajramovic, R. and Ford, J. D., "Droplet Size Distribution: An Improved Method for Fitting Experimental Data," Canadian Journal of Chemical Engineering, Vol. 54, 1976.

[37] Lekic, A., "Direct Contact Condensation of Vapor on Spray of Subcooled Liquid Drops," Ph.D. Thesis, University of Waterloo, 1976.

[38] Lekic, A. and Ford, J. D., "Direct Contact Condensation of Vapor on a Spray of Subcooled Liquid Droplets," Int. J. Heat Mass Transfer, Vol. 23, 1980.

[39] Azzopardi, B. J., "Measurement of Drop Sizes," Int. J. Heat Mass Transfer, Vol. 22, 1979.

[40] Mugele, R. A. and Evans, H. D., "Drop Size Distribution in Sprays," Industrial and Engineering Chemistry, June 1951.

[41] Kashiwagi, T. and Oketani, K., "Direct Contact Condensation on Coolant Fluid Jets," presented at Winter Annual Meeting of ASME, Nov. 1980.

[42] Tanaka, M., "Heat Transfer of a Spray Droplet in a Nuclear Reactor Containment," Nuclear Technology, Vol. 47, 1980.

[43] Ohba, K., Kitada, H. and Nishiguchi, A., "Direct Contact Condensation of Steam on a High Speed Spray Jet of Subcooled Water," submitted for 1980 International Seminar on Nuclear Reactor Safety Heat Transfer, 1980.

[44] Parlange, J. Y., "A Theory of Water Bells," J. Fluid Mech., Vol. 29, Part 2, 1967.

[45] Bark, F. H., Wallin, H., Gallstedt, M. G. and Kristiansson, L. P., "Swirling Water Bells," J. Fluid Mech., Vol. 90, Part 4, 1979.

[46] Clift, R., Grace, J. R. and Weber, M. E., "Bubbles, Drops and Particles," Academic Press, 1978.

[47] Yuen, M. C. and Chen, L. W., "On Drag of Evaporating Liquid Droplets," Combustion Science and Technology, Vol. 14, 1976.

[48] Stachniak, R. E., "Pulsed Holography of Two Phase Air and Water Mixtures Using a Q-Switched Nd:YAG Laser," M.S. Thesis, Northwestern University, 1979.

[49] Trolinger, J. D., "Laser Instrumentation for Flow Field Diagnostics," AGARD Report, March 1974.

[50] Chan, F. W.-K., Chan, R. K.-C. and Stuhmiller, J. H., "Single Nozzle Spray Distribution Analysis," EPRI Report, NP-1344, 1980.

[51] Taylor, G. I., "The Dynamics of Thin Sheets of Fluid," Proc. Roy. Soc. London, Ser. A, Vol. 253, 1959.

[52] Huang, J. C. P., "The Breakup of Axisymmetric Liquid Sheets," J. Fluid Mech., Vol. 43, Part 2, 1970.

[53] Hagerty, W. W. and Shea, J. F., "A Study of the Stability of Plane Liquid Sheets," J. of Applied Mech., 1955.

[54] Sandoz, S. A., private communications, Dec. 1981.

NRC FORM 335 (7-77)

U.S. NUCLEAR REGULATORY COMMISSION

BIBLIOGRAPHIC DATA SHEET

1. REPORT NUMBER *(Assigned by DDC)*
NUREG/CR-2784

4. TITLE AND SUBTITLE *(Add Volume No., if appropriate)*
Behavior of Water Spray Injected into Air/Steam Environment

2. *(Leave blank)*

3. RECIPIENT'S ACCESSION NO.

7. AUTHOR(S)
S. Y. Lee and R. S. Tankin

5. DATE REPORT COMPLETED
MONTH: May | YEAR: 1982

9. PERFORMING ORGANIZATION NAME AND MAILING ADDRESS *(Include Zip Code)*
Northwestern University
Department of Mechanical and Nuclear Engineering
Evanston, Illinois 60201

DATE REPORT ISSUED
MONTH: August | YEAR: 1982

6. *(Leave blank)*

8. *(Leave blank)*

12. SPONSORING ORGANIZATION NAME AND MAILING ADDRESS *(Include Zip Code)*
U.S. Nuclear Regulatory Commission
Office of Nuclear Regulatory Research
Division of Accident Evaluation
Washington, DC 20555

10. PROJECT/TASK/WORK UNIT NO.

11. CONTRACT NO.
Grant No. G-1000

13. TYPE OF REPORT
Topical Report

PERIOD COVERED *(Inclusive dates)*
June 1981 - May 1982

15. SUPPLEMENTARY NOTES

14. *(Leave blank)*

16. ABSTRACT *(200 words or less)*

The behavior of water spray injected into both an air and a steam environment was studied. The water spray was divided into two parts - sheet portion and droplet portion. An analytical model is proposed for explaining the spray behavior. Experiments were performed to substantiate the analytical results. The holographic pictures were used to obtain the droplet size distribution. These size distributions were used for computing the motion of spray droplets in the analytical model. For the sprays used in this study, most of the heat transfer occurs in the sheet portion rather than at the droplet portion of the spray. In addition, the spray angle is primarily governed by the sheet portion. The axial extent (length) of sheet is a very important parameter in determining the spray angle. A correlation is obtained experimentally for breakup length in terms of the Weber number and the Jakob number.

17. KEY WORDS AND DOCUMENT ANALYSIS
Water Spray
Hologram Reconstruction
Liquid Sheet Breakup Length
Jakob Number

17a. DESCRIPTORS

17b. IDENTIFIERS/OPEN-ENDED TERMS

18. AVAILABILITY STATEMENT
UNLIMITED

19. SECURITY CLASS *(This report)*
Unclassified

20. SECURITY CLASS *(This page)*
Unclassified

21. NO. OF PAGES

22. PRICE
$

NRC FORM 335 (7-77)

UNITED STATES
NUCLEAR REGULATORY COMMISSION
WASHINGTON, D.C. 20555

OFFICIAL BUSINESS
PENALTY FOR PRIVATE USE, $300

FOURTH CLASS MAIL
POSTAGE & FEES PAID
USNRC
WASH. D.C.
PERMIT No. G67

120555078877 1 ANR2
US NRC
ADM DIV OF TIDC
POLICY & PUBLICATIONS MGT BR
PDR NUREG COPY
LA 212
WASHINGTON DC 20555